The Geometry of the Space of 2D Shapes and the Weil-Petersson Metric

by

Sergey Kushnarev

B.Sc., Moscow State University, Russia 2003

Sc.M., Brown University, RI, 2004

A dissertation submitted in partial fulfillment of the

requirements for the degree of Doctor of Philosophy

in the Division of Applied Mathematics at Brown University

PROVIDENCE, RHODE ISLAND

May 2010

Abstract of "The Geometry of the Space of 2D Shapes and the Weil-Petersson Metric" by Sergey Kushnarev, Ph.D., Brown University, May 2010

This thesis investigates three related topics on the geometry of the space of planar shapes.

In the first part, we setup the EPDiff (Euler-Poincaré equation on the group of diffeomorphisms) and investigate its singular solutions, Teichons, analogues of solitons. A symplectic integration scheme has been implemented to solve a Hamiltonian problem that arises in this part.

In the second part, the formula for the sectional curvature of the Weil-Petersson metric has been derived. It has been shown that the formula coincides with Arnold's formula in the case of the metric without a null space.

The third part concerns numerical implementation of optimization problem of finding geodesics by minimizing the Weil-Petersson energy. The comparison of methods is shown alongside with the examples of geodesics.

This dissertation by Sergey Kushnarev is accepted in its present form
by the Division of Applied Mathematics as satisfying the
dissertation requirement for the degree of Doctor of Philosophy.

Date_______________ ______________________________

David Mumford, Ph.D., Advisor

Recommended to the Graduate Council

Date_______________ ______________________________

Peter Michor, Ph.D., Reader

Date_______________ ______________________________

Stuart Geman, Ph.D., Reader

Approved by the Graduate Council

Date_______________ ______________________________

Sheila Bonde, Dean of the Graduate School

The Vita of Sergey Kushnarev

Born on June 12, 1981 in Smolensk, Russia.

Education

- M.Sc. in Applied Mathematics, Brown University, May 2004.
- B.Sc. in Mathematics and Mechanics, Moscow State University, Russia, June 2003.

Publications/Preprints

- S. Kushnarev, *Teichons: Soliton-like Geodesics on Universal Teichmller Space*, journal Experimental Mathematics, Volume 18, Number 3, 2009.

Research Interests

- Geometry of shape spaces, Riemannian metrics on the spaces of shapes, mathematical representation and comparison of shapes.
- Euler-Poincare equation on the group of diffeomorphisms.
- Numerical Methods for Finding Geodesics.

Academic Experience

- Research Assistant: Division of Applied Mathematics, Brown University, June 2005 – May 2009.
- Teaching Assistant: *Statistical Inference I, II*, Division of Applied Mathematics, Brown University, September 2004 – May 2005.

Modeling the World with Mathematics, Division of Applied Mathematics, Brown University, Spring 2006.

Mathematics of Shape, Division of Applied Mathematics, Brown University, Spring 2006.

Awards and Honors

- Graduate Student Fellowship, Division of Applied Mathematics, Brown University, 2003-2004.
- Gold Medal, award for graduating with distinction, Moscow State University, Russia, 2003.

Acknowledgments

My thanks go to my adviser David Mumford for his enormous patience and scientific guidance. I would like to thank my readers Peter Michor and Stuart Geman for their time and valuable suggestions in regards of my research. I would also like to thank Eitan Sharon, whose code I have built on in the minimization algorithm of the Weil-Petersson energy. I would like to acknowledge the Vision Group at LEMS, Brown University for providing the outlines of fish for numerical experiments.

My thanks go to Johns Hopking University and their merry bunch: Michael Miller, Laurent Younes, Tilak Ratnanather. I would like to thank Prof. Darryl Holm for his insights and for his suggestions to study the singular solutions of the EPDiff(S^1).

My friends: Jessica Libertini, Mario Micheli, Matt Feizsli, Wei Zhang. To my officemates Yanchun Wu, Christian Pfrang, Lo-Bin Chang, Luan Lin, Oren Freifeld. I am eternally grateful to my friend Akil Narayan for his enormous help with the numerical problems I was faced with while working on my thesis.

I would like to express my appreciation to the amazing staff in the Division of Applied Math for maintaining a friendly and supporting environment.

I am thanking my parents, Sergey Kupriyanovich and Iraida Nikitichna, and my brother Denis for not asking too often "How is your thesis going, son/brother?"

Contents

List of Tables

List of Figures

Chapter 1

Introduction and Preliminary Material

1.1 Introduction

The study of shapes and their similarities is the central problem in computer vision. Of particular interest are 2D shapes, such as the outline of an object in a photo, the shape of a bacteria under a microscope, or an image of body tissue from an X-ray. The natural questions arise: how different are these shapes? Can we quantify the measure of their difference? Can we infer some extra information?

In order to answer these questions from the mathematical point of view, we need to formalize the concept of all possible shapes, and devise a mechanism that will yield the quantifiable difference between shapes. It turns out that the tools to study the shape space and to answer the above questions are given to us by Riemannian geometry. We can treat a collection of all planar shapes as a manifold. Riemannian geometry allows us to put a metric on this manifold. Equipped with the metric we can analyze the shape space: connect shapes with paths of shortest length, and thus get a geodesic; obtain curvature of the shape space, and infer the overall geometry of the shape space.

Recently the space of planar curves equipped with different metrics has been extensively studied in [YMSM08], [MM05], [MM06], [MM07], [KSMJ04], [SM06]. By endowing the shape space with a metric, we will be able to measure a certain similarity between shapes. If the shapes are similar, in some sense, then the distance between them is small; if two shapes are different, then the distance between them is large.

Why is it important to compute distances between shapes? For example: in computer vision it aides classification, recognition and segmentation tasks. Given a set of shapes from some class (say, outlines of cats) and a metric, one can construct the so-called mean shape, or Karcher mean. The mean shape will be, in some sense, an 'average', or 'typical' shape from this class. By measuring the distance between any given shape and a mean shape, one can tell whether it is a cat or, say, a dog, thus performing a classification task. In computational anatomy, given a metric on a shape space, one can construct the average shape of a diseased tissue (it could be a failing heart or a brain of an Alzheimer's patient, for example). By computing the distance between a patient's tissue and an average diseased tissue, an automatic diagnosis can be rendered, or a doctor can start early treatment if the patient's heart is 'close' in the shape space to a failing one.

Many types of metrics has been proposed previously [Mu91]. For example, one can measure the distance between shapes by taking the area of the symmetric difference of interiors of two shapes. This is an L^1-type metric. There is an L^∞-type metric, such as Hausdorff metric: the distance between two shapes, which is calculated as a maximum distance of the points on one of the shapes to the points on the other.

The curvature of the underlying shape space is of particular importance to appli-

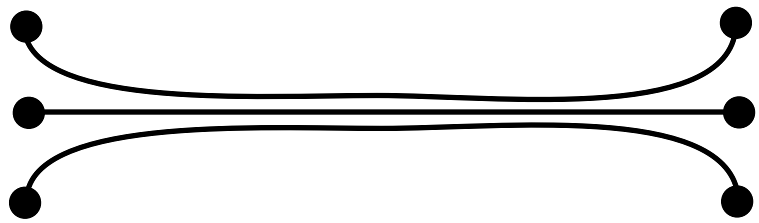

Figure 1.1: Behavior of the neighboring geodesics in the case of negative sectional curvature.

cations. It influences the numerical computation and the behavior of geodesics. The goal of this thesis is to look at a particular metric on the space of planar shapes, the so-called Weil-Petersson metric, to find geodesics in this space, and to investigate the influence of curvature on the theoretical and numerical behavior of the geodesics.

It turns out that one can associate all possible smooth shapes (represented by smooth, simple, closed curves) with a certain coset space $\mathrm{PSL}_2(\mathbb{R})\backslash\mathbf{Diff}(S^1)$. It is a right coset space of a subgroup $\mathrm{PSL}_2(\mathbb{R})$ (stands for projective special linear group) in the group $\mathbf{Diff}(S^1)$. The group $\mathbf{Diff}(S^1)$ is the group of diffeomorphism of the circle S^1 onto itself. We equip the above space with a specific metric, the Weil-Petersson metric (WP). The resulting shape space has two major properties. The first one is that all of its sectional curvatures are negative. It is believed REF (as in finite dimensional case) that between any two shapes we can find a unique geodesic, the path of shortest length. Also it introduces a sort of 'stability' in the geodesic finding problem. Given any geodesic between two shapes, the geodesic between 'nearby' shapes will be close to the initial geodesic (see Figure 1.1). Secondly, the resulting space is homogeneous with respect to the right translations by a diffeomorphism. This means that if we apply a diffeomorphism from the right to a given geodesic in the shape space, it will transform the initial and final shapes into new ones, and the geodesic into another geodesic connecting the new shapes, while preserving the WP distance.

The coset space $\mathrm{PSL}_2(\mathbb{R})\backslash\mathbf{Diff}(S^1)$ (or its completion in the WP metric or in the Teichmüller topology, see for example [Takht]) is known as the universal Teichmüller space and is well-known in many contexts: in the classification of Riemann surfaces [Hu06], conformal and quasi-conformal maps [Leh87], string theory [BR87] and most recently computer vision [SM06]. Its completion in the WP metric is an infinite dimensional homogeneous complex Kähler-Hilbert manifold ([TT06]). The coset space $\mathrm{PSL}_2(\mathbb{R})\backslash\mathbf{Diff}(S^1)$ has another realization as the space of smooth, simple, closed curves mod translations and scalings. By studying the geodesics in the space $\mathrm{PSL}_2(\mathbb{R})\backslash\mathbf{Diff}(S^1)$, we get a corresponding path in the space of the planar shapes, modulo translations and scalings.

This thesis is organized as follows. Chapter 1 will cover the basic definitions and theorems that will be used throughout the thesis. Chapter 2 will introduce the Euler-Poincaré equation on the group of diffeomorphisms of the circle S^1, or EPDiff(S^1), i.e. the geodesic equation on the shape space. Chapter 3 will be dedicated to the study of singular solutions of the EPDiff(S^1), so called *Teichons*. I will prove the existence of a Teichon solution for infinite time in one ansatz example. Numerical solution of the ODE that governs the Teichon evolution will be presented. Chapter 4 will deal with the computation of the sectional curvature of the universal Teichmüller space. I will show that the formula coincides with the Arnold's formula for curvature in [Ar66]. The last chapter will be dedicated to the numerical methods of finding geodesics in the space of 2D shapes, and presenting some example geodesics. The effects of negative curvature on the geodesic behavior will be demonstrated.

1.2 Lie groups and Lie algebras

1.2.1 Lie group

A *Lie group* is a smooth manifold G, with the property that the multiplication map $m : G \times G \to G$ and inversion map $i : G \to G$, given by

$$m(g, h) = gh, \; i(g) = g^{-1},$$

which are both smooth maps.

Examples.

- $\mathrm{Aff}(\mathbb{R})$. Consider $\mathrm{Aff}(\mathbb{R})$, the group of affine transformations of the real line $\mathbb{R}$. An element of the group $g \in \mathrm{Aff}(\mathbb{R})$ acts on $x \in \mathbb{R}$ in the following way: $x \mapsto ax + b$, where $a \in \mathbb{R}, \; a > 0$ and $b \in \mathbb{R}$. In other words, $\mathrm{Aff}(\mathbb{R}) = \{(a, b) \mid a \in \mathbb{R}, \; a > 0, b \in \mathbb{R}\}$

- *Projective special linear group* $\mathrm{PSL}_2(\mathbb{R})$. This group consists of the Möbius maps that preserve the unit circle, i.e. $A \in \mathrm{PSL}_2(\mathbb{R})$ such that:

  $$A(z) = \frac{az + b}{\bar{b}z + \bar{a}}, \quad |a|^2 - |b|^2 = 1.$$

  In general, a Möbius map $A(z)$ has the form:

  $$A(z) = \frac{az + b}{cz + d}, \quad ad - bc = 1.$$

  It is defined by four complex numbers a, b, c, d. Since multiplying all of them by a constant does not change a map, the normalization $ad - bc = 1$ is chosen. This is a 6-dimensional group. If one considers all of the coefficients to be real, i.e. $a, b, c, d \in \mathbb{R}$, then it is easy to check that the Möbius map $A(z)$ will preserve the upper half-plane. Take a map $C(z) = \frac{z+i}{iz+1}$. It maps a unit disk, centered at zero to the upper half-plane. Therefore, the map $C \circ A \circ C^{-1}$ will map a unit disk onto itself. It is easy to check that, in this case, the map $C \circ A \circ C^{-1}$ will take the form:

$$\begin{aligned} C \circ A \circ C^{-1}(z) &= \frac{((a+d) - i(b-c))z + (b+c) - i(a-d)}{((b+c) + i(a-d))z + (a+d) + i(b-c)} \\ &= \frac{\alpha z + \beta}{\bar{\beta} z + \bar{\alpha}}, \quad |\alpha|^2 - |\beta|^2 = 1. \end{aligned}$$

These are the elements of $\mathrm{PSL}_2(\mathbb{R})$, a 3-dimensional subgroup of Möbius transformations. The name of the group stands for the *projective special linear group*. This name comes from the fact that a Möbius map with real coefficients can be regarded as an element of $\mathrm{SL}_2(\mathbb{R})$, 2-by-2 real matrices with determinant 1. Projective special linear group is the quotient of $\mathrm{SL}_2(\mathbb{R})$, obtained by identifying each element with its negative, i.e. $\mathrm{PSL}_2(\mathbb{R}) = \mathrm{SL}_2(\mathbb{R})/\{+1, -1\}$.

The action of $\mathrm{PSL}_2(\mathbb{R})$ on the circle can be written as:

$$\tan(A(\theta)/2) = \frac{(a_2 + b_2) + (a_1 - b_1)\tan(\theta/2)}{(a_1 + b_1) - (a_2 - b_2)\tan(\theta/2)}.$$

- *Group of diffeomorphisms.* The group of diffeomorphisms mapping the domain $M \subset \mathbb{R}^n$ to itself is a Lie group. It will be denoted by $\mathbf{Diff}(M)$.

Remark. If M is a compact manifold, then $\mathbf{Diff}(M)$ is a Lie group modeled on the infinite-dimensional locally convex vector spaces. See [KM97] for details. Many of the results for the finite-dimensional Lie groups can be applied in the infinite-dimensional case.

1.2.2 Lie algebra

A *Lie algebra* $\mathfrak{g}$ is a tangent space at the identity e of the Lie group G, endowed with the *Lie bracket* map, denoted by $(X, Y) \mapsto [X, Y]$, which satisfies the following properties for all $X, Y, Z \in \mathfrak{g}$:

- bilinearity,
- antisymmetry,
- Jacobi identity, i.e. $[X, [Y, Z]] + [Y, [Z, X]] + [Z, [X, Y]] = 0$.

Examples.

- In the case of the group of affine transformations $\mathrm{Aff}(\mathbb{R})$, let us represent $g \in \mathrm{Aff}(\mathbb{R})$ as a pair (a, b), where $a > 0, b \in \mathbb{R}$. Therefore, we can identify the group $\mathrm{Aff}(\mathbb{R})$ as a right half-plane. The identity element is $e = (1, 0)$. The tangent space at e is the whole $\mathbb{R}^2$.
- Let us determine the Lie algebra $psl_2(\mathbb{R})$. First, consider a tangent space to the group $\mathrm{PSL}_2(\mathbb{R})$ at the identity element. It could be shown that a Lie algebra $psl_2(\mathbb{R})$ consists of vector fields $v(z)$ of the form:

$$v(z) = (a_{-1}z^{-1} + a_0 + a_1 z)iz\frac{\partial}{\partial z}.$$

For $z = e^{i\theta}$ this vector field is tangent to the unit circle. Since $\partial/\partial\theta$ pushes to $iz\partial/\partial z$ under the embedding $\theta \mapsto e^{i\theta}$, we can rewrite this in the coordinate θ on the circle:

$$v(\theta) = (b\cos\theta + c\sin\theta + a_0)\frac{\partial}{\partial\theta},$$

where $b = a_{-1} + a_1, c = i(a_1 - a_{-1})$, and $b, c \in \mathbb{R}$, since $a_{-1} = \bar{a}_1$.

- The tangent space $T_e\mathbf{Diff}(M)$ is the space of smooth vector fields with support on M. It will be denoted as $\mathbf{Vec}(M)$.

1.2.3 The adjoint representation

For all $g \in G$, we can define the left and right translation maps on G:

$$L_g : h \mapsto gh, \quad R_g : h \mapsto hg.$$

We can also define the conjugate map: $h \mapsto ghg^{-1} = L_g R_{g^{-1}} h$. It induces a map on the tangent space at the identity e, denoted by Ad_g. For any vector $X \in \mathfrak{g}$, it is given by:

$$\begin{aligned} &\mathrm{Ad}_g : \mathfrak{g} \to \mathfrak{g}, \\ &X \mapsto DR_{g^{-1}} DL_g X. \end{aligned}$$

The map Ad that associates any element $g \in G$ with a bijective linear mapping Ad_g of the Lie algebra $\mathfrak{g}$ onto itself. This map is called the *adjoint representation of the Lie group G*. Finally, the derivative of the map Ad at the identity e is denoted by ad and associates a linear map ad_X with any vector $X \in \mathfrak{g}$. It is called the *adjoint representation of the Lie algebra* $\mathfrak{g}$. The adjoint representation ad is related to the Lie bracket by

$$\mathrm{ad}_X Y = [X, Y], \quad \forall X, Y \in \mathfrak{g}.$$

Examples.

Consider the group of affine transformations $\mathrm{Aff}(\mathbb{R})$. Let us compute the differential of the left multiplication $L_g : h \mapsto gh$ and the right multiplication maps

$R_g : h \mapsto hg$, where $g = (a_g, b_g)$

$$dL_g : Y \mapsto a_g Y, \text{ and } dR_g : Y = \begin{pmatrix} Y_1 \\ Y_2 \end{pmatrix} \mapsto \begin{pmatrix} a_g Y_1 \\ b_g Y_1 + Y_2 \end{pmatrix}.$$

Therefore the adjoint map Ad for the affine group will be:

$$\mathrm{Ad}_g : Y = \begin{pmatrix} Y_1 \\ Y_2 \end{pmatrix} \mapsto \begin{pmatrix} Y_1 \\ a_g Y_2 - b_g Y_1 \end{pmatrix}.$$

The map ad, in this case, will be: $g(t) = (a_g(t), b_g(t)) \in G$, $g(0) = e = (1, 0)$, $\dot{g}(0) = (\dot{a}_g(0), \dot{b}_g(0))^T = X$. So

$$\mathrm{ad}_X(Y) = \frac{d}{dt}\left[\mathrm{Ad}_{g(t)} Y\right]_{t=0} = \frac{d}{dt}(Y_1, a_g(t)Y_2 - b_g(t)Y_1)^T_{t=0}$$

$$= (0, \dot{a}_g(0)Y_2 - \dot{b}_g(0)Y_1)^T = (0, X_1Y_2 - X_2Y_1)^T.$$

Therefore, $\mathrm{ad}_X(Y) = (0, X_1Y_2 - X_2Y_1)^T$. Hence, we have an expression for the Lie bracket of the group of affine transformations of $\mathbb{R}$:

$$\left[\begin{pmatrix} X_1 \\ X_2 \end{pmatrix}, \begin{pmatrix} Y_1 \\ Y_2 \end{pmatrix}\right] = \begin{pmatrix} 0 \\ X_1Y_2 - X_2Y_1 \end{pmatrix}.$$

1.3 Universal Teichmüller space

1.3.1 Definitions

Let Δ be an open disk in the complex plane $\mathbb{C}$, i.e. $\Delta = \{z \in \mathbb{C} \mid |z| < 1\}$, and let $\Delta^* = \{z \in \mathbb{C} \mid |z| > 1\}$ be its exterior. We denote by $L^\infty(\Delta)$ the space of bounded Beltrami differentials on Δ, and by $L^\infty(\Delta)_1$ the open unit ball in $L^\infty(\Delta)$.

A quasiconformal mapping is a generalization of the conformal mapping. It is a mapping with bounded distortion. Consider a mapping $f : D \to D'$. The characteristic of the distortion of this map is the coefficient $k_f(z)$, called the *coefficient of quasi-conformality of function f at point z*, and is defined as follows:

$$k_f(z) = \limsup_{r \to 0} \frac{\sup_{|w-z|=r} |f(w) - f(z)|}{\inf_{|w-z|=r} |f(w) - f(z)|}.$$

The quantity k_f is called the *coefficient of quasi-conformality of f in the domain D*:

$$k_f = \sup_{z \in D} k_f(z).$$

If $k_f \leqslant k$, then mapping f is called *k-quasi-conformal*. Geometrically, the coefficient k_f could be viewed as follows: f maps infinitesimal circles to the infinitesimal ellipses. The ratio of the major to the minor axis of the infinitesimal ellipses will be at most k for a k-quasiconformal map f. The 1-quasiconformal map is conformal (circles are mapped to circles).

The Beltrami differential equation is the equation of the type:

$$\frac{\partial f}{\partial \bar{z}} = \mu(z) \frac{\partial f}{\partial z}, \tag{1.1}$$

where $\mu(z)$ is a known measurable function on some region $\Omega \subset \mathbb{C}$. We are looking for the function f, that will satisfy equation (1.1). The function $\mu(z)$ is called the *Beltrami differential*. The name comes from the fact that we can symbolically rewrite the Beltrami equation as $\frac{\partial f}{\partial \bar{z}} = \mu(z) \frac{dz}{d\bar{z}} \frac{\partial f}{\partial z}$.

For the construction of the universal Teichmüller space we will need the extension of the usual Riemann Mapping Theorem, called the Measurable Riemann Mapping Theorem.

Theorem 1. *Equation (1.1) gives a one-to-one correspondence between $QC_{fix}(\hat{\mathbb{C}})$*

and the unit ball $L^\infty(\mathbb{C})_1$. The space $QC_{fix}(\hat{\mathbb{C}})$ is the set of quasiconformal mappings f on $\hat{\mathbb{C}}$ that fix the points 0, 1, and ∞. The space $L^\infty(\mathbb{C})_1$ is the set of measurable complex-valued functions μ on $\mathbb{C}$ for which $\|\mu\|_\infty < 1$.

The general solution of the equation (1.1) in D will be a quasiconformal homeomorphism f, which is defined up to a composition with any analytic function F, i.e. $F \circ f(z)$ is also a solution.

1.3.2 Two models for the universal Teichmüller space

Consider a Beltrami differential $\mu \in L^\infty(\Delta)_1$. We now define two models: model A and model B.

Model A: Fingerprints Homeo$_{qs}(S^1)$.

Extend μ into $\hat{\mathbb{C}}$ by the reflection

$$\mu\left(\frac{1}{\bar{z}}\right) = \bar{\mu}(z)\frac{z^2}{\bar{z}^2}.$$

Thus we get a new map $\mu \in L^\infty(\hat{\mathbb{C}})$. Denote by f_μ the unique solution to the Beltrami equation

$$(f_\mu)_{\bar{z}} = \mu(f_\mu)_z,$$

normalized to preserve three points $(-1, -i, 1)$. Then, due to the reflection symmetry of μ, we have

$$\frac{1}{f_\mu(z)} = \bar{f}_\mu\left(\frac{1}{\bar{z}}\right).$$

As a result, f_μ preserves the unit circle S^1, Δ and Δ^*. Given two Beltrami differentials $\mu, \nu \in L^\infty(\Delta)_1$, set $\mu \sim \nu$ if $f_\mu\mid_{S^1} = f_\nu \mid_{S^1}$. The universal Teichmüller space is the set of equivalence classes of mappings μ:

$$Teich(\Delta) = L^{\infty}(\Delta)_1 / \sim .$$

An orientation preserving homeomorphism f of the circle S^1 is *quasisymmetric* if there is a constant M such that for every x and every $t \leqslant \pi/2$

$$\frac{1}{M} \leqslant \frac{f(e^{i(x+t)}) - f(e^{ix})}{f(e^{ix}) - f(e^{i(x-t)})} \leqslant M.$$

Note that the definition implies that $M \geqslant 1$. The set of all quasisymmetric homeomorphisms of the circle is denoted $\mathbf{Homeo}_{qs}(S^1)$, which is a group under the composition of maps. The link with the quasiconformal mappings on the exterior of the disc is given by the Beurling-Ahlfors extension theorem, stating that an orientation preserving homeomorphism of the circle admits a quasiconformal extension to the disk if and only if it is quasisymmetric. Therefore, one may equally consider homeomorphisms of the circle; the restriction of f_μ to S^1 is a quasisymmetric homeomorphism of the circle, unique up to the self-maps of the circle, i.e. the elements of the Möbius subgroup $\mathrm{PSL}_2(\mathbb{R})$. Define

$$T(1) = \mathbf{Homeo}_{qs}(S^1)/\mathrm{PSL}_2(\mathbb{R}).$$

The function $\Psi(\theta) \in \mathbf{Homeo}_{qs}(S^1)/\mathrm{PSL}_2(\mathbb{R})$ will be called a *fingerprint* (in the Techmüller theory it is called a *welding map*). We are interested in smooth fingerprints, i.e. fingerprints that lie in the subgroup $\mathbf{Diff}(S^1)$ of the group $\mathbf{Homeo}_{qs}(S^1)$.

Model B: quasicircles.

A quasicircle is an image of a circle under the quasiconformal map. This is the planar shape that corresponds to the fingerprint, constructed above.

Extend μ into $\hat{\mathbb{C}}$ by setting $\mu(z) = 0$ outside of the unit disk. Denote f^μ as the solution to the Beltrami equation

$$(f^\mu)_{\bar{z}} = \mu(f^\mu)_z,$$

normalized so that $f^\mu(z) = z + O\left(\frac{1}{|z|}\right)$ near infinity. On the exterior of the unit disk Δ^*, f^μ is a conformal map onto its image $D^\mu := f(\Delta^*)$. Set $\mu \sim \nu$ if $f^\mu|_{\Delta^*} = f^\nu|_{\Delta^*}$. The universal Teichmüller space is the set of equivalence classes of mappings μ,

$$T(1) = L^\infty(\Delta)_1 / \sim .$$

Since exterior maps f^μ are in one-to-one correspondence with the quasicircles ∂D^μ, we can treat $T(1)$ as a set of equivalence classes of quasicircles.

The two models A and B are equivalent since $f_\mu|_{S^1} = f_\nu|_{S^1} \Leftrightarrow f^\mu|_{\Delta^*} = f^\nu|_{\Delta^*}$. Therefore, we set up a correspondence between a fingerprint (or a welding map) and a quasicircle (a shape).

1.3.3 Passing between the two models.

In this section, we will show how to pass from the fingerprints to the shapes and vice versa. The numerical aspect of these procedures is treated in Chapter 5.

From shapes to fingerprints

In this thesis, 'shape' means a simple closed smooth curve Γ in the plane, which is associated with the complex plane $\mathbb{C}$. We also need an extended complex plane (or Riemann sphere), which is denoted by $\hat{\mathbb{C}} = \mathbb{C} \cup \{\infty\}$. As stated previously, the universal Teichmüller space is isomorphic to a space of shapes, modulo translations and scalings. In other words:

$$\boxed{\mathrm{PSL}_2(\mathbb{R})\backslash\mathbf{Diff}(S^1) \cong \text{ set of shapes}/\{\text{translations, scalings}\}.}$$

Denote the interior of the unit disk as $\mathbb{D}_{\text{int}} = \{z \mid |z| < 1\}$ and the infinite region outside (including ∞) as $\mathbb{D}_{\text{ext}} = \{z \mid |z| > 1\}$. For every simple closed curve Γ in $\mathbb{C}$, denote Γ_{int} as its union with the region enclosed by it, and denote by Γ_{ext} its union with the infinite region outside of Γ (including ∞).

Then, by the Riemann mapping theorem, for all Γ there exists a conformal map

$$\phi_{\text{int}} : \mathbb{D}_{\text{int}} \to \Gamma_{\text{int}}.$$

This map is unique up to replacing ϕ_{int} by $\phi_{\text{int}} \circ A$ for any Möbius transformation $A : \mathbb{D}_{\text{int}} \to \mathbb{D}_{\text{int}}$, where A is defined as:

$$A(z) = \frac{az + b}{\bar{b}z + \bar{a}},\ |a|^2 - |b|^2 = 1.$$

Similarly, we obtain a conformal map of the exteriors:

$$\phi_{\text{ext}} : \mathbb{D}_{\text{ext}} \to \Gamma_{\text{ext}}.$$

As above, ϕ_{ext} is also unique up to any Möbius transformation. But in this, case we normalize. We choose a unique Möbius map A, such that $\phi_{\text{ext}} \circ A$ maps ∞ to ∞, and that its differential carries the real positive axis of the D-plane at infinity to the real positive axis of the Γ-plane at infinity. Thus, the ambiguity in the choice of ϕ_{ext} is eliminated for every Γ.

The goal of this construction is to define on the unit circle S^1 the map, called the 'fingerprint' of the shape:

$$\psi = \phi_{\text{int}}^{-1} \circ \phi_{\text{ext}} \in \text{PSL}_2(\mathbb{R})\backslash\textbf{Diff}(S^1).$$

Note that $\phi_{\text{int}}(S^1) = \Gamma,\ \phi_{\text{ext}}^{-1}(\Gamma) = S^1$. The fingerprint $\psi : S^1 \to S^1$ is a real-valued orientation-preserving diffeomorphism. It is a uniquely identifying fingerprint of the shape Γ. The fingerprint of the eye-shape is shown in Figure 1.2. Due to Möbius transformation ambiguity in the choice of ϕ_{int}, we can see by construction that ψ is a member of the right coset space $\text{PSL}_2(\mathbb{R})\backslash\textbf{Diff}(S^1)$, where $\text{PSL}_2(\mathbb{R})$ is a group of Möbius maps.

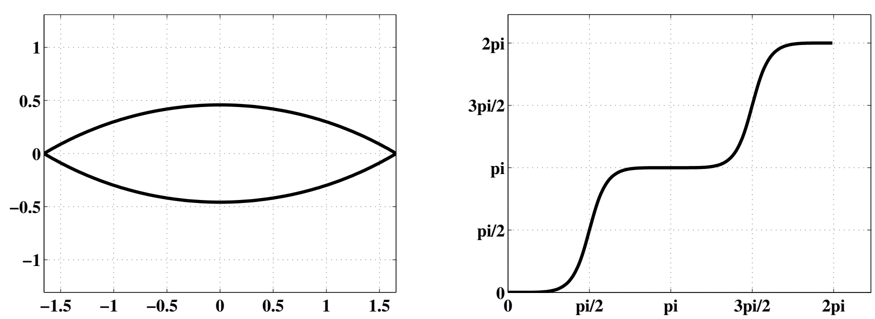

Figure 1.2: Example of the eye-shape and its fingerprint ψ as given by equation (3.14).

Note that one can equally define the fingerprint to be

$$\psi^i = \phi_{\text{ext}}^{-1} \circ \phi_{\text{int}} \in \textbf{Diff}(S^1)/\text{PSL}_2(\mathbb{R}),$$

which is simply the inverse of our fingerprint. This alternate version is the definition used in [SM06]. However, in this thesis, we choose *right* cosets and put the Möbius ambiguity on the left.

Remark. It is easy to see the relationship between these equivalent definitions of the fingerprint by defining two sets of points, $\{\theta^{\text{int}}\}$ and $\{\theta^{\text{ext}}\}$, on the circle:

$$\theta_k^{\text{int}} = \phi_{\text{int}}^{-1}(\Gamma_k),$$
$$\theta_k^{\text{ext}} = \phi_{\text{ext}}^{-1}(\Gamma_k),$$

where Γ_k are points that define the shape. In this notation we can write the fingerprints:

$$\psi^i(\theta^{\text{int}}) = \theta^{\text{ext}}, \quad \psi(\theta^{\text{ext}}) = \theta^{\text{int}}.$$

By construction, the fingerprint encodes the geometry of the shape. These results have been extensively studied by M. Feiszli in [Fe08]. Consider the conformal map $f : \mathbb{D}_{\text{int}} \to \Gamma_{\text{int}}$ and some point z on the boundary of the shape $\partial\Gamma_{\text{int}}$. M. Feiszli has shown that the boundary derivative $|f' \circ f^{-1}(z)|$ is influenced by two factors. The first one accounts for the local geometry of $\partial\Gamma_{\text{int}}$ near z and is stated in terms of the boundary curvature κ at point z, and R, the radius of the medial circle tangent at z. The second factor says that boundary derivatives increase exponentially with hyperbolic distance d from the point $f(0)$. In other words:

$$|f' \circ f^{-1}(z)| \approx \frac{R}{2 - R\kappa} e^d. \tag{1.2}$$

From fingerprints to shapes

Given the quasisymmetric homeomorphism $\Psi(\theta)$, extend it to the quasiconformal map $F(z)$ of the disk. It will give an associated Beltrami differential μ:

$$\mu = \frac{\partial_{\bar{z}} F}{\partial_z F}.$$

Extend this $\mu(z)$ to the complex plane $\mathbb{C}$ by reflections, as in Model A in Section 1.3.2. By solving the Beltrami equation we will obtain $f_\mu(z)$. The fingerprint $\Psi(\theta)$ will be

Fingerprint	$\Phi = f_{\text{int}}^{-1} \circ f_{\text{ext}}$	$\Phi = f_{\text{ext}}^{-1} \circ f_{\text{int}}$
Domain vs. range	$\Phi(\theta_{\text{ext}}) = \theta_{\text{int}}$	$\Phi(\theta_{\text{int}}) = \theta_{\text{ext}}$
Protrusions	Φ has low derivatives	Φ has high derivatives
Intrusions	Φ has high derivatives	Φ has low derivatives
Space	$\text{PSL}_2(\mathbb{R})\backslash\textbf{Diff}(S^1)$	$\textbf{Diff}(S^1)/\text{PSL}_2(\mathbb{R})$
Metric	Right invariant, with velocity: $v = \Phi_t \circ \Phi^{-1}$	Left invariant with velocity: $v = \frac{\Phi_t}{\Phi_\theta}$
Energy of the path	$E = \int_0^1 \lVert\Phi_t \circ \Phi^{-1}\rVert^2 dt$	$E = \int_0^1 \lVert\Phi_t/\Phi_\theta\rVert^2 dt$

Table 1.1: Comparison of two equivalent constructions of the fingerprint representation.

defined as:

$$\Psi(\theta) = f_\mu \mid_{S^1} .$$

The fingerprint is defined up to an action of the $\text{PSL}_2(\mathbb{R})$ group on the left (or, equivalently, on the right if $\Psi \in \textbf{Diff}(S^1)/\text{PSL}_2(\mathbb{R})$). This ambiguity arises from the fact that Ψ can be extended non-uniquely to the quasiconformal map of the disk. But the resulting shape does not depend on the choice of extension. For details see [Hu06]. For the numerical implementation of the welding see Section 5.2.

1.3.4 Left vs. right

In the table 1.1 we are comparing two equivalent ways of defining a fingerprint of the shape $\phi_{\text{int}}^{-1} \circ \phi_{\text{ext}}$ vs $\phi_{\text{ext}}^{-1} \circ \phi_{\text{int}}$, and how it affects the rest of the theory.

1.4 Weil-Petersson Norm

1.4.1 Weil-Petersson norm on $T(1)$

It is customary to define the Weil-Petersson norm on the universal Teichmüller space $T(1)$ in the following way. Let $N(\Delta)$, the subspace of $L^\infty(\Delta)$ denote the space of *infinitesimaly trivial* Beltrami differentials. Specifically, $\nu \in N(\Delta)$ if

$$\int_\Delta \nu(z)\phi(z)dxdy = 0$$

for all quadratic differentials ϕ defined on Δ. We can identify the space $L^\infty(\Delta)/N(\Delta)$ with the tangent space to $T(1)$ at the origin.

Given two Beltrami differentials $\mu, \nu \in L^\infty(\Delta)/N(\Delta)$, the Weil-Petersson inner product is defined as

$$\langle \mu, \nu \rangle_{WP} = \int\int_\Delta \mu\bar{\nu}\rho^2 dxdy,$$

where $\rho = \frac{2}{1-|z|^2}$ defines the Poincaré measure on the disk Δ. Using right translations this inner product will be defined for all the $T(1)$.

We have chosen to work on one of the realizations of the universal Teichmüller space, on the space of fingerprints $\mathbf{Diff}(S^1)$. This is, in fact, a subspace of $T(1)$. Nag and Verjovsky [NV90] have shown how the Weil-Petersson metric is induced on $\mathrm{PSL}_2(\mathbb{R})\backslash\mathbf{Diff}(S^1)$.

1.4.2 Weil-Petersson norm on the lie algebra of $\mathbf{Diff}(S^1)$

The Lie algebra of the group $\mathbf{Diff}(S^1)$ is given by the vector space $\mathbf{Vec}(S^1)$ of smooth periodic vector fields $v(\theta)\partial/\partial\theta$ on the circle.

Expanding such a v in a Fourier series $v(\theta) = \sum_{n=-\infty}^{\infty} v_n e^{in\theta}$ (where $\overline{v_n} = v_{-n}$ for the vector field to be real), we can define the Weil-Petersson norm on $\mathbf{Vec}(S^1)$ as

$$\|v\|_{WP}^2 = \sum_{n\in\widehat{\mathbb{Z}}} |n^3 - n||v_n|^2. \tag{1.3}$$

Here, $\widehat{\mathbb{Z}} = \mathbb{Z}\backslash\{n = 0, \pm 1\}$. Notice that this is an '$H^{3/2}$'-type of metric on the space $\mathbf{Vec}(S^1)$.

The null space of this norm is given by the vector fields whose only Fourier coefficients are v_{-1}, v_0 and v_1, i.e. vector fields of the type $(a + b\cos\theta + c\sin\theta)\partial/\partial\theta$. These vector fields are exactly in the Lie algebra $psl_2(\mathbb{R})$ of the Lie group $\mathrm{PSL}_2(\mathbb{R})$.

The motivation for this particular definition is the fact that for all $A \in \mathrm{PSL}_2(\mathbb{R})$ and $v \in \mathbf{Vec}(S^1)$, one can verify that

$$\|\mathrm{Ad}_A(v)\|_{WP} = \|v\|_{WP}.$$

1.4.3 Extending the WP Metric to $\mathrm{PSL}_2(\mathbb{R})\backslash\mathbf{Diff}(S^1)$

Consider any Lie group G and a subgroup H, and let $\mathfrak{g}$ and $\mathfrak{h}$ be their corresponding Lie algebras. Quite generally, any norms $\|\cdot\|$ on the Lie algebra of G which are zero on the Lie subalgebra of H and which satisfy $\|\mathrm{Ad}_h(v)\| = \|v\|$ for all $h \in H$ induce a Riemannian metric on coset spaces $H\backslash G$ which are invariant by all right multiplication maps $R_g : H\backslash G \to H\backslash G$, $g \in G$.

Applied to $G = \mathbf{Diff}(S^1), H = \mathrm{PSL}_2(\mathbb{R})$ and the above WP norm on vector fields, we get the right-invariant *WP-Riemannian metric* on the coset space $\mathrm{PSL}_2(\mathbb{R})\backslash\mathbf{Diff}(S^1)$.

1.4.4 The WP Green's Function

The Weil-Petersson norm can also be defined via a differential operator L

$$\begin{aligned} \|v\|_{WP}^2 &= \langle Lv, v\rangle, \\ L &= -\mathcal{H}(\partial_\theta^3 + \partial_\theta), \end{aligned}$$

where $\mathcal{H}$ is the periodic Hilbert transform defined by convolution with $\frac{1}{2\pi}\mathrm{ctn}(\theta/2)$. This is because in the Fourier space, $\mathcal{H}$ acts as multiplication by $-i.\mathrm{sign}(n)$. Hence:

$$-\mathcal{H}(\partial_\theta^3 + \partial_\theta)e^{in\theta} = i\mathrm{sign}(n)((in)^3 + in)e^{in\theta} = |n^3 - n|e^{in\theta}.$$

Because our later analysis will require it, we will find here the inverse of the operator L, i.e. its Green's function $G(\theta)$, using the representation of L in the Fourier basis (1.3). We will therefore need to find

$$G(\theta) = \sum_{n\in\widehat{\mathbb{Z}}} \frac{e^{in\theta}}{|n^3 - n|}.$$

Using the following series from [GR00],

$$\sum_{k=1}^{\infty} \frac{\cos(k\theta)}{k} = \frac{1}{2}\ln\frac{1}{2(1-\cos\theta)}, \text{ for } \theta \in (0, 2\pi),$$

and employing the decomposition $\frac{1}{n^3-n} = \frac{1}{2}\frac{1}{n+1} + \frac{1}{2}\frac{1}{n-1} - \frac{1}{n}$, we find that the Green's function of the WP operator L has the form

$$G(\theta) = (1-\cos\theta)\log[2(1-\cos\theta)] + \frac{3}{2}\cos\theta - 1. \tag{1.4}$$

One can easily verify that $LG(\theta) = \delta_0(\theta) - 1 - 2\cos\theta$, the projection of δ_0 onto the subspace of distributions orthogonal to $1, \cos(\theta), \sin(\theta)$. The profile of Green's function can be seen in Figure 1.3. Note that it is smooth everywhere except for the logarithmic pole in $G''(\theta)$ at $\theta = 0$.

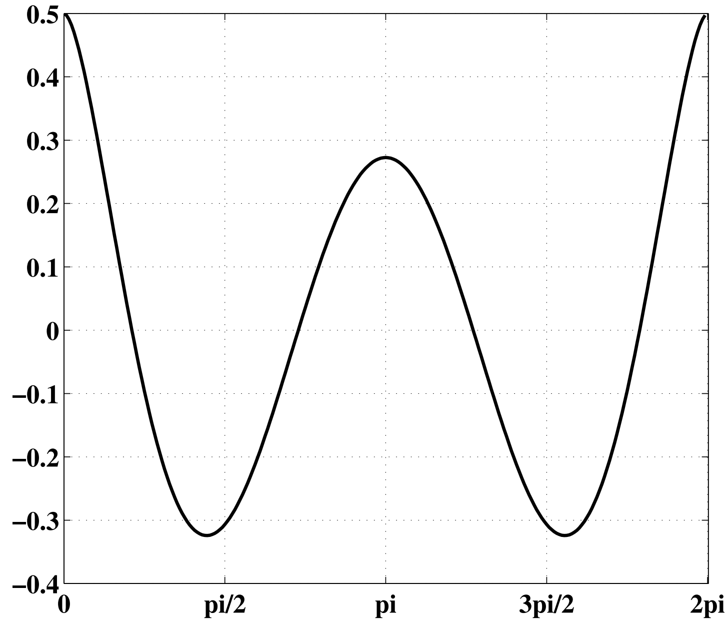

Figure 1.3: Green's function (1.4) of the Weil-Peterson operator L_{WP}. It is smooth except for a log-pole in its *second* derivative at $\theta = 0$.

1.4.5 WP metric on the plane

In [MM05] and [MM06] Michor and Mumford considered different metrics, defined on the planar curves. It will be instructive to see how the Weil-Petersson metric is expressed as a metric on the shapes themselves, not as a metric on the fingerprint representation.

Consider $\mathcal{S}$, the space of smooth, simple, closed curves. Let $C \in \mathcal{S}$ be a fixed curve, parametrized by the arclength $s \mapsto C(s)$. Then nearby curve C_a can be represented as:

$$s \mapsto C_a(s) = C(s) + a(s).\vec{n}(s),$$

where $\vec{n}(s)$ is the unit normal to the curve C at point s, and $a(s)$ is a smooth function, chosen in such a way that curve C_a stays smooth and simple. The space of all normal vector fields $a\vec{n}_C$ to the curve C is naturally isomorphic to the space tangent space $T_C\mathcal{S}$. The simplest inner product on $T_C\mathcal{S}$ is the L^2 inner product: $\langle a, b\rangle = \int_C a.b.ds$, where s is the arclength along C. This metric and many others have been studied in [MM05], [MM06].

In case of the Weil-Petersson metric, welding map takes fingerprints and maps them to the corresponding shapes. In [Fe08] it was shown that the derivative of the welding map D_0 at the identity (i.e. circle shape) is defined by:

$$V(\theta) \mapsto \frac{1}{2}(iV(\theta) + \mathcal{H}V(\theta))e^{i\theta}\frac{\partial}{\partial\theta},$$

where $V(\theta) \in \mathbf{Vec}(S^1)$, and $\mathcal{H}$ is the Hilbert transform. The normal component of the vector field on the plane is $\tilde{V} = \frac{1}{2}\mathcal{H}V(\theta)$. Taking into account that $\widehat{(\mathcal{H}f)}_n = -i.\mathrm{sgn}(n)f_n$ we have:

$$\langle V, V\rangle_{WP} = \int_{S^1} LV(\theta).V.d\theta = 4\int_{S^1} L\tilde{V}.\tilde{V}d\theta.$$

In terms of the setup of papers [MM05], [MM06] the metric involves the same Weil-Petersson operator, which is an '$H^{3/2}$'-type of metric.

Notice that the above expression is given for the normal vector fields to the circle. In the case of a general curve, the expression will involve the Hilbert transform on an arbitrary domain, and no close form of it is available. Knowing explicitly the conformal map between the disk and the domain in interest will give us the required expression for map $\mathcal{H}$, but this is beyond the scope of this thesis.

Chapter 2

EPDiff

In this chapter we will discuss EPDiff(Ω), which stands for Euler-Poincaré equation on the group of diffeomorphisms of some manifold Ω. EPDiff describes the geodesic on this group, and it is usually denoted EPDiff(Ω). We will derive the EPDiff(S^1), the geodesic equation on the group $\mathbf{Diff}(S^1)$, and demonstrate conserved quantities of the geodesic motion.

2.1 EPDiff

Geodesic equations of groups of diffeomorphisms on a manifold Ω were first studied in Arnold's ground-breaking paper [Ar66]. The Lie group in question is denoted by $\mathbf{Diff}(\Omega)$, its tangent space at identity is the space of smooth vector fields on Ω and is denoted by $\mathbf{Vec}(\Omega)$. Taking the tangents to a geodesic in $\mathbf{Diff}(\Omega)$ and translating them back to the Lie algebra $\mathbf{Vec}(\Omega)$, we get a time varying vector field $\vec{u}(x,t)$ on Ω from which we can recover the geodesic by integrating. The geodesic equation now becomes a differential equation for $\vec{u}$, *first order* in t.

This general construction gives rise to a huge number of seemingly unrelated equations. For example, Arnold considered the group of volume preserving diffeomorphisms of domain $\Omega \subset \mathbb{R}^n$ with the L^2 metric and found the geodesic equation for the vector field $\vec{u}(\vec{x}, t)$ to be Euler's fluid flow equation (see [AK98] for a full exposition).

If we consider a group of diffeomorphisms of the circle $\mathbf{Diff}(S^1)$ with the L^2 metric then the geodesic equation becomes inviscid Burgers equation.

Another examples of geodesic flow on Virasoro group, a central extension by S^1 of the group $\mathbf{Diff}(S^1)$, include both the periodic Korteweg-deVries equation (KdV) for a function $u(\theta, t)$:

$$u_t = -3u.u_\theta - u_{\theta\theta\theta}$$

and the periodic Camassa-Holm equation or C-H (see [CH93])

$$m_t = -2m.u_\theta - u.m_\theta - u_{\theta\theta\theta}, \text{ where } m = u - u_{\theta\theta}$$

with L^2 and H^1 metrics respectively.

In general, when we are provided with a right-invariant metric on a group of diffeomorphisms of some domain Ω, then the geodesic equation on this group is called EPDiff(Ω), i.e. Euler-Poincaré equation for diffeomorphisms of the domain Ω. In this thesis the domain of interest is the circle S^1. The general EPDiff follows from [Ar66] and has the form

$$\frac{\partial}{\partial t} Lv + (v \cdot \nabla)(Lv) + \mathrm{div} v.Lv + Dv^t \cdot Lv = 0,$$

The statement of Arnold's theorem for the general case of a Lie group G is the following.

Theorem 2. *Let G be any Lie group. Let $\langle v_1, v_2 \rangle_L = (L(v_1), v_2)$ be a positive-definite symmetric inner product on the Lie algebra $\mathfrak{g}$, defined by a symmetric linear map*

$L : \mathfrak{g} \to \mathfrak{g}^*$ (the braces denote the canonical pairing of elements from $\mathfrak{g}^*$ and $\mathfrak{g}$). For $v_1, v_2 \in T_gG$ the inner product is defined via the right translations: $\langle v_1, v_2\rangle_g = \langle D_gR_{g^{-1}}v_1, D_gR_{g^{-1}}v_2\rangle_e = \langle v_1 \cdot g^{-1}, v_2 \cdot g^{-1}\rangle$. Let $g(t)$ be any path in G and define $u(t) = g_t \cdot g^{-1}$ to be its tangent path in $\mathfrak{g}$. Then:

$$g(t) \subset G \text{ is a geodesic } \iff Lu_t = -\mathrm{ad}_u^*(Lu) \text{ in } \mathfrak{g}^*$$

where $\mathrm{ad}_u^* : \mathfrak{g}^* \to \mathfrak{g}^*$ is the adjoint of $\mathrm{ad}_u, u \in \mathfrak{g}$.

Remark. The statement of the theorem holds with minor alteration for the left-invariant metric. The evolution equation in this case becomes $Lu_t = \mathrm{ad}_u^*(Lu)$.

We can apply the above result in the case when G is an infinite-dimensional group (e.g. a group of diffeomorphisms of a circle S^1). We omit the technicalities of this more general approach and render the proof heuristically, largely following [Ar66].

Proof. Notice, that the energy $E = \frac{1}{2}\langle g_t \cdot g^{-1}, g_t \cdot g^{-1}\rangle$ is invariant under the right translations. By Noether's theorem this implies that $L_g^*(Lg_t) \in \mathfrak{g}^*$ is conserved, where L_g^* is the pullback of the left translation L_g. We denote it as m^L, i.e. $m^L = L_g^*(Lg_t) = \text{const}$. Moreover, notice that

$$Lu(t) = L(g_t \cdot g^{-1}(t)) = R_{g(t)}^* Lg_t = Ad_{g^{-1}(t)}^* L_{g(t)}^* Lg_t = Ad_{g^{-1}(t)}^* m^L.$$

Differentiating the above identity in t at $t = 0$, and assuming that $g(0) = e$ we obtain the statement of the theorem. The right-invariance of the metric implies that the right-hand side depends only on Lu_t, but not on $g(t)$, and therefore the equation is satisfied for every $g(t)$. ∎

Example

Take $G = \text{Aff}(\mathbb{R})$, the group of affine transformations of the real line. Recall that $\text{Aff}(\mathbb{R}) = \{(a,b) \mid a > 0, b \in \mathbb{R}\}$. The Lie algebra $\mathfrak{g}$ is the whole $\mathbb{R}^2$. In Subsection 1.2.3 we have derived the expression for the adjoint map for the group $\text{Aff}(\mathbb{R})$. It has the form:

$$\text{ad}_u(v) = \begin{pmatrix} 0 \\ u_1 v_2 - u_2 v_1 \end{pmatrix}, \text{ where } u = \begin{pmatrix} u_1 \\ u_2 \end{pmatrix}, v = \begin{pmatrix} v_1 \\ v_2 \end{pmatrix} \in T_e G.$$

For the metric we will fix the quadratic form $da^2 + db^2$ on the tangent space at the identity $e = (1,0)$. So the metric on $T_{(1,0)}G$ is the usual Euclidean metric:

$$\langle u, v \rangle = g_{ij}.u^i.v^j, \text{ where } g = \left(\begin{smallmatrix} 1 & 0 \\ 0 & 1 \end{smallmatrix}\right).$$

We extend it to all of TG via left translations, in other words:

$$u, v \in T_g G, \ \langle u, v \rangle_g = \langle dL_{g^{-1}} u, dL_{g^{-1}} v \rangle_e.$$

Therefore the metric on $T_{(a,b)}$ is $g = \left(\begin{smallmatrix} 1/a^2 & 0 \\ 0 & 1/a^2 \end{smallmatrix}\right)$ (see Subsection 1.2.3 for the expression for dL_g).

The self-adjoint, symmetric, positive definite operator $L : \mathfrak{g} \to \mathfrak{g}^*$ in our case is $L = \left(\begin{smallmatrix} 1 & 0 \\ 0 & 1 \end{smallmatrix}\right)$. It defines an inner product on $\mathfrak{g}$: $\forall u, v \in \mathfrak{g}$, $\langle u, v \rangle = (Lu, v) = (Lv, u)$, where round braces indicate the canonical pairing of a functional from $\mathfrak{g}^*$ and an element from $\mathfrak{g}$.

Now we derive the expression for the ad_v^* map. It is defined as following: $\langle u, \text{ad}_v w \rangle =$

$(Lu, \mathrm{ad}_v w) = (\mathrm{ad}_v^* Lu, w)$. In our case the left-hand side becomes

$$\langle \begin{pmatrix} u_1 \\ u_2 \end{pmatrix}, \begin{pmatrix} 0 \\ v_1 w_2 - v_2 w_1 \end{pmatrix} \rangle = u_2 v_1 w_2 - u_2 v_2 w_1$$
$$= (\mathrm{ad}_v^* u, w).$$

Therefore $\mathrm{ad}_v^* u = \begin{pmatrix} -u_2 v_2 \\ u_2 v_1 \end{pmatrix}$.

The velocity $u(t) = dL_{g(t)^{-1}} \dot{g}(t)$ is translated back to the tangent space at identity, i.e. it lies in the Lie algebra $\mathfrak{g}$. Since $g(t)^{-1} = \left(\frac{1}{a(t)}, -\frac{b(t)}{a(t)}\right)^T$ the expression for the velocity is $u(t) = \left(\frac{\dot{a}(t)}{a(t)}, \frac{\dot{b}(t)}{a(t)}\right)^T$.

According to Arnold's theorem, $t \mapsto g(t)$ is a geodesic on G if and only if:

$$Lu_t = \mathrm{ad}_u^*(Lu).$$

Putting everything together:

$$u(t) = \begin{pmatrix} \frac{\dot{a}(t)}{a(t)} \\ \frac{\dot{b}(t)}{a(t)} \end{pmatrix}, \ Lu(t) = \begin{pmatrix} \frac{\dot{a}(t)}{a(t)} \\ \frac{\dot{b}(t)}{a(t)} \end{pmatrix}, \ \mathrm{ad}_v^* u = \begin{pmatrix} -u_2 v_2 \\ u_2 v_1 \end{pmatrix}.$$

The geodesic equation becomes:

$$\begin{pmatrix} \frac{\dot{a}(t)}{a(t)} \\ \frac{\dot{b}(t)}{a(t)} \end{pmatrix}^{\cdot} = \begin{pmatrix} -u_2(t)^2 \\ u_1(t) u_2(t) \end{pmatrix}$$
$$= \begin{pmatrix} -\frac{\dot{b}(t)^2}{a(t)^2} \\ \frac{\dot{a}(t)\dot{b}(t)}{a(t)^2} \end{pmatrix}.$$

Taking the derivative on the left-hand side:

$$\begin{cases} \dfrac{\ddot{a}(t)a(t)-\dot{a}(t)^2}{a(t)^2} = -\dfrac{\dot{b}(t)^2}{a(t)^2}, \\ \dfrac{\ddot{b}(t)a(t)-\dot{a}(t)\dot{b}(t)}{a(t)^2} = \dfrac{\dot{a}(t)\dot{b}(t)}{a(t)^2}; \end{cases} \Leftrightarrow \begin{cases} \ddot{a} = \dfrac{1}{a}\left(\dot{a}^2 - \dot{b}^2\right), \\ \ddot{b} = \dfrac{2\dot{a}\dot{b}}{a}. \end{cases}$$

This is exactly the geodesic equation for the Poincaré half-plane model. The geodesics here are straight lines $b = \text{const}$, and circles with centers on the line $a = 0$.

2.1.1 Variation of energy

The EPDiff can also be derived (as in the 1998 Insitut Henri Poincaré notes to be published in [MD10]) via the first variation of energy $E(\psi)$ of the path $\psi(x,t) \in$ $\mathbf{Diff}(\mathbb{R}^n)$:

$$E(\psi) = \int_0^1 \left\| \frac{\partial \psi}{\partial t}(\psi^{-1}(x,t),t) \right\|_L^2 dt,$$

where $\left\| \frac{\partial \psi}{\partial t}(\psi^{-1}(x,t),t) \right\|_L$ is the right-invariant metric, given by the symmetric operator L: $\langle u, v \rangle = \int_{\mathbb{R}^n} Lu.vdx = \int_{\mathbb{R}^n} Lv.udx$, for $u, v \in \mathbf{Vec}(\mathbb{R}^n)$.

In our case consider a fingerprint $\psi(x,t) \in \mathbf{Diff}(S^1)$ (for now we do not consider the quotient space, which will be addressed later in the chapter). What is $\frac{\delta E}{\delta \psi}$? If we vary $\psi \rightsquigarrow \psi + \varepsilon\delta\psi$, the energy varies too $E \rightsquigarrow E + \varepsilon\delta E$. Energy has the form

$$E = \int\int Lv \cdot v d\theta dt,$$

where $v(\theta,t) = \psi_t(\psi^{-1}(\theta,t),t) = \psi_t \circ \psi^{-1}$.

First, we compute the variation of the velocity δv

$$\begin{aligned} v &\rightsquigarrow (\psi_t + \varepsilon\delta\psi_t) \circ (\psi + \varepsilon\delta\psi)^{-1}, \\ (\psi + \varepsilon\delta\psi)^{-1} &= [(I + \varepsilon\delta\psi \circ \psi^{-1}) \circ \psi]^{-1} \\ &= \psi^{-1} \circ (I + \varepsilon\delta\psi \circ \psi^{-1})^{-1} \\ &= \psi^{-1} \circ (I - \varepsilon\delta\psi \circ \psi^{-1}). \end{aligned}$$

Now composing $\psi_t + \varepsilon\delta\psi_t$ with $\psi^{-1} \circ (I - \varepsilon\delta\psi \circ \psi^{-1})$ and disregarding terms with ε^2 and higher:

$$\begin{aligned} v + \varepsilon\delta v &= (\psi_t + \varepsilon\delta\psi_t) \circ \psi^{-1} \circ (I - \varepsilon\delta\psi \circ \psi^{-1}) \\ &= \psi_t \circ \psi^{-1} \circ (I - \varepsilon\delta\psi \circ \psi^{-1}) + \varepsilon\delta\psi_t \circ \psi^{-1} \circ (I - \varepsilon\delta\psi \circ \psi^{-1}) \\ &= \psi_t \circ \psi^{-1} - \varepsilon(\psi_t \circ \psi^{-1})_\theta \cdot \delta\psi \circ \psi^{-1} + \varepsilon\delta\psi_t \circ \psi^{-1} \\ &= \psi_t \circ \psi^{-1} + \varepsilon(\delta\psi_t \circ \psi^{-1} - v_\theta \cdot \delta\psi \circ \psi^{-1}). \end{aligned}$$

Therefore

$$\delta v = \delta\psi_t \circ \psi^{-1} - v_\theta \cdot \delta\psi \circ \psi^{-1}.$$

Finally we have

$$\delta E = 2 \int \int Lv \cdot [\delta\psi_t \circ \psi^{-1} - v_\theta \cdot \delta\psi \circ \psi^{-1}] d\theta dt.$$

We need to simplify the above variation further. First, let us compute the full derivative $\frac{d}{dt}(\delta\psi \circ \psi^{-1})$ using the fact that $\psi_t^{-1} = -v\psi_\theta^{-1}$:

$$\begin{aligned} \frac{d}{dt}(\delta\psi \circ \psi^{-1}) &= \delta\psi_t \circ \psi^{-1} + \delta\psi_\theta \circ \psi^{-1} \cdot \psi_t^{-1} \\ &= \delta\psi_t \circ \psi^{-1} - \delta\psi_\theta \circ \psi^{-1} \cdot v \cdot \psi_\theta^{-1} \\ &= \delta\psi_t \circ \psi^{-1} - v \cdot (\delta\psi \circ \psi^{-1})_\theta. \end{aligned}$$

Therefore

$$\begin{aligned}\delta v &= \delta\psi_t \circ \psi^{-1} - v_\theta \cdot \delta\psi \circ \psi^{-1} \\ &= (\delta\psi \circ \psi^{-1})_t + v \cdot (\delta\psi \circ \psi^{-1})_\theta - v_\theta \cdot \delta\psi \circ \psi^{-1}.\end{aligned}$$

Finally by applying integration by parts, the variation of energy E becomes:

$$\begin{aligned}\delta E &= 2\int\int Lv \cdot \delta v \; d\theta dt \\ &= 2\int\int Lv[(\delta\psi \circ \psi^{-1})_t + v \cdot (\delta\psi \circ \psi^{-1})_\theta - v_\theta \cdot \delta\psi \circ \psi^{-1}] d\theta dt \\ &= 2\int\int [-(Lv)_t - (Lv \cdot v)_\theta - Lv \cdot v_\theta]\delta\psi \circ \psi^{-1} d\theta dt \\ &= -2\int\int [(Lv)_t + 2Lv \cdot v_\theta + Lv_\theta \cdot v]\delta\psi \circ \psi^{-1} d\theta dt.\end{aligned}$$

Therefore another formula for the variation of the WP energy E has the form:

$$\delta E = -2\int\int [(Lv)_t + 2Lv \cdot v_\theta + Lv_\theta \cdot v]\delta\psi \circ \psi^{-1} d\theta dt.$$

Since the variation $\delta\psi$ of the path is arbitrary, we can conclude that the geodesic equation, i.e. the evolution equation for the fingerprint, should be

$$(Lv)_t + 2Lv \cdot v_\theta + Lv_\theta \cdot v = 0,$$

where $v(\theta, t) = \psi_t \circ \psi^{-1}$.

2.1.2 Case of a quotient group

What we have derived in the previous subsection is a geodesic equation on the quotient group $\mathrm{PSL}_2(\mathbb{R})\backslash\mathbf{Diff}(S^1)$. It is a special case of the generalized Theorem 2. In this general case, we have a homogeneous space $H\backslash G$. Fortunately, Arnold's formula for geodesics on groups extends with only small changes to equations for geodesics on homogeneous spaces $H\backslash G$:

Theorem 3. *Let G be any Lie group and H a subgroup. Let $\langle v_1, v_2\rangle_L = (L(v_1), v_2)$ be a non-negative symmetric inner product on $\mathfrak{g}$ with null space $\mathfrak{h}$, defined by a non-negative symmetric linear map $L : \mathfrak{g} \to \mathfrak{g}^*$. Assume this inner product is invariant under Ad_h, $h \in H$. As explained in the Introduction, this defines a G-invariant metric on $H\backslash G$. Let $g(t)$ be any path in G and define $u(t) = g_t \cdot g^{-1}$ to be its tangent path in $\mathfrak{g}$. Then:*

$$\{H \cdot g(t)\} \subset H\backslash G \text{ is a geodesic } \Longleftrightarrow Lu_t = -\mathrm{ad}^*_u(Lu) \text{ in } \mathfrak{g}^*$$

where $\mathrm{ad}^*_u : \mathfrak{g}^* \to \mathfrak{g}^*$ *is the adjoint of* $\mathrm{ad}_u, u \in \mathfrak{g}$.

Remark. As mentioned before, the theorem holds in case of the left-invariant metric, the evolution equation becomes $Lu_t = \mathrm{ad}^*_u(Lu)$.

Proof. Denote by $\overline{g}(t)$ any path in $H\backslash G$. Let us take any lift of $\overline{g}(t)$ to the Lie group G, and define a velocity $v(t)$ of this path in the Lie algebra $\mathfrak{g}$: $v(t) = DR_{g^{-1}}(\dot{g}(t))$. The energy of the path $\overline{g}(t)$ is defined as

$$E(\overline{g}(t)) = \int_0^1 \int_{S^1} Lv.vd\theta dt. \tag{2.1}$$

This energy does not depend on the choice of the lift $g(t)$. To be specific, let $A(t)\cdot g(t)$ be another lift, where $A(t) \in H$. This lift has a time varying action from the left by members of the subgroup H. Then the velocity $\tilde{v}(t) = DR_{\left[A\cdot g(t)\right]^{-1}}\left[A \cdot g(t)\right]^{\cdot}$ of this lift will be:

$$\begin{aligned}
\big[A \cdot g(t)\big]^{\cdot} &= A_t \cdot g(t) + A_\theta \cdot g(t).g_t, \\
\big[A \cdot g(t)\big]^{-1} &= g^{-1} \cdot A^{-1}(t), \\
\tilde{v}(t) &= A_t \cdot g \cdot g^{-1} \cdot A^{-1} + [A_\theta \cdot g \cdot g^{-1} \cdot A^{-1}].[g_t \cdot g^{-1} \cdot A^{-1}] \\
&= A_t \cdot A^{-1} + [A_\theta \cdot A^{-1}].[g_t \cdot g^{-1} \cdot A^{-1}] \\
&= A_t \cdot A^{-1} + [A_\theta \cdot A^{-1}].[v \cdot A^{-1}] \\
&= A_t \cdot A^{-1} + \mathrm{Ad}_A v.
\end{aligned}$$

Therefore, since $A_t \cdot A^{-1} \in \mathfrak{h}$ and the metric is Ad-invariant under the action of the subgroup H, we have $\|\tilde{v}(t)\|_L = \|v(t)\|_L$. In other words, the energy (2.1) is independent of the choice of the lift $g(t)$.

Choose a perturbation $\delta g(t)$ of the path $g(t)$. The perturbed path is $\tilde{g}(t) = \delta g \cdot g$, where infinitesimally $\delta g = Id + \delta v$. The velocity of the perturbed path becomes:

$$\begin{aligned}
(\delta g \cdot g)^{\cdot} \cdot (g^{-1} \cdot \delta g^{-1}) &= \delta \dot{g} \cdot g \cdot g^{-1} \cdot \delta g^{-1} + \delta g \cdot \dot{g} \cdot g^{-1} \cdot \delta g^{-1} \\
&= \delta \dot{v} \cdot \delta g^{-1} + \delta g \cdot v \cdot \delta g^{-1} \text{ (upto the first order)} \\
&= v + \delta \dot{v} + \delta v \cdot v - v \cdot \delta v \\
&= v + \delta \dot{v} - \mathrm{ad}_v \delta v.
\end{aligned}$$

Therefore, the velocity $\tilde{v}$ of the perturbed path is $\tilde{v} = v + \delta\dot{v} - \mathrm{ad}_v \delta v$. The energy of the perturbed path becomes (upto the terms of the second order):

$$
\begin{aligned}
E(\tilde{g}) &= \|\tilde{v}\|_L^2 \\
&= \|v + \delta\dot{v} - \mathrm{ad}_v \delta v\|_L^2 \\
&= \|v\|^2 + 2\langle v, \delta\dot{v} - \mathrm{ad}_v \delta v\rangle_L \\
&= \|v\|^2 + 2\big(Lv, \delta\dot{v} - \mathrm{ad}_v \delta v\big) \\
&= \|v\|^2 - 2\big((Lv)^{\cdot} + \mathrm{ad}_v^* Lv, \delta v) \text{ (using integration by parts)} \\
&= E(g) + \delta E.
\end{aligned}
$$

From the above we derive the familiar EPDiff equation, $(Lv)_t + \mathrm{ad}_v^* Lv = 0$. □

2.1.3 Quotient group $\mathrm{PSL}_2(\mathbb{R})\backslash\mathbf{Diff}(S^1)$

This applies to our case of $\mathrm{PSL}_2(\mathbb{R})\backslash\mathbf{Diff}(S^1)$. On the Lie algebra level, $\mathrm{PSL}_2(\mathbb{R})$ becomes the vector fields spanned by 1, cos and sin, i.e. those whose only non-zero Fourier coefficients are those with indices $-1, 0, +1$. The simplest complement W are the vector fields with these coefficients zero. The geodesic equation is therefore simply another special case of EPDiff. Given a path $\psi(\theta, t)$ in $\mathbf{Diff}(S^1)$, let $v(\theta, t) = \frac{\partial\psi}{\partial t}(\psi^{-1}(\theta, t), t)$ be the scalar vector field it defines on a circle and let L be the Weil-Petersson differential operator $L = -\mathcal{H}(\partial_\theta^3 + \partial_\theta)$. Then EPDiff takes the form

$$(Lv)_t + v.(Lv)_\theta + 2v_\theta.Lv = 0. \tag{2.2}$$

2.2 Conserved quantities

In this section we will demonstrate the conserved quantities of the EPDiff(S^1), namely the energy and momenta. The EPDiff is given by the following formula:

$$m_t + 2m.v_\theta + m_\theta.v = 0, \quad m = Lv, \quad v = G * m.$$

Quantities $v(\theta)$ and $m(\theta)$ are called velocity and momenta respectively.

Energy

Momentum and energy conservation for the EPDiff readily follow from the Noether's theorem and the fact that the action (this is just energy), associated to the path $g(\theta, t)$:

$$E(g) = \int_0^1 \|v\|_{WP}^2 dt$$

is invariant under the time translation and right translation. Here $v = g_t \circ g^{-1}$.

Specifically since E does not depend on time t, hence it is invariant under the transformation $t \mapsto t' = t + \tau$. This time symmetry, according to Noether's, theorem yields the conservation of energy, in other words:

$$\|v\|_{WP}^2 = \text{const}.$$

Momentum

In general, for the geodesic equation on $\mathbf{Diff}(\mathbb{R}^n)$, to derive conservation of momentum we can rewrite EPDiff($\mathbb{R}^n$) as:

$$\frac{d}{dt}(m \cdot dx \otimes dV) = 0, \text{ along the path } \frac{dx}{dt} = v = G * m.$$

The above expression is a conservation law of a one-form density of momentum along the path $dx/dt = v$. It is an integrated version of the original EPDiff($\mathbb{R}^n$). We can check this by taking the derivative and we will get the EPDiff($\mathbb{R}^n$) back:

$$
\begin{aligned}
\frac{d}{dt}(m \cdot dx \otimes dV) &= \frac{d}{dt}m \cdot dx \otimes dV + m \cdot d\frac{dx}{dt} \otimes dV + m \cdot dx \otimes \frac{d}{dt}dV \\
&= \left(\frac{\partial}{\partial t}m + v \cdot \nabla m + \nabla v^T \cdot m + m(\mathrm{div} v)\right) \cdot dx \otimes dV.
\end{aligned}
$$

Therefore, the quantity $m \cdot dx \otimes dV$ is constant along the trajectories $dx/dt = v$.

In case of a geodesic path $g(t) \in \mathbf{Diff}(S^1)$ with right-invariant metric, Noether's theorem implies that the momentum carried back by the pullback of left translations is conserved:

$$
\begin{aligned}
(DL_g)^*(L\dot{g}) &= \text{const, or equivalently,} \\
\mathrm{Ad}_g^\dagger v &= \text{const, where } v = \dot{g} \circ g^{-1}.
\end{aligned}
$$

where $(DL_g)^*$ is the pullback of the left translation L_g by the element g, and $\mathrm{Ad}_g^\dagger$ is the transpose of the Adjoint map defined by: $\langle u, \mathrm{Ad}_g^\dagger v\rangle = \langle \mathrm{Ad}_g u, v\rangle$. Since $(DL_g)^*(L\dot{g}) \in \mathfrak{g}^*$ we need to pair it with a vector from $\mathfrak{g}$. Now we will show that two expressions above are indeed equivalent:

$$
\begin{aligned}
(DL_g^*(L\dot{g}), X) &= (L\dot{g}, DL_g X) \\
&= \langle \dot{g}, DL_g X\rangle_g \\
&= \langle DR_{g^{-1}}\dot{g}, DR_{g^{-1}} DL_g X\rangle_e \quad \text{(right-invariance)} \\
&= \langle v, \mathrm{Ad}_g X\rangle_e \quad \text{(definition of Ad)} \\
&= \langle \mathrm{Ad}_g^\dagger v, X\rangle_e.
\end{aligned}
$$

Remark. In the case of the left-invariant metric, the conservation of momentum takes the form: $(DR_{g(t)})^* L\dot{g}(t) = \text{const}$ or, equivalently, $\mathrm{Ad}^\dagger_{g^{-1}(t)} v(t) = \text{const}$.

Now we compute the projection of the conserved momenta $\mathrm{Ad}_g^\dagger v$ onto any $X(\theta) \in \mathbf{Vec}(S^1)$:

$$\begin{aligned}\langle \mathrm{Ad}_g^\dagger v, X\rangle_e &= \langle v, \mathrm{Ad}_g X\rangle_e \\ &= \langle DR_{g^{-1}}\dot{g}, DR_{g^{-1}}DL_g X\rangle_e \\ &= \langle \dot{g}\circ g^{-1}, (g_\theta \circ g^{-1}).(X\circ g^{-1})\rangle_e \\ &= \int L(\dot{g}\circ g^{-1}).(g_\theta\circ g^{-1}).(X\circ g^{-1})d\theta \\ &= \int_{S^1} m\circ g(\theta).g_\theta^2.X.d\theta.\end{aligned}$$

Therefore the conservation of momentum states, that for any $X \in \mathbf{Vec}(S^1)$, i.e. any smooth function $X(\theta)$ on the circle S^1 the following quantity is conserved along the geodesic $g(t) \in \mathbf{Diff}(S^1)$:

$$\boxed{\int_{S^1} m\circ g(\theta).g_\theta^2.X.d\theta = \mathrm{const.}} \tag{2.3}$$

For any smooth $X(\theta) \in \mathbf{Vec}(S^1)$ we get the above conservation law. Thus we have infinitely many conserved quantities. But they all represent the projection of momentum onto X, so in fact we have just one conserved momentum. The fact that it is conserved is expressed by the conservation of its 'coordinates', i.e. projections on X.

In general for the EPDiff equation on the Lie group $\mathbf{Diff}(\mathbb{R}^n)$ with the right-invariant metric the conserved quantity is:

$$g(t)^*\omega(t) = \mathrm{const},$$

Here ω is a measure-valued differential 1-form:

$$\omega(t) = (m_1.dx^1 + \ldots + m_n.dx^n)\otimes dV,$$

where $dV = dx^1 \wedge dx^2 \wedge \ldots \wedge dx^n$, is the volume form on R^n, $m = Lv = L(\dot{g} \circ g^{-1})$ is the momenta. Coordinate expression in case of $\mathbf{Diff}(\mathbb{R}^n)$:

$$g(t)^* \omega(t) = \det(Dg(t)).\langle Dg(t)^t.(m \circ g(t)), dx \rangle \otimes dV. \tag{2.4}$$

Determinant $\det(Dg(t))$ corresponds to the change of the volume form dV under the flow $g(t)$, $Dg(t)^t.(m \circ g(t))$ is the pullback of $m.dx$.

In the case of $\mathbf{Diff}(S^1)$ quantities $\det(Dg(t))$ and $Dg(t)^t$ both give $g_\theta(t)$. Volume form dV and dx will both give $d\theta$. Therefore our expression (2.3) is in line with the general expression (2.4) for $\mathbf{Diff}(\mathbb{R}^n)$.

In Chapter 3, Section 3.5 we will demonstrate how these conserved quantities are expressed in the case of Teichons, singular solutions to the EPDiff(S^1). We will also show how well the numerical scheme preserves the energy and the momenta.

Chapter 3

Teichons

In this chapter we study the singular solutions of the EPDiff(S^1). The EPDiff(S^1) admits a class of soliton like solutions (we will call them Teichons) in which the "momentum" m is a distribution. In this chapter we study closely the solution in the special case where m is expressed as a sum of four delta functions. We prove the existence of the solution for infinite time and find bounds on its longterm behavior. We then show a series of numerical experiments on Teichons with more delta functions and argue that this is can be one of the ways of finding geodesics in the space of 2D shapes. This Chapter is larger following the paper [Ku09].

3.1 Introduction

As we mentioned in Chapter 2 periodic Korteweg-deVries equation (KdV) for a function $u(\theta, t)$:

$$u_t = -3u.u_\theta - u_{\theta\theta\theta}$$

and the periodic Camassa-Holm equation or C-H (see [CH93])

$$m_t = -2m.u_\theta - u.m_\theta - u_{\theta\theta\theta}, \text{ where } m = u - u_{\theta\theta}$$

are examples of an EPDiff on the Virasoro group (a central extension by S^1 of the group $\mathbf{Diff}(S^1)$) with L^2 and H^1 metrics respectively. These are two completely integrable partial differential equations and have soliton solutions. More recently, Holm and collaborators have found that quite generally the geodesic equation on $\mathbf{Diff}(\mathbf{R}^n)$ admits special solutions with many of the properties of solitons: for each fixed time, they are diffeomorphisms which are largely localized in space and, as time varies, they retain their general shape and can interact somewhat like solitons for KdV [HM04]. There are not, however, infinitely many conserved quantities so they are not true solitons. A discussion of EPDiff and solitons in the case of template matching in computational anatomy can be found in [Ho04].

In this chapter we study a new example of singular solutions closely related to KdV and C-H. We consider the geodesic equation on the group $\mathrm{PSL}_2(\mathbb{R})\backslash\mathbf{Diff}(S^1)$ with the Weil-Petersson metric. As in Chapter 2 the equation is:

$$m_t = -2m.u_\theta - u.m_\theta, \text{ where } m = -\mathcal{H}(u_\theta + u_{\theta\theta\theta}). \tag{3.1}$$

This is an integro-differential equation with the Hilbert transform operator $\mathcal{H}$, defined by the convolution with $\frac{1}{2\pi}\cot(\theta/2)$.

Here, we may invert the relationship between m and u and write:

$$u(\theta, t) = \int_{S^1} G(\theta - \xi) m(\xi, t) d\xi = G * m.$$

The integral kernel, or Green's function, $G(\theta)$ is given in the Fourier domain by

$$G(\theta) = 2\sum_{n=2}^{\infty} \frac{\cos(n\theta)}{(n^3 - n)}.$$

Note that $m(\cdot, t)$ is always orthogonal to 1, cos and sin.

It is not known if this new equation is completely integrable but it admits a class of soliton like solutions which we study here, namely the solutions in which m is a distribution. In fact, we want $m(\cdot, t)$ to be a weighted sum of delta functions for one and hence all t. Because m is orthogonal to 1, cos and sin, there must be at least 4 delta functions. Following a suggestion of Darryl Holm, we call these and their corresponding geodesics in Teichmüller space *Teichons*.

In general, solutions to the above equation integrate to geodesics on the universal Teichmüller space $\mathrm{PSL}_2(\mathbb{R})\backslash\mathbf{Diff}(S^1)$. As we have explained in Chapter 1, the universal Teichmüller space has another realization, namely as the space of smooth simple closed curves mod translations and scalings. Therefore the solutions of this equation can also be thought of as paths in the space of simple closed plane curves which minimize a certain energy. The soliton property means that, in a certain sense, their momentum is concentrated at a finite set of points.

Below we study the solution in the special case where the momentum m is expressed as a sum of four delta functions. We prove the existence of the solution for infinite time and find bounds on its longterm behavior.

3.2 Setup

We call $v(\theta, t)$ the velocity of the path and $m(\theta, t) = Lv(\theta, t)$ the momentum. Then inversely $v(\theta, t) = G * m(\theta, t)$. Note that momenta can be distributions. Both m and v will have vanishing $-1, 0, +1$ Fourier coefficients. We consider an ansatz, a special form of momentum which we call a Teichon (or an N-Teichon), given by a sum of N delta-functions, i.e.

$$\begin{aligned} m(\theta,t) &= \sum_{j=1}^{N} a_j \delta(\theta - b_j), \\ v(\theta,t) &= \sum_{j=1}^{N} a_j G(\theta - b_j). \end{aligned}$$

Plugging this expressions into the EPDiff (3.1) we get a system of ODEs describing the evolution of a_k's and b_k's:

$$\begin{cases} \dot{a}_k = -a_k \sum_{j=1}^{N} a_j G'(b_k - b_j), \\ \dot{b}_k = \sum_{j=1}^{N} a_j G(b_k - b_j). \end{cases} \tag{3.2}$$

where a_j, b_j are functions of time t. For well-posedness of the problem, $m(\theta, t)$ should have its 0th, $\pm$1st Fourier coefficients zero, i.e. we have the following constraints:

$$\sum_{j=1}^{N} a_j = \sum_{j=1}^{N} a_j e^{ib_j} = \sum_{j=1}^{N} a_j e^{-ib_j} = 0. \tag{3.3}$$

If they are satisfied at time $t = 0$ they will be satisfied for all t.

What is the minimal number N, such that momenta m will lie in the splitting, i.e. three relations (3.3) should hold.

- $N = 1$. In this case $\hat{m}_k = e^{ik(\theta - b_k)}$, obviously does not work.

- $N = 2$. Then we have $a_1 = -a_2$, and from the relation $a_1 e^{ib_1} + a_2 e^{ib_2} = 0$ we deduce that $b_1 = b_2$. Therefore two Teichons are not enough.

- $N = 3$. In this case the above conditions are equivalent to

$$\det \begin{pmatrix} 1 & 1 & 1 \\ \cos b_1 & \cos b_2 & \cos b_3 \\ \sin b_1 & \sin b_2 & \sin b_3 \end{pmatrix} = 0.$$

  This is impossible for distinct b_k's.

- $N = 4$. This is the minimal number of Teichons, such that $m(\theta)$ lies in the splitting. For example, choose $(a_1, a_2, a_3, a_4) = (1, -1, 1, -1)$ and $b_k = \frac{\pi(k-1)}{2}, k = 1, \ldots, 4$.

Note that EPDiff is invariant under the action $\mathrm{Ad}_A, A \in \mathrm{PSL}_2$, so we may always normalize Teichons by the Möbius group.

3.3 Estimates

3.3.1 4-Teichon ODE

Recall that operator $L : T_e(H\backslash G) \to T_e(H\backslash G)^*$ is bijective (and hence invertible), if we choose momentum m to be in the horizontal splitting, which is a space, orthogonal to the $psl_2(\mathbb{R})$ Lie algebra. In other words the Fourier coefficients of the momenta $\hat{m}_k$ are zero for $k = 0, \pm 1$.

Therefore we consider the case of $N = 4$ deltas:

$$m(\theta) = \sum_{k=1}^{4} a_k \delta(\theta - b_k).$$

Due to the Möbius invariance, we can normalize the initial conditions giving us the following initial configuration for momentum $m(\theta)$:

$$m(\theta, t=0) = \sum_{j=1}^{4} a_j \delta(\theta - b_j), \text{ where}$$

$$(a_1, a_2, a_3, a_4) = (a_0, -a_0, a_0, -a_0),$$
$$(b_1, b_2, b_3, b_4) = (2\pi - \tfrac{d_0}{2}, \tfrac{d_0}{2}, \pi - \tfrac{d_0}{2}, \pi + \tfrac{d_0}{2}),$$
$$a_0 = 1, \ d_0 \in (0, \epsilon).$$

If this holds for time 0, then it is easy to check that for all times t

$$\begin{aligned}(a_1, a_2, a_3, a_4) &= (a(t), -a(t), a(t), -a(t)), \\ (b_1, b_2, b_3, b_4) &= \left(2\pi - \frac{d(t)}{2}, \frac{d(t)}{2}, \pi - \frac{d(t)}{2}, \pi + \frac{d(t)}{2}\right).\end{aligned}$$

for some functions $a(t), d(t)$. Then the system (3.2) becomes a system of just two variables $a(t)$ and $d(t)$

$$\begin{aligned}\dot{a} &= a^2[G'(-d) + G'(\pi - d)], \\ \dot{d} &= -2a[G(0) - G(-d) + G(\pi) - G(\pi - d)].\end{aligned}$$

Equivalently, if $E(d)$ denotes $G(0) - G(-d) + G(\pi) - G(\pi - d)$ and prime is the differentiation in d, then the system is:

$$\begin{aligned}\dot{a} &= a^2 E'(d), \\ \dot{d} &= -2aE(d).\end{aligned} \tag{3.4}$$

Notice that (3.4) is a Hamiltonian system with the conserved energy $H = a^2 E(d) = k^2$, for some constant k. Therefore we can have the equation just in terms of d

$$\dot{d} = -2k\sqrt{E(d)}, \text{ where } k = a_0\sqrt{E(d_0)}. \tag{3.5}$$

The other equation is a conserved quantity, which relates $a(t)$ and $d(t)$:

$$a(t)\sqrt{E(d(t))} = k.$$

Geodesic in the universal Teichmüller space with the above initial momentum $m(\theta)$ could be seen on Figure 3.1 (evolution of $\log|a_k|$'s and b_k's is shown on Figure 3.2).

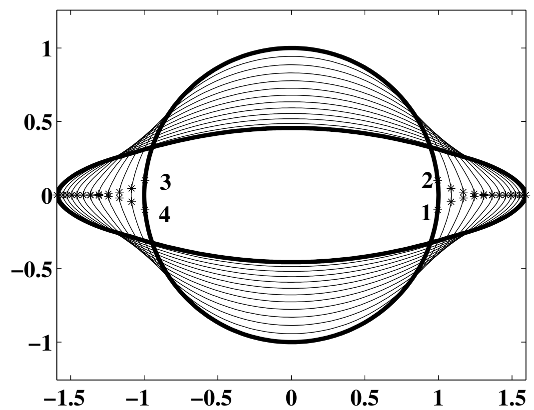

Figure 3.1: Geodesic with initial momentum $m(\theta) = \sum_{k=1}^{4} a_k \delta(\theta - b_k)$ upto time T=6, $(a_{k=1}^4)_{t=0} = (1, -1, 1, -1), (b_{k=1}^4)_{t=0} = (2\pi - 0.1, 0.1, \pi - 0.1, \pi + 0.1)$. Position of delta functions (i.e. b_k's) is marked by asterisks.

3.3.2 Estimates of $a(t)$, $d(t)$

For small $d \in (0, \epsilon)$ we have an expansion of $E(d) = G(0) - G(-d) + G(\pi) - G(\pi - d)$:

$$E(d) = d^2 \left(\frac{1}{2} - \log \frac{d}{2} \right) - d^4 \left(\frac{3}{48} - \frac{1}{12} \log \frac{d}{2} \right) + O(d^6 \log d).$$

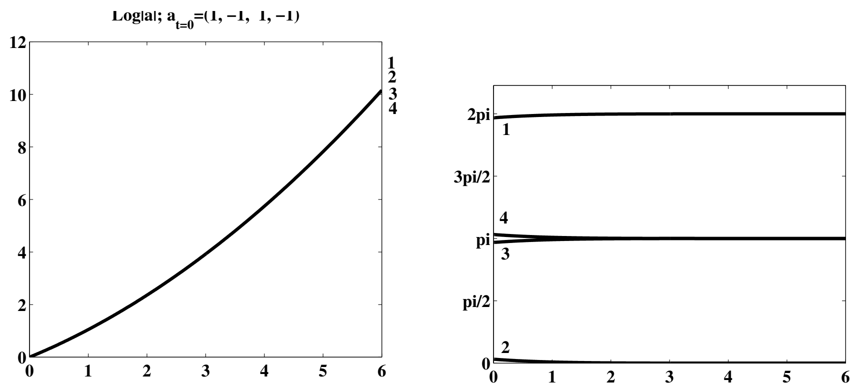

Figure 3.2: Time evolution of $\log|a_k|$'s (left) and b_k's (right) for the 4-Teichon: $(a^4_{k=1})_{t=0} = (1, -1, 1, -1), (b^4_{k=1})_{t=0} = (2\pi - 0.1, 0.1, \pi - 0.1, \pi + 0.1)$.

And the basic inequality is

$$d^2\left(\frac{1}{2} - \log\frac{d}{2} - \gamma\right) \leq E(d) \leq d^2\left(\frac{1}{2} - \log\frac{d}{2}\right). \tag{3.6}$$

Here γ is chosen to guarantee that $-\gamma d^2 \leq E(d) - d^2\left(\frac{1}{2} - \log\frac{d}{2}\right)$, or in other words $\gamma \geq -E(d)/d^2 + \left(\frac{1}{2} - \log\frac{d}{2}\right)$. Since the RHS is an increasing function of d, and $d(t)$ will be decreasing with t it suffices to take any $\gamma \geq -E(d_0)/d_0^2 + \left(\frac{1}{2} - \log\frac{d_0}{2}\right)$ (in simulations the value used was $d_0 = .2$, hence we may take $\gamma = .0102$).

Based on this we get the following inequalities for the RHS of the equation (3.5):

$$-2kd\sqrt{\frac{1}{2} - \log\frac{d}{2}} \leq -2k\sqrt{E(d)} \leq -2kd\sqrt{\frac{1}{2} - \log\frac{d}{2} - \gamma}. \tag{3.7}$$

From the theory of ODEs we can conclude that for all $t \in [0, +\infty)$ if $d_0 \in (0, \epsilon)$ $(d(t)$

will stay in $(0, \epsilon)$ for all t), then the following estimate for $d(t)$ is valid:

$$\boxed{\begin{array}{l} 2\exp\left\{\frac{1}{2} - (kt + c_1)^2\right\} \leq d(t) \leq 2\exp\left\{\frac{1}{2} - (kt + c_2)^2 - \gamma\right\}, \\ \\ \text{where } k = a_0\sqrt{E(d_0)} > 0, \\ c_1 = \sqrt{\frac{1}{2} - \log\frac{d_0}{2}}, \\ c_2 = \sqrt{\frac{1}{2} - \log\frac{d_0}{2} - \gamma};\ c_1 > c_2. \end{array}} \tag{3.8}$$

Denote the bounds

$$\begin{aligned} d_1(t) &:= 2\exp\left\{\frac{1}{2} - (kt + c_1)^2\right\}, \\ d_2(t) &:= 2\exp\left\{\frac{1}{2} - (kt + c_2)^2 - \gamma\right\}. \end{aligned} \tag{3.9}$$

Using inequalities (3.6) we get the following estimates:

$$\frac{1}{\sqrt{\frac{1}{2} - \log\frac{d}{2}}} \leq \frac{d}{\sqrt{E(d)}} \leq \frac{1}{\sqrt{\frac{1}{2} - \log\frac{d}{2} - \gamma}}.$$

Combining it with the estimates on $d(t)$ and the fact that both bounds are increasing functions of d we conclude that the product ad decreases as $1/t$, or specifically

$$\begin{gathered} \frac{k}{\sqrt{\frac{1}{2} - \log\frac{d_1}{2}}} \ \leq\ a(t)d(t) = k\frac{d}{\sqrt{E(d)}} \ \leq\ \frac{k}{\sqrt{\frac{1}{2} - \log\frac{d_2}{2} - \gamma}}, \\ \boxed{\frac{k}{kt + c_1} \ \leq\ a(t)d(t) \ \leq\ \frac{k}{kt + c_2}.} \end{gathered} \tag{3.10}$$

Finally an estimate for $a(t)$:

$$\frac{k}{d_2\sqrt{\frac{1}{2}-\log\frac{d_2}{2}}} \;\le\; a(t)=\frac{k}{\sqrt{E(d)}} \;\le\; \frac{k}{d_1\sqrt{\frac{1}{2}-\log\frac{d_1}{2}-\gamma}}, \tag{3.11}$$

$$\boxed{\frac{k\exp\left\{(kt+c_2)^2-\frac{1}{2}+\gamma\right\}}{2\sqrt{(kt+c_2)^2+\gamma}} \;\le\; a(t) \;\le\; \frac{k\exp\left\{(kt+c_1)^2-1/2\right\}}{2\sqrt{(kt+c_1)^2-\gamma}}}.$$

3.3.3 Estimating the velocity field $v(\theta, t)$

For $\theta \in I = [\delta, \pi-\delta]\cup[\pi+\delta, 2\pi-\delta]$ (away from points $0, \pi, 2\pi$, where $G(\theta), G(\theta+\pi)$ are only C^1) we have the following Taylor expansion:

$$G(\theta+\Delta\theta) = G(\theta)+\Delta\theta\, G'(\theta)+\frac{\Delta\theta^2}{2}G''(\theta)+\frac{\Delta\theta^3}{6}G'''(\theta)+\frac{\Delta\theta^4}{24}G^{(iv)}(\theta)+O(\Delta\theta^5).$$

Therefore using the above we have the following expansion of the velocity field $v(\theta, t)$

$$\begin{aligned} v(\theta,t) &= a[G(\theta+d/2)-G(\theta-d/2)+G(\theta+\pi+d/2)-G(\theta+\pi-d/2)] \\ &= ad[G'(\theta)+G'(\theta+\pi)]+ad^3/24[G'''(\theta)+G'''(\theta+\pi)]+O(ad^5). \end{aligned}$$

For derivatives of the Green's function we get

$$\begin{aligned} G'(\theta)+G'(\theta+\pi) &= 2\sin\theta\log|\tan\theta/2|, \\ G'''(\theta)+G'''(\theta+\pi) &= -2\sin\theta\log|\tan\theta/2|+2\cot\theta. \end{aligned}$$

And applying estimates (3.8), (3.10) for ad, ad^3 we finally arrive at

$$\boxed{\begin{array}{l} \textbf{First order approximation:} \\ v(\theta,t) \approx 2\frac{k}{kt+c}\sin\theta\log|\tan\theta/2| + O\left(\frac{1}{te^{2kt^2}}\right), \text{ for some } c. \\ \\ \textbf{Third order approximation:} \\ v(\theta,t) \approx 2\frac{k}{kt+c}\sin\theta\log|\tan\theta/2| \\ +r(t)(\cot\theta - \sin\theta\log|\tan\theta/2|) + O\left(\frac{1}{t\exp(4kt^2)}\right), \\ \text{where } r(t) \text{ s.t. } \frac{k}{3}\frac{\exp(1-2(kt+c_1)^2)}{kt+c_1} \le r(t) \le \frac{k}{3}\frac{\exp(1-2(kt+c_2)^2-2\gamma)}{kt+c_2}. \end{array}} \tag{3.12}$$

Here as before $k = a_0\sqrt{E(d_0)}$, and we can choose c somewhere between c_2 and c_1 ($c_2 = \sqrt{1/2 - \log\frac{d_0}{2} - \gamma} < c_1 = \sqrt{1/2 - \log\frac{d_0}{2}}$).

Remark. Notice that $\|v(\theta,t)\|_{WP}$ should be constant, but in the first order expansion there is a t-term which is monotonically decreasing. It is actually the case that $\sin\theta\log|\tan\theta/2|$ has infinite WP-norm.

3.3.4 Estimating the fingerprint $\psi(\theta,t)$

The fingerprint $\psi(\theta,t)$ evolves under the action of the velocity field $v(\theta,t)$ according to

$$\psi_t(\psi^{-1}(\theta,t),t) = v(\theta,t).$$

Denote $\psi^i(\theta,t)$ the inverse of $\psi(\theta,t)$ in θ-variable for each fixed t-variable, i.e. $\psi^i(\psi(\theta,t),t) = \psi(\psi^i(\theta,t),t) = \theta$. It is easy to check that $\psi^i(\theta,t)$ satisfies the transport equation:

$$\psi^i_t(\theta,t) = -v(\theta,t)\psi^i_\theta(\theta,t). \tag{3.13}$$

Remark. In this case $\psi^i(\theta,t)$ is in the left coset space $\mathbf{Diff}(S^1)/\mathrm{PSL}_2(\mathbb{R})$ and we have the same setup as in [SM06].

We are going to solve the transport equation (3.13) for the inverse fingerprint ψ^i with *first order approximation* of v (3.12).

Note that $G(\theta)$ is smooth, except for the logarithmic pole in $G''(\theta)$ at $\theta = 0$. Let us write out the first order Taylor's series with the remainder term in the integral form:

$$\begin{aligned} G(\theta+\delta) &= G(\theta) + G'(\theta)\delta + R_1(\theta), \\ & \quad \text{where } R_1(\theta) = \int_{\theta}^{\theta+\delta} G''(t)(\theta+\delta-t)dt. \end{aligned}$$

The remainder term $R_1(\theta)$ for all δ's small will be uniformly bounded for all θ away from zero. Employing the fact that $G''(\theta) = \cos\theta\log[2(1-\cos\theta)] + 1/2\cos\theta + 1$ one can easily verify that the remainder term $R_1(\theta)$ at $\theta = 0$:

$$R_1(0) = \int_0^{\delta} G''(t)(\delta - t)dt = \int_0^{\delta} ((2-t^2)\log t + 3/2 + O(t^2))(\delta - t)dt = O(\delta^2\log\delta).$$

Therefore the first order estimate of $v(\theta,t)$ in (3.12) is valid uniformly for all $\theta \in [0, 2\pi]$ and t, while the third order estimate is valid uniformly away from $\theta = 0, \pi$.

From PDE theory it is known that the solution remains constant along the characteristics of the equation (3.13). The characteristic equations are:

$$\begin{cases} \dfrac{\partial\theta}{\partial s} = 2\dfrac{k}{kt+c}\sin\theta\log|\tan\theta/2|, \\ \\ \dfrac{\partial t}{\partial s} = 1. \end{cases}$$

Using the fact that $\int \frac{d\theta}{\sin\theta} = \log|\tan\theta/2|$ we get

$$\frac{\log|\tan(\theta-\pi)/2|}{\log|\tan(\theta_0-\pi)/2|} = \left(\frac{kt+c}{c}\right)^2.$$

Given point (θ, t) a characteristic passes through the point $(\theta_0, 0)$, where θ_0 is expressed using the previous formula, i.e.

$$\theta_0 = 2\arctan\left[(\tan(\theta-\pi)/2)^{\left(\frac{c}{kt+c}\right)^2}\right] + \pi.$$

Since ψ^i stays constant along characteristics and since $\psi^i(\theta, t=0) = \theta$:

$$\begin{aligned}&\psi^i(\theta,t) = \psi^i(\theta_0,0) = \theta_0 = 2\arctan\left[(\tan(\theta-\pi)/2)^{\left(\frac{c}{kt+c}\right)^2}\right] + \pi,\\ &\text{where } \tan^\beta = \text{sign}(\tan)|\tan|^\beta.\end{aligned} \tag{3.14}$$

If we denote $\left(\frac{c}{kt+c}\right)^2 = \beta$, then the above inverse fingerprint is the fingerprint of the 'eye' shape with angles at its corners $\alpha\pi$, $\alpha = 2\beta/(\beta+1)$ (example of the fingerprint on Figure 3.3, see also [SM06]). In other words the curve starts as a circle (angles at the corners of the 'eye' are π) and angle gets smaller with time as $\frac{2\pi}{1+(kt/c+1)^2}$.

Invert expression (3.14) to get the approximate evolution of the fingerprint $\psi \in \mathrm{PSL}_2(\mathbb{R})\backslash\mathbf{Diff}(S^1)$:

$$\boxed{\begin{aligned}&\psi(\theta,t) = 2\arctan\left[(\tan(\theta-\pi)/2)^{\left(\frac{kt+c}{c}\right)^2}\right] + \pi,\\ &\text{where } \tan^\beta = \text{sign}(\tan)|\tan|^\beta.\end{aligned}} \tag{3.15}$$

This fingerprint still defines an eye-shaped figure (see Figure 3.3), one just needs to perform welding using the fact that $\psi = \phi_{\text{int}}^{-1} \circ \phi_{\text{ext}}$.

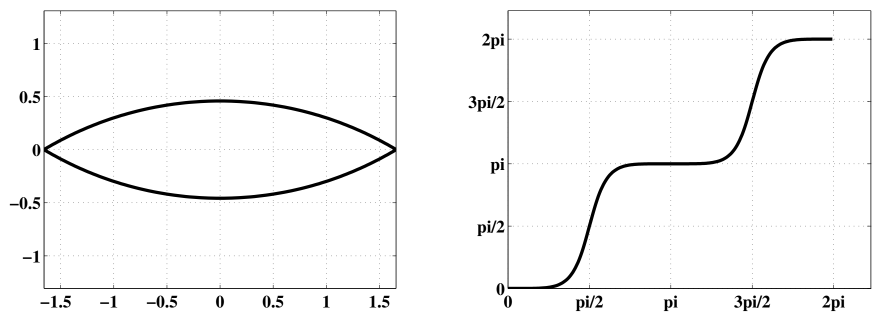

Figure 3.3: Example of the eye-shape and its fingerprint ψ as given by equation (3.14).

The limiting fingerprint is

$$\psi_\infty(\theta) = \begin{cases} \pi/2, \text{ for } \theta \in (0, \pi); \\ 3\pi/2, \text{ for } \theta \in (\pi, 2\pi). \end{cases}$$

We have proved the existence of the solution for infinite time and have found bounds on its longterm behavior. In the limit, the shape represented by the fingerprint (3.15) will become an infinite slit on the plane. Note, that our soliton trajectory is asymptotic to the following one parameter subgroup in $\mathbf{Diff}(S^1)$:

$$\begin{aligned} \psi_\beta(\theta) &= 2 \arctan(\tan(\theta/2)^\beta), \\ &\quad \text{where } \tan^\beta = \text{sign}(\tan)|\tan|^\beta, \\ \psi_{\beta_1\beta_2} &= \psi_{\beta_1} \circ \psi_{\beta_2}. \end{aligned}$$

3.4 Numerical Experiments

3.4.1 Numerical methods

System (3.2) is in fact a Hamiltonian system with Hamiltonian $H_{ab} = \sum_{i,j=1}^{N} a_i a_j G(b_i - b_j)$ and it could be rewritten as

$$\begin{cases} \dot{a}_k = -\dfrac{\partial H_{ab}}{\partial b_k}, \\ \dot{b}_k = \dfrac{\partial H_{ab}}{\partial a_k}. \end{cases} \tag{3.16}$$

That is why it is reasonable to use symplectic methods (i.e. preserving the Hamiltonian H_{ab}) of integration of system (3.2). Also notice on Figure 3.4 how conventional Runge-Kutta method (`ode45` solver in Matlab) fails to conserve the energy.

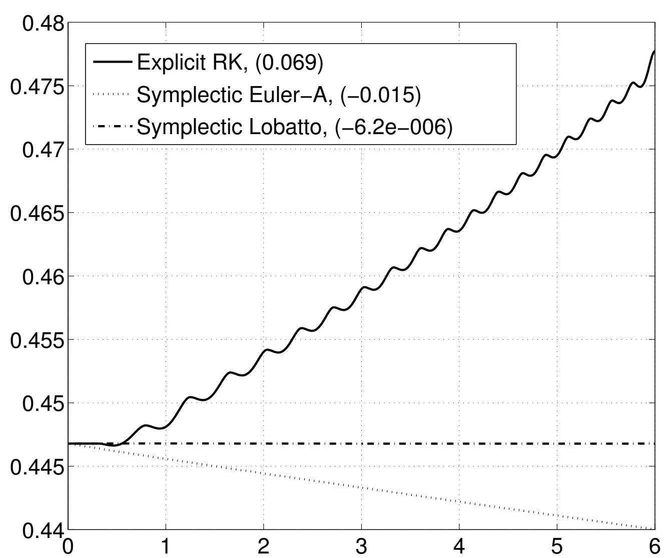

Figure 3.4: Evolution of conserved Hamiltonian H_{ab} in numerical simulations. Case of a 4-Teichon, $\Delta t = .01$, $(a^4_{k=1})_{t=0} = (1, -1, 1, -1), (b^4_{k=1})_{t=0} = (2\pi - 0.1, 0.1, \pi - 0.1, \pi + 0.1)$. Method used, relative change of H_{ab}.

We are going to describe shortly the main definitions behind Euler-A and Lobatto methods (mainly from [Ha02]).

We treat non-autonomous systems of first-order ordinary differential equations

$$\dot{y} = f(t, y), \quad y(t_0) = y_0.$$

Definition. *Let β_i, α_{ij} $(i, j = 1, \ldots, s)$ be real numbers, h is a constant step size and let $\sigma_i = \sum_{j=1}^{s} \alpha_{ij}$. An* **s-stage Runge-Kutta method** *is given by*

$$\begin{aligned} k_i &= f(t_0 + \sigma_i h, y_0 + h \textstyle\sum_{j=1}^{s} \alpha_{ij} k_j), \quad i = 1, \ldots, s \\ y_1 &= y_0 + h \textstyle\sum_{i=1}^{s} \beta_i k_i. \end{aligned} \tag{3.17}$$

Here we allow a full matrix (α_{ij}) of non-zero coefficients, thus making this an *implicit* integrator. In case when $\alpha_{ij} = 0$ for $i \leq j$ the method becomes an *explicit* Runge-Kutta method.

It is customary to display coefficients in the following way:

$$\begin{array}{c|ccc} \sigma_1 & \alpha_{11} & \ldots & \alpha_{1s} \\ \vdots & \vdots & \ddots & \vdots \\ \sigma_s & \alpha_{s1} & \ldots & \alpha_{ss} \\ \hline & \beta_1 & \ldots & \beta_s \end{array}$$

Definition. *We consider differential equations in the partitioned form*

$$\dot{y} = f(y, z), \quad \dot{z} = g(y, z), \tag{3.18}$$

where y, z may be vectors of different dimensions.

The idea is to take two different Runge-Kutta methods, and to treat the y-variables with the first method (α_{ij}, β_i), and the z-variables with the second method $(\hat{\alpha}_{ij}, \hat{\beta}_i)$.

Let α_{ij}, β_i and $\hat{\alpha}_{ij}, \hat{\beta}_i$ be the coefficients of two Runge-Kutta methods. A **partitioned Runge-Kutta method** *for the solution of (3.18) is given by*

$$\begin{aligned} k_i &= f\left(y_0 + h\sum_{j=1}^{s}\alpha_{ij}k_j, z_0 + h\sum_{j=1}^{s}\hat{\alpha}_{ij}l_j\right), \\ l_i &= g\left(y_0 + h\sum_{j=1}^{s}\alpha_{ij}k_j, z_0 + h\sum_{j=1}^{s}\hat{\alpha}_{ij}l_j\right), \\ y_1 &= y_0 + h\sum_{i=1}^{s}\beta_i k_i, \quad z_1 = z_0 + h\sum_{i=1}^{s}\hat{\beta}_i l_i. \end{aligned} \tag{3.19}$$

A particular example of this method is a *symplectic Euler-A (or Euler-B)* method:

$$\begin{cases} y_{n+1} = y_n + hf(y_n, z_{n+1}) \\ z_{n+1} = z_n + hg(y_n, z_{n+1}), \end{cases} \quad \text{or} \quad \begin{cases} y_{n+1} = y_n + hf(y_{n+1}, z_n) \\ z_{n+1} = z_n + hg(y_{n+1}, z_n). \end{cases}$$

Here implicit Euler method with $\beta_1 = 1, \alpha_{11} = 1$ is combined with the explicit Euler method with $\hat{\beta}_1 = 1, \hat{\alpha}_{11} = 0$ (or vice versa).

Another example of the 3-stage partitioned RK method is Lobatto IIIA-B method. The coefficients of the method are given in Table 3.1

Table 3.1: Coefficients of the 3-stage Lobatto IIIA-B pair

$$\begin{array}{c|ccc} 0 & 0 & 0 & 0 \\ 1/2 & 5/24 & 1/3 & -1/24 \\ 1 & 1/6 & 2/3 & 1/6 \\ \hline & 1/6 & 2/3 & 1/6 \end{array} \qquad \begin{array}{c|ccc} 0 & 1/6 & -1/6 & 0 \\ 1/2 & 1/6 & 1/3 & 0 \\ 1 & 1/6 & 5/6 & 0 \\ \hline & 1/6 & 2/3 & 1/6 \end{array}$$

In the figure 3.4 you can see the performance of three algorithms in preserving the Hamiltonian H_{ab}. Clearly, Lobatto IIIA-B method does the best job. This is due to the fact that Lobatto IIIA-B is a fourth order method, while Euler-A is just a first order method. In table 3.2 the comparison data is provided.

Table 3.2: Comparison of numerical methods used

Method	Explicit RK		Euler-A		Lobatto IIIA-B
Δt	10^{-2}	10^{-2}	10^{-3}	10^{-4}	10^{-2}
Time spent	.3 sec	2 sec	22 sec	734 sec	13 sec
Change in H_{ab}	7.0e10^{-2}	-1.5e10^{-2}	-1.5e10^{-3}	-1.5e10^{-4}	-6.0e10^{-6}

Simplecticity.

Theorem 4. *If the coefficients of a partitioned Runge-Kutta method (3.19) satisfy*

$$\begin{aligned} &\beta_i \hat{\alpha}_{ij} + \hat{\beta}_j \alpha_{ji} = \beta_i \hat{\beta}_j, \quad \textit{for } i, j = 1, \ldots, s, \\ &\beta_i = \hat{\beta}_i \quad \textit{for } i = 1, \ldots, s, \end{aligned}$$

then it conserves quadratic invariants of the form $Q(y, z) = y^T D z$, where D is the matrix of the appropriate dimensions.

We consider Hamiltonian equations

$$\dot{p}_k = -\frac{\partial H}{\partial q_k}(p, q), \quad \dot{q}_k = \frac{\partial H}{\partial p_k}(p, q), \quad k = 1, \ldots, d.$$

Denoting $y = (p, q)$ we write the above Hamiltonian system along with its variational equation in the form

$$\begin{aligned} &\dot{y} = J^{-1} \nabla H(y), \text{ where } J = \begin{pmatrix} 0 & I \\ -I & 0 \end{pmatrix}, \quad \nabla H(y) = H'(y)^T. \\ &\dot{\Psi} = J^{-1} \nabla^2 H(y) \Psi, \text{ where } \Psi = \partial y / \partial y_0. \end{aligned}$$

Note that the symplecticity condition is a quadratic first integral of the variational equation, i.e. $\Psi^T J \Psi = \text{const}$.

To understand the symplecticity of *partitioned* Runge-Kutta methods, we write the solution Ψ of the variational equation as

$$\Psi = \begin{pmatrix} \Psi^p \\ \Psi^q \end{pmatrix}.$$

Then, the Hamiltonian system together with its variational equation is a partitioned system with variables (p, Ψ^p) and (q, Ψ^q). And we have

$$\Psi^T J \Psi = (\Psi^p)^T \Psi^q - (\Psi^q)^T \Psi^p.$$

Then the simplecticity of the Lobatto IIIA-B pair follows from the above theorem, since we have a difference of two quadratic quantities which are conserved.

3.4.2 Numerical experiments with N-Teichons

In this section we will show that using a relatively small number of Teichons (around 20) we can get a wide variety of shapes. In other words, first we set an initial momentum on the circle as a sum of 20 delta functions $a_i\delta(\theta - b_i)$ scattered at positions b_i on the circle and satisfying conditions (3.3). Then solve the the system (3.16) forward in time until time $T = 1$ (using Lobatto IIIA-B scheme). This gives us the evolution of the vector $v(\theta, t) = \sum_{i=1}^{N} a_i\delta(\theta - b_i)$. We integrate this time varying vector $\Psi_t = v \circ \Psi$ to produce fingerprints $\Psi(\theta, t)$, corresponding to some shape evolution. One of the ideas is to learn heuristically the 'syntax' of Teichon interaction: how they repel or attract each other and what kind of shapes are produced as a result of these interactions. From the experiments we can say a few certain rules of this 'syntax'.

To simplify the discussion we can say that shapes basically have two sets of features: some number of extremities (or limbs) and some number of concavities (or dents). We are going to state the conjecture on the formation of these two features and provide figures of randomly generated shapes to support it.

Extremities are obtained via 'pinching', i.e. two (or more) close Teichons are attracted towards each other. The faster they are heading (large values of a_j's) the pointier is the extremity.

Concavities, or the dents, are obtained via 'ripping': two (or more) close Teichons running away from each other. The faster they are running the more concave that part of the shape will be.

Parts of the shape with no Teichons, or with Teichons moving slowly (small values of a_j) remain circular.

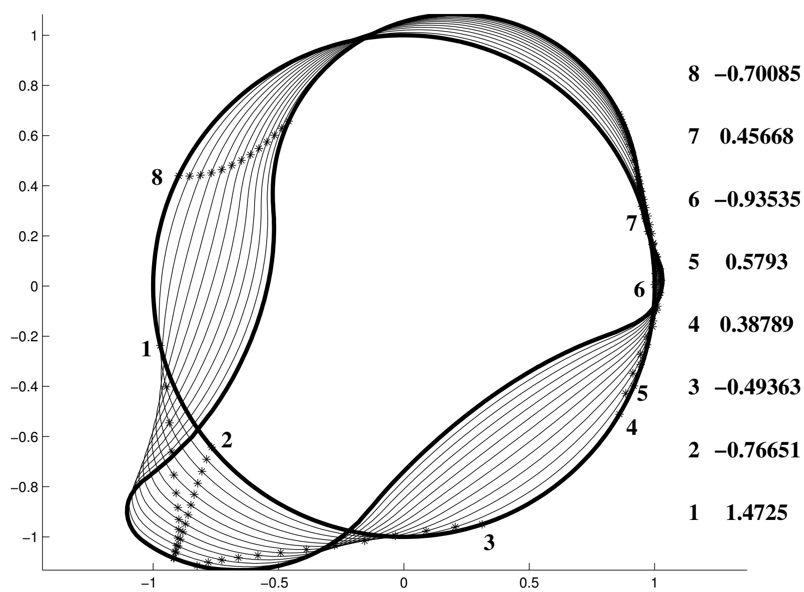

Figure 3.5: Evolution of an 8-Teichon from the circle to a Donald-Duck-like shape. Positions of individual 1-Teichons are marked by asterisks. The initial values of $(a_k)_{k=1}^{8}$ are given on the right.

Let us see how these rules apply to a Donald-Duck-like shape on Figure 3.5 (evolution of a_k, b_k is shown on Figure 3.6). It is comprised of the pointier end

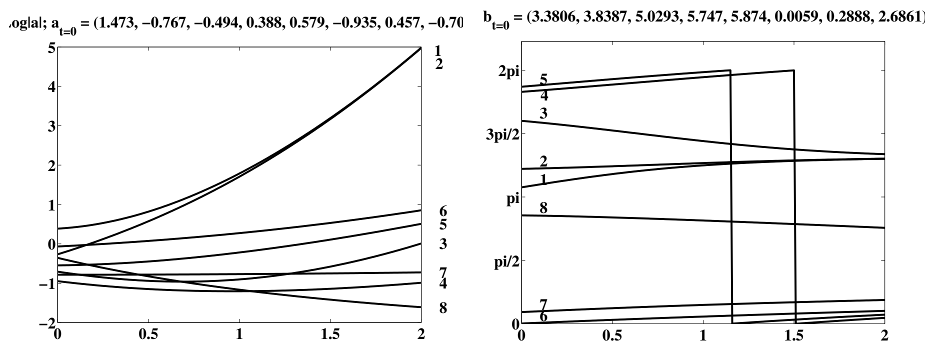

Figure 3.6: Time evolution of $\log|a_k|$'s (left) and b_k's (right) for the solitons representing Donald-Duck-like shape (Figure 3.5)

formed by 'large' Teichons $1, 2, 3$ and the dull end formed by solitons $4, 5, 6, 7$. The sharper end is formed by 'fast running' solitons $1, 2, 3$. The 'ripping' by Teichons $1, 8$ is somewhat bigger than the 'ripping' done by solitons $3, 4$, since Teichons $1, 8$ run faster away from each other than $3, 4$. The upper part of the Donald's head remains circular due to the absence of any solitons.

One can see how these general rules hold true most of the time in Figures 3.7, 3.8, 3.9. Here there are five more figures with random shapes generated by 16-Teichons. To the right from the shape you can see the 1-Teichon number j and the corresponding value of a_j at the initial time.

3.5 Conserved quantities

In Section 2.2 we have demonstrated that the energy and momentum are conserved in the solution of EPDiff(S^1). Here we will demonstrate what these translates into in the case of singular solutions.

For the N-Teichon evolution we have $v = \sum_{k=1}^{N} a_k G(\theta - b_k)$, and $m = \sum_{k=1}^{N} a_k \delta(\theta -$

b_k), then the energy becomes:

$$\begin{aligned}
\int_{S^1} Lv.v d\theta &= \int_{S^1} L\left(\sum_{k=1}^{N} a_k G(\theta - b_k)\right)\left(\sum_{k=1}^{N} a_j G(\theta - b_j)\right) d\theta \\
&= \int_{S^1} \left(\sum_{k=1}^{N} a_k \delta(\theta - b_k)\right)\left(\sum_{k=1}^{N} a_j G(\theta - b_j)\right) d\theta \\
&= \sum_{j,k=1}^{N} a_j a_k G(b_k - b_j).
\end{aligned}$$

This is exactly the Hamiltonian in the equations (3.2) of evolution of Teichons. In Figure 3.4 you can see how well it is preserved by the Lobatto IIIA-B symplectic integrator.

Recall (see Section 2.2) that the conserved momenta for the geodesic $g(\theta, t)$ has the expression:

$$\int L(\dot{g} \circ g^{-1}).(g_\theta \circ g^{-1}).(X \circ g^{-1}).d\theta = \int_{S^1} Lv.(g_\theta \circ g^{-1}).(X \circ g^{-1}).d\theta.$$

In the case of an N-Teichon we have $v = \dot{g} \circ g^{-1} = \sum_{k=1}^{N} a_k G(\theta - b_k)$. Therefore:

$$\begin{aligned}
\int L(\dot{g} \circ g^{-1}).(g_\theta \circ g^{-1}).(X \circ g^{-1}) d\theta &= \int L\left(\sum_{k=1}^{N} a_k G(\theta - b_k)\right).(g_\theta \circ g^{-1}).(X \circ g^{-1}) d\theta \\
&= \sum_{k=1}^{N} a_k \int \delta(\theta - b_k).(g_\theta \circ g^{-1}).(X \circ g^{-1}) d\theta \\
&= \sum_{k=1}^{N} a_k.(g_\theta \circ g^{-1}(b_k)).(X \circ g^{-1}(b_k)).
\end{aligned}$$

This means that momenta m at any time t is equal to momenta at time $t = 0$:

$$\sum_{k=1}^{N} a_k(t).(g_\theta \circ g^{-1}(b_k(t), t)).\delta(\theta - g^{-1}(b_k(t), t)) = \sum_{k=1}^{N} a_k(0)\delta(\theta - b_k(0)).$$

Therefore, conservation of momenta for Teichons yields:

$$\boxed{a_k(t) = \frac{a_k(0)}{g_\theta(b_k(0), t)}, \quad b_k(t) = g(b_k(0), t).} \tag{3.20}$$

See Figure 3.10 for numerical evidence of the conserved quantities.

3.6 Final remarks

It should be noted that evolution of Teichons is governed by the same system as the evolution of landmark points (see, for example, [M08]). But there is a difference. In the case of landmarks, landmarks are characteristic points on some shape, and the geodesic is calculated by matching one set of landmarks to another, thus matching one shape to another. Landmarks *are* the shape in this case. In contrast, position of Teichons on the circle does not tell us what the shape is. Teichon evolution only gives us the velocity $v(t)$ on the tangent space, that could be integrated to a geodesic path. Because of homogeneity of the underlying space we can integrate this vector starting from any shape $\Psi(\theta)$ and we will get a geodesic.

In this section we have not addressed the problem of finding the geodesic between two given shapes. This problem will be treated in Chapter 5 by minimizing the WP energy. To find the geodesic connecting two shapes in the Teichon setting one needs to consider the following numerical problem. Given two shapes with fingerprints Ψ_0 and Ψ_1 find $v(\theta, t)$ which is represented by

$$v(\theta, t) = \sum_{k=1}^{N} a_k(t) G(\theta - b_k),$$

(for some suitable N). The evolution of $v(\theta, t)$ will be governed by the evolution $a_k(t), b_k(t)$ via ODE (3.2). After integrating the equation $\Psi_t = v \circ \Psi$ the boundary conditions $\Psi(t=0)=\Psi_0, \Psi(t=1)=\Psi_1$ should be met.

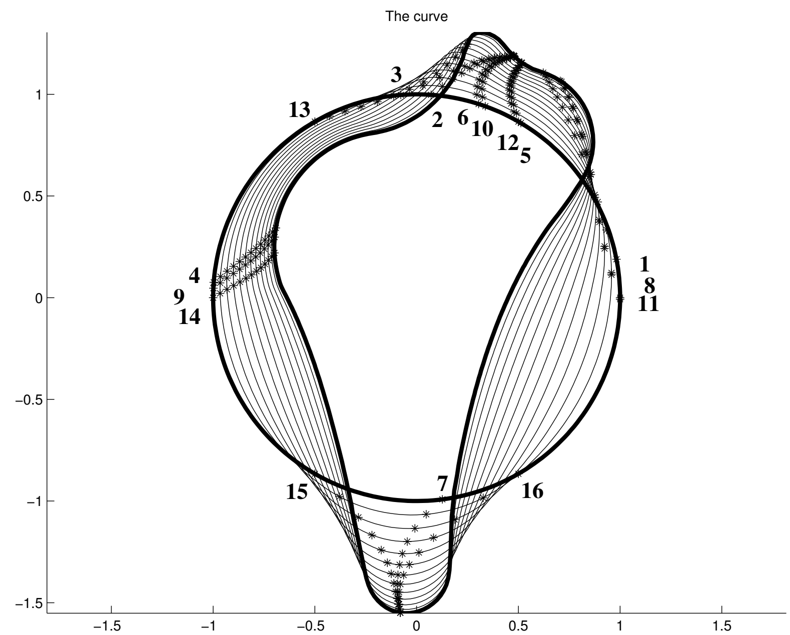

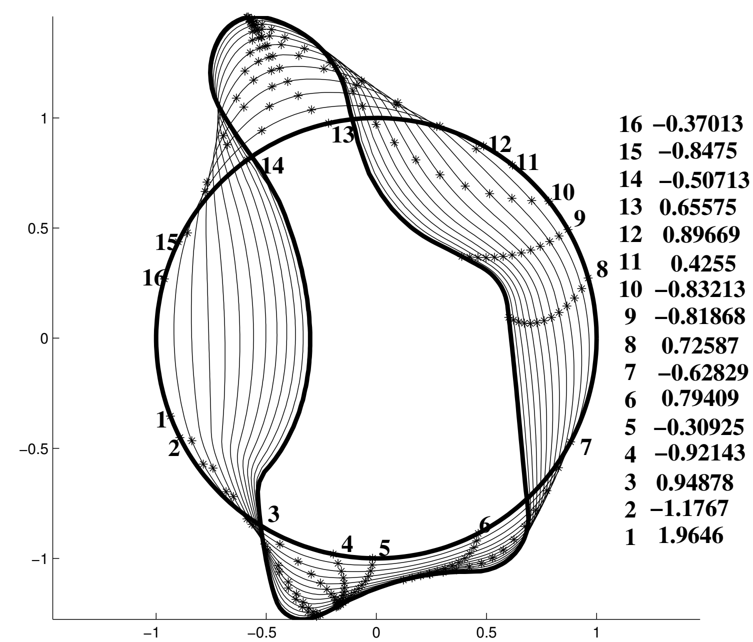

Figure 3.7: Evolution of a 16-Teichon from the circle to the bird-like shape (top) and to the bottle-like shape (bottom). Positions of individual 1-Teichons are marked by asterisks. Initial values of $(a_k)_{k=1}^{16}$ are given on the right. (Data for the bird-like shape is not available.)

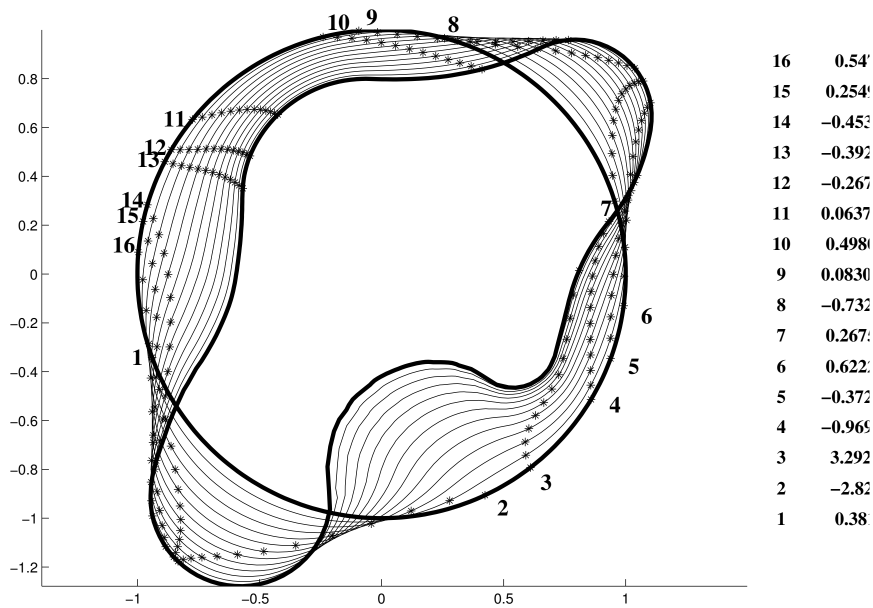

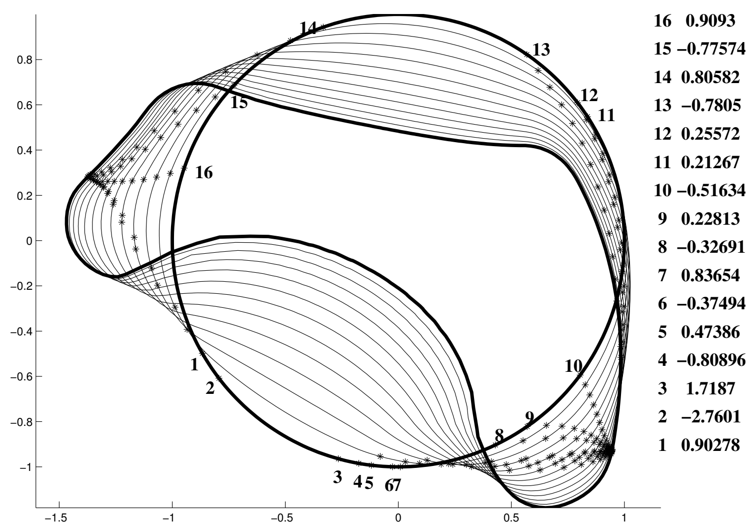

Figure 3.8: Evolution of a 16-Teichon from the circle to the amoeba-like shape (top) and the boomerang-like shape (bottom), represented by a 16-Teichon. Positions of individual 1-Teichons are marked by asterisks. Initial values of $(a_k)_{k=1}^{16}$ are given on the right.

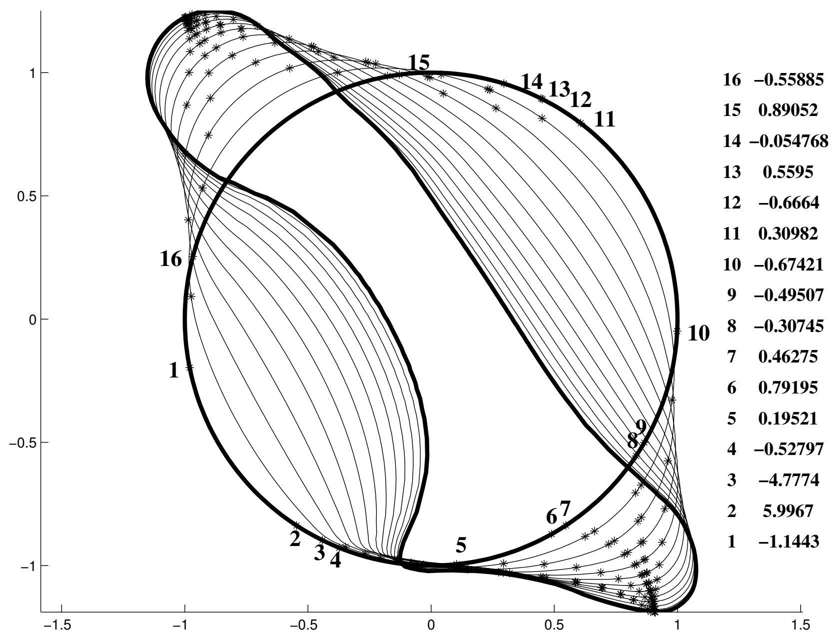

Figure 3.9: Evolution of a 16-Teichon from the circle to the sock-like shape, represented by a 16-Teichon. Positions of individual 1-Teichons are marked by asterisks. Initial values of $(a_k)_{k=1}^{16}$ are given on the right.

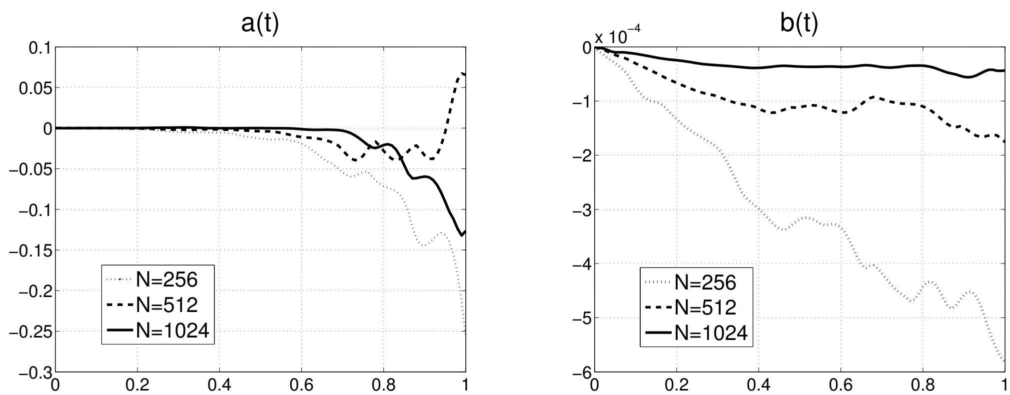

Figure 3.10: Left: difference between the computed $a_k(t)$ and the conserved $a_k(t) = \frac{a_k(0)}{g_\theta(b_k(0),t)}$. Right: difference between the computed $b_k(t)$ and the conserved $b_k(t) = g(b_k(0), t)$. Differences computed for different θ-discretizations: $N = 256, 512, 1024$.

Chapter 4

Curvature

It is an established fact, that all sectional curvatures of the Weil-Petersson metric on $T(1)$ are negative [Wo86]. In this chapter we show that the Arnold's formula (see [Ar66]) for sectional curvature on the Lie group G turns out to be valid in our case, for the metric with the null space, the Weil-Petersson metric. We make explicit computations of some sectional curvatures that agree with results in [BL88]. The discussion of the results is presented at the end of the chapter.

4.1 Introduction

Curvature is a very important characteristic of a metric on a given space. Its effects are usually not accounted for, due to the complexity of computation of the curvature tensor, or the impossibility of the computation in some cases. The Weil-Petersson metric has unique curvature properties — all of its sectional curvatures are negative. It is believed that this, as in a finite dimensional case, guarantees unique geodesics, connecting two shapes. Moreover, negative curvature gives us a certain 'stability' in the geodesic finding problem, as depicted in Figure 1.1. Unfortunately, the 'shooting' type of algorithms for finding geodesics suffer from negative sectional curvature — there is exponential divergence of geodesics with slightly different initial conditions. In other words geodesics are very sensitive to the changes of the initial vector. In subsection 4.2.7 we argue that this is not a big issue in the case of a Weil-Petersson metric. Now we are going to present the curvature computation using Jacobi vector fields.

4.2 Curvature computation

4.2.1 Jacobi vector field

Given the Riemannian manifold M, $P \in M$, $v \in T_P M$, we define the exponential map (it is defined in the neighborhood of a point P)

$$\exp_P : T_P M \to M, \quad \exp_P v = \gamma(p, v, 1),$$

where $\gamma(p, v, t)$ is a geodesic starting at P, launched in the direction v. Note, we can always write $\exp_p tv = \gamma(P, tv, 1) = \gamma(P, v, t)$ (for sufficiently small t).

The derivative of this map will look like

$$(d \exp_P)_{tv} : T_{tv}(T_P M) \equiv T_P M \to T_{\gamma(t)} M,$$

i.e. given $w \in T_P M$ we will have $(d \exp_P)_{tv} w = \partial / \partial s [\exp_P tv(s)]_{s=0}$, where $v(s)$ is a path in the tangent space $T_P M$ such that $v(0) = v, v'_s(0) = w$.

The *Jacobi field* $J(t)$ along the geodesic $\gamma(t)$ is defined as

$$J(t) = (d \exp_P)_{tv} tw,$$

and it satisfies the Jacobi equation

$$D_t^2 J - R(\gamma'(t), J(t))\gamma'(t) = 0, \;\; J(0) = 0, \;\; J'(0) = w.$$

Here, $R(X, Y)Z$ is the Riemannian curvature tensor. The Jacobi vector field essentially tells us how the geodesic $\exp_P(tv)$ will vary if we perturb the initial velocity v to be $v + s.w$, for some small value s. As you can see from the formula above the behavior of Jacobi vector fields is governed by the curvature of the underlying space. In fact we have the following theorem, that relates Jacobi vector fields with sectional curvature.

Theorem 5. *The Jacobi field $J(t)$ has a Taylor expansion, namely for $t \to 0$*

$$J(t) = P^t \left[wt - R(\gamma'(0), w)\gamma'(0)\frac{t^3}{3!} \right] + O(t^4).$$

Here, $P^t : T_{\gamma(0)}M \to T_{\gamma(t)}M$ is parallel translation.

A proof of this result can be found in [Jo05].

Let us take two vectors $v, w \in T_P M$, such that $\|v\| = \|w\| = 1, \langle v, w\rangle = 0$, and consider the geodesic $\gamma(t) = \exp_P tv$. Then:

$$\begin{aligned}
\exp_P^*(tv)\langle w, w\rangle_P &= \langle (d\exp_P)_{tv} w, (d\exp_P)_{tv} w\rangle_{\gamma(t)} \\
&= \left\langle \frac{1}{t}J(t), \frac{1}{t}J(t) \right\rangle_{\gamma(t)} \\
&= \left\langle P^t \left[w - R(v, w)v\frac{t^2}{3!} \right], P^t \left[w - R(v, w)v\frac{t^2}{3!} \right] \right\rangle_{\gamma(t)} \\
&= \left\langle w - R(v, w)v\frac{t^2}{3!}, w - R(v, w)v\frac{t^2}{3!} \right\rangle_P \\
&= \langle w, w\rangle - K(v, w)\frac{t^2}{3} + O(t^3). \qquad (4.1)
\end{aligned}$$

Here, $K(v, w)$ is a sectional curvature in the directions v, w. Intuitively, the sectional curvature $K(v,w)$ could be explained in the following way. Take two vectors v, w in the tangent space to the manifold M at some point P. They will define a 2D plane, a subspace of the tangent space at P. We launch geodesics, originating from point P with initial vectors in the tangent two-dimensional plane. These geodesics will 'carve' the 2D surface in the manifold M. The sectional curvature $K(v,w)$ is the Gaussian curvature of this 2D surface. All sectional curvatures of the Weil-Petersson metric are negative. That means that in every tangent plane the shape space 'looks' locally like a saddle, a 2D surface with negative Gaussian curvature.

We are going to employ the above construction involving Jacobi vector fields to compute sectional curvatures of the WP metric.

4.2.2 Taylor expansion of $\Phi(\theta,t) \in \mathbf{Diff}(S^1)/\mathrm{PSL}_2(\mathbb{R})$

In order to use Theorem 5 we need to find Taylor expansion of the geodesic $\exp_P tv$ for small t. In fact we will have *two* expressions for the geodesic $\exp_P tv$, depending which metric we are going to use, left- or right-invariant. They will be denoted $\exp_P^L tv \in \mathbf{Diff}(S^1)/\mathrm{PSL}_2(\mathbb{R})$ and $\exp_P^R tv \in \mathrm{PSL}_2(\mathbb{R})\backslash\mathbf{Diff}(S^1)$.

Take $v(\theta,t)$ and corresponding $m(\theta,t)$ and expand them in series in t-variable:

$$\begin{aligned} v(\theta,t) &= v_0(\theta) + v_1(\theta)t + v_2(\theta)t^2 + O(t^3), \\ m(\theta,t) &= m_0(\theta) + m_1(\theta)t + m_2(\theta)t^2 + O(t^3). \end{aligned}$$

To make this path a geodesic we need to make sure that the velocity $v(\theta,t)$ is such that it solves the EPDiff, in other words:

$$m_t = -2m.v_\theta - v.m_\theta, \quad \text{where } m = Lv, \quad v = G * m = L^{-1}m.$$

Plugging in the above expressions for v and m into the EPDiff we get:

$$\begin{aligned} m_1 + 2tm_2 + 3t^2m_3 + O(t^3) &= -2(m_0 + tm_1 + t^2m_2 + O(t^3))(v_0' + v_1't + v_2't^2 + O(t^3)) \\ &= -(m_0' + tm_1' + t^2m_2' + O(t^3))(v_0 + v_1t + v_2t^2 + O(t^3)). \end{aligned}$$

Which yields the following relations:

$$\begin{aligned} Lv_1 &= -2m_0v_0' - m_0'v_0 \\ &= -2Lv_0 \cdot v_0' - Lv_0' \cdot v_0, \qquad (4.2) \\ 2Lv_2 &= -2Lv_0v_1' - 2Lv_1v_0' - Lv_0'v_1 - Lv_1'v_0. \end{aligned}$$

In terms of the velocity field:

$$\begin{aligned} v_1 &= -L^{-1}(2Lv_0 \cdot v_0' + Lv_0' \cdot v_0), \\ v_2 &= L^{-1}\Big[Lv_0 \cdot L^{-1}(2Lv_0 \cdot v_0' + Lv_0' \cdot v_0)' + \frac{1}{2}Lv_0' \cdot L^{-1}(2Lv_0 \cdot v_0' + Lv_0' \cdot v_0) \\ &\quad + v_0'(2Lv_0 \cdot v_0' + Lv_0' \cdot v_0) + \frac{1}{2}v_0(2Lv_0 \cdot v_0' + Lv_0' \cdot v_0)'\Big]. \end{aligned}$$

Take a geodesic $\Psi(\theta, t) \in \mathrm{PSL}_2(\mathbb{R})\backslash\mathbf{Diff}(S^1)$. Then the vector field $w(\theta, t)$ is given by

$$\Psi_t(\Psi^{-1}(\theta, t), t) = w(\theta, t).$$

If we instead consider $\Phi(\theta, t) := \Psi(\theta, t)^{-1} \in \mathbf{Diff}(S^1)/\mathrm{PSL2}$ (inverse is taken in θ-variable), then we obtain that Φ satisfy the transport equation:

$$\Phi_t(\theta, t) = -w(\theta, t)\Phi_\theta(\theta, t).$$

Here, vector field $w(\theta, t)$ is the same as in the previous formula.

Consider $\Phi(\theta,t)=\theta+t\cdot\Phi_1(\theta)+t^2\cdot\Phi_2(\theta)+t^3\cdot\Phi_3(\theta)+O(t^4)$. We have

$$\begin{aligned}\Phi_t(\theta,t) &= \Phi_1+2\Phi_2t+3\Phi_3t^2+O(t^3),\\ \Phi_\theta(\theta,t) &= 1+\Phi_1't+\Phi_2't^2+\Phi_3't^3+O(t^4).\end{aligned}$$

Then the transport equation for $\Phi(\theta,t)$ becomes:

$$\Phi_1+2\Phi_2t+3\Phi_3t^2+O(t^3)=-(v_0+v_1t+v_2t^2+O(t^3))(1+\Phi_1't+\Phi_2't^2+O(t^3)).$$

Which yields

$$\begin{aligned}\Phi_1 &= -v_0,\\ 2\Phi_2 &= -v_0\Phi_1'-v_1\\ &= v_0v_0'+L^{-1}(2Lv_0\cdot v_0'+Lv_0'\cdot v_0),\\ 3\Phi_3 &= -v_0\Phi_2'-v_1\Phi_1'-v_2\\ &= -\frac{v_0}{2}[v_0v_0'+L^{-1}(2Lv_0\cdot v_0'+Lv_0'\cdot v_0)]'-v_0'L^{-1}(2Lv_0\cdot v_0'+Lv_0'\cdot v_0)\\ &\quad -L^{-1}\Big[Lv_0\cdot L^{-1}(2Lv_0\cdot v_0'+Lv_0'\cdot v_0)'+\frac{1}{2}Lv_0'\cdot L^{-1}(2Lv_0\cdot v_0'+Lv_0'\cdot v_0)\\ &\qquad +v_0'(2Lv_0\cdot v_0'+Lv_0'\cdot v_0)+\frac{1}{2}v_0(2Lv_0\cdot v_0'+Lv_0'\cdot v_0)'\Big].\end{aligned}\tag{4.3}$$

Therefore, the geodesic $\Phi(\theta,t)$ has the following expansion (substituting v for v_0)

$$\Phi(\theta,t)=\theta-vt+\frac{1}{2}[vv'+L^{-1}(2Lv\cdot v'+Lv'\cdot v)]t^2+\Phi_3t^3+O(t^4).$$

Where Φ_3 is defined by (4.3). The above is the expression for the left exponential, i.e. $\Phi(\theta,t)=\exp_P^L(-tv)\in\mathbf{Diff}(S^1)/\mathrm{PSL}_2(\mathbb{R})$.

4.2.3 Taylor expansion of $\Psi(\theta,t) \in \mathrm{PSL}_2(\mathbb{R})\backslash\mathbf{Diff}(S^1)$

Knowing the Taylor expansion of $\Phi(\theta,t)$ we obtain the expansion of $\Psi = \Phi^{-1}$. Given $\Phi(\theta,t) := \Psi^{-1}(\theta,t) = \theta + \Phi_1(\theta)t + \Phi_2(\theta)t^2 + O(t^3)$. We have the following:

$$\begin{aligned}
\frac{\partial}{\partial t}\Psi^{-1}(\Psi(\theta,t),t) &= 0,\\
\Psi_\theta^{-1}(\Psi(\theta,t),t)\Psi_t(\theta,t) + \Psi_t^{-1}(\Psi(\theta,t),t) &= 0,\\
\Psi_t(\theta,t) &= -\frac{\Psi_\theta^{-1}(\Psi(\theta,t),t)}{\Psi_t^{-1}(\Psi(\theta,t),t)}.
\end{aligned}$$

$$\begin{aligned}
\frac{\Psi_t^{-1}(\theta,t)}{\Psi_\theta^{-1}(\theta,t)} &= \frac{\Phi_1 + 2\Phi_2 t + 3\Phi_3 t^2 + O(t^3)}{1 + \Phi_1' t + \Phi_2' t^2 + O(t^3)}\\
&= (\Phi_1 + 2\Phi_2 t + 3\Phi_3 t^2 + O(t^3))(1 - \Phi_1' t - \Phi_2' t^2 + \Phi_1'^2 t^2 + O(t^3))\\
&= \Phi_1 + t(2\Phi_2 - \Phi_1\Phi_1') + t^2(3\Phi_3 - 2\Phi_1'\Phi_2 - \Phi_1\Phi_2' + \Phi_1\Phi_1'^2) + O(t^3).
\end{aligned}$$

Combining two expressions we have

$$\begin{aligned}
\Psi_t(\theta,t) = &-\frac{\Psi_\theta^{-1}(\Psi(\theta,t),t)}{\Psi_t^{-1}(\Psi(\theta,t),t)}\\
= &-\left[\Phi_1(\theta) + t(2\Phi_2(\theta) - \Phi_1(\theta)\Phi_1'(\theta))\right.\\
&\left.+t^2(3\Phi_3 - 2\Phi_1'\Phi_2 - \Phi_1\Phi_2' + \Phi_1\Phi_1'^2) + O(t^3)\right]_{\theta=\Psi(\theta,t)}.
\end{aligned}$$

Therefore

$$\begin{aligned}
\Psi_t(\theta,t=0) &= v_0,\\
\Psi_{tt}(\theta,t=0) &= v_0v_0' - L^{-1}(2Lv_0\cdot v_0' + Lv_0'\cdot v_0),\\
\Psi_{ttt}(\theta,t=0) &= v_0(v_0v_0')' - 2v_0L^{-1}(2Lv_0\cdot v_0' + Lv_0'\cdot v_0)' \qquad (4.4)\\
&\quad - v_0'L^{-1}(2Lv_0\cdot v_0' + Lv_0'\cdot v_0) + 2v_2. \qquad (4.5)
\end{aligned}$$

Using the series for $\Phi(\theta,t)$ we have obtained the series for the right exponential

$\Psi(\theta, t) = \exp_P^R(tv) \in \mathrm{PSL2}\backslash\mathbf{Diff}(S^1)$ (substituting v for v_0):

$$\Psi(\theta, t) = \theta + vt + \frac{1}{2}[vv' - L^{-1}(2Lv \cdot v' + Lv' \cdot v)]t^2 + \Psi_3 t^3 + O(t^4),$$

where $\Psi_3 = \frac{1}{6}\Psi_{ttt}$.

4.2.4 Exponential maps

We have two exponential maps, right and left exponential maps, which correspond to geodesics in left- or right-invariant metrics:

$$\exp^L(-tv) = \Psi(\theta, -v, t) \in \mathbf{Diff}(S^1)/\mathrm{PSL2},$$
$$\exp^R(tv) = \Phi(\theta, v, t) \in \mathrm{PSL2}\backslash\mathbf{Diff}(S^1).$$

We have explicit formulae for them, up to a third order terms:

$$\begin{aligned} \exp^L(-tv) &= \theta - vt + \frac{1}{2}\left[vv' + L^{-1}(2Lv \cdot v' + Lv' \cdot v)\right]t^2 + \Phi_3 t^3, \\ \exp^R(tv) &= \theta + vt + \frac{1}{2}\left[vv' - L^{-1}(2Lv \cdot v' + Lv' \cdot v)\right]t^2 + \Psi_3 t^3, \end{aligned} \tag{4.6}$$

where Φ_3, Ψ_3 are defined as in (4.3) and (4.5).

4.2.5 Concise way

In order to write the expression for the sectional curvature in the concise manner we will introduce new notation. For any $u, v \in \mathfrak{g}$ we have the *transpose of the adjoint* *map*:

$$\begin{aligned}
\mathrm{ad}_u^\dagger v : \mathfrak{g} &\to \mathfrak{g}, \\
v &\mapsto \mathrm{ad}_u^\dagger v.
\end{aligned}$$

It is defined in the following way:

$$\begin{aligned}
\langle \mathrm{ad}_u^\dagger v, w \rangle &= \langle v, \mathrm{ad}_u w \rangle \\
&= \langle v, [u, w] \rangle.
\end{aligned}$$

We will derive the formula for the $\mathrm{ad}^\dagger$ using integration by parts:

$$\begin{aligned}
\langle \mathrm{ad}_u^\dagger v, w \rangle &= \langle v, [u, w] \rangle \\
&= \int Lv(uw' - wu')dx \\
&= \int -Lv \cdot u'w + Lv \cdot uw'dx \\
&= \int (-2Lv \cdot u' - Lv' \cdot u)wdx.
\end{aligned}$$

Therefore:

$$\mathrm{ad}_u^\dagger v = -L^{-1}(2Lv \cdot u' + Lv' \cdot u).$$

Notice, that $\mathrm{ad}_u^\dagger v = \beta(v, u)$ in Arnold's notation in [Ar66].

In terms of the transpose of the adjoint map exponential maps (4.6) take more concise form (we can write v instead of tv, for small $\|v\|$):

$$\begin{aligned}\exp^R v &= \theta + v + \frac{1}{2}\big[vv' + \mathrm{ad}_v^\dagger v\big] \\ &\qquad + \frac{1}{6}\big[v(vv')' + v'\mathrm{ad}_v^\dagger v + 2v(\mathrm{ad}_v^\dagger v)' + \mathrm{ad}_v^\dagger(\mathrm{ad}_v^\dagger v) + \mathrm{ad}^\dagger_{\mathrm{ad}_v^\dagger v} v\big] + O(\|v\|^4), \\ \exp^L v &= \theta + v + \frac{1}{2}\big[vv' - \mathrm{ad}_v^\dagger v\big] \\ &\qquad + \frac{1}{6}\big[v(vv')' - v(\mathrm{ad}_v^\dagger v)' - 2v'\mathrm{ad}_v^\dagger v + \mathrm{ad}_v^\dagger(\mathrm{ad}_v^\dagger v) + \mathrm{ad}^\dagger_{\mathrm{ad}_v^\dagger v} v\big] + O(\|v\|^4).\end{aligned}$$

Now we compute $\widetilde{u} = D\exp_v^R u$, in other words how the vector u is carried by the flow generated by the vector v (keeping the terms of the third order and below):

$$\begin{aligned}\widetilde{u} = D\exp_v^R u = u &+ \frac{1}{2}\big[(uv)' + \mathrm{ad}_u^\dagger v + \mathrm{ad}_v^\dagger u\big] + \frac{1}{6}\Big[u(vv')' + v(uv')' + v(vu')' \\ &+ u'\mathrm{ad}_v^\dagger v + v'(\mathrm{ad}_u^\dagger v + \mathrm{ad}_v^\dagger u) + 2u(\mathrm{ad}_v^\dagger v)' + 2v(\mathrm{ad}_u^\dagger v + \mathrm{ad}_v^\dagger u)' \\ &+ \mathrm{ad}_u^\dagger \mathrm{ad}_v^\dagger v + \mathrm{ad}_v^\dagger(\mathrm{ad}_u^\dagger v + \mathrm{ad}_v^\dagger u) + \mathrm{ad}^\dagger_{\mathrm{ad}_u^\dagger v + \mathrm{ad}_v^\dagger u} v + \mathrm{ad}^\dagger_{\mathrm{ad}_v^\dagger v} u\Big]. \end{aligned} \tag{4.7}$$

In order to compute the WP norm of $\widetilde{u}$ we translating it back to the tangent space at the identity $T_{Id}\mathrm{PSL}_2(\mathbb{R})\backslash\mathbf{Diff}(S^1)$ and keep all the terms upto $O(\|v\|^2)$. We will get a rather long formula:

$$\begin{aligned}&\widetilde{u}(\exp^R(v)^{-1}) = \widetilde{u}(\exp^L(-v)) = \\ &u - vu' + \frac{1}{2}[vv'u' - u'\mathrm{ad}_v^\dagger v + v^2u''] + \frac{1}{2}\big[(uv)' + \mathrm{ad}_u^\dagger v + \mathrm{ad}_v^\dagger u\big] - \frac{1}{2}v\big[(uv)' + \mathrm{ad}_u^\dagger v + \mathrm{ad}_v^\dagger u\big]' \\ &\quad + \frac{1}{6}\Big[u(vv')' + v(uv')' + v(vu')' + u'\mathrm{ad}_v^\dagger v + v'(\mathrm{ad}_u^\dagger v + \mathrm{ad}_v^\dagger u) + 2u(\mathrm{ad}_v^\dagger v)' + \\ &2v(\mathrm{ad}_u^\dagger v + \mathrm{ad}_v^\dagger u)' + \mathrm{ad}_u^\dagger \mathrm{ad}_v^\dagger v + \mathrm{ad}_v^\dagger(\mathrm{ad}_u^\dagger v + \mathrm{ad}_v^\dagger u) + \mathrm{ad}^\dagger_{\mathrm{ad}_u^\dagger v + \mathrm{ad}_v^\dagger u} v + \mathrm{ad}^\dagger_{\mathrm{ad}_v^\dagger v} u\Big]. \end{aligned} \tag{4.8}$$

After some simplification the formula turns into

$$
\begin{aligned}
&\widetilde{u}(\exp^R(v)^{-1}) = u + \underbrace{\frac{1}{2}[u,v] + \frac{1}{2}\left[\mathrm{ad}_u^\dagger v + \mathrm{ad}_v^\dagger u\right]}_{I_1} \\
&\underbrace{+\frac{1}{6}\left[uv'^2 - uvv'' - vv'u' + v^2u'' - 2u'\mathrm{ad}_v^\dagger v - v(\mathrm{ad}_u^\dagger v + \mathrm{ad}_v^\dagger u)' + v'(\mathrm{ad}_u^\dagger v + \mathrm{ad}_v^\dagger u) + 2u(\mathrm{ad}_v^\dagger v)'\right]}_{I_2} \\
&\quad + \frac{1}{6}\Bigg[u(vv')' + v(uv')' + v(vu')' + u'\mathrm{ad}_v^\dagger v + v'(\mathrm{ad}_u^\dagger v + \mathrm{ad}_v^\dagger u) + 2u(\mathrm{ad}_v^\dagger v)' + \\
&\underbrace{2v(\mathrm{ad}_u^\dagger v + \mathrm{ad}_v^\dagger u)' + \mathrm{ad}_u^\dagger \mathrm{ad}_v^\dagger v + \mathrm{ad}_v^\dagger(\mathrm{ad}_u^\dagger v + \mathrm{ad}_v^\dagger u) + \mathrm{ad}^\dagger_{\mathrm{ad}_u^\dagger v + \mathrm{ad}_v^\dagger u} v + \mathrm{ad}^\dagger_{\mathrm{ad}_v^\dagger v} u\Bigg]}_{I_3}. \quad (4.9)
\end{aligned}
$$

One can check that

$$
\begin{aligned}
\langle u + I_1, u + I_1\rangle &= \|u\|^2 + \frac{1}{4}\|[u,v]\|^2 + \frac{1}{4}\|\mathrm{ad}_u^\dagger v + \mathrm{ad}_v^\dagger u\|^2 + \frac{1}{2}\langle [u,v], \mathrm{ad}_u^\dagger v + \mathrm{ad}_v^\dagger u\rangle, \\
\langle u, I_2\rangle &= -\frac{1}{6}\langle [u,v], \mathrm{ad}_v^\dagger u\rangle + \frac{1}{3}\langle \mathrm{ad}_u^\dagger u, \mathrm{ad}_v^\dagger v\rangle - \frac{1}{6}\langle \mathrm{ad}_v^\dagger u, \mathrm{ad}_v^\dagger u + \mathrm{ad}_u^\dagger v\rangle, \\
\langle u, I_3\rangle &= -\frac{1}{6}\langle [u,v], \mathrm{ad}_v^\dagger u + \mathrm{ad}_u^\dagger v\rangle - \frac{1}{6}\langle \mathrm{ad}_u^\dagger u, \mathrm{ad}_v^\dagger v\rangle - \frac{1}{6}\langle \mathrm{ad}_u^\dagger v, \mathrm{ad}_v^\dagger u + \mathrm{ad}_u^\dagger v\rangle.
\end{aligned}
$$

Combining the above one gets the WP norm of $\widetilde{u}$ (again up to the terms quadratic in v):

$$
\begin{aligned}
\langle \widetilde{u}(\exp^R(v)^{-1}), \widetilde{u}(\exp^R(v)^{-1})\rangle &= \langle u + I_1 + I_2 + I_3, u + I_1 + I_2 + I_3\rangle \\
&= \langle u + I_1, u + I_1\rangle + 2\langle u, I_2 + I_3\rangle.
\end{aligned}
$$

$$
\begin{aligned}
&\langle \widetilde{u}(\exp^R(v)^{-1}), \widetilde{u}(\exp^R(v)^{-1})\rangle = \\
&\qquad \|u\|^2 + \frac{1}{4}\|[u,v]\|^2 - \frac{1}{12}\|\mathrm{ad}_u^\dagger v + \mathrm{ad}_v^\dagger u\|^2 \\
&\qquad\qquad + \frac{1}{6}\langle [u,v], \mathrm{ad}_u^\dagger v - \mathrm{ad}_v^\dagger u\rangle + \frac{1}{3}\langle \mathrm{ad}_u^\dagger u, \mathrm{ad}_v^\dagger v\rangle. \quad (4.10)
\end{aligned}
$$

Since $\langle \widetilde{u}(\exp^R(v)^{-1}), \widetilde{u}(\exp^R(v)^{-1})\rangle = \|u\|^2 + \frac{1}{3}K(u,v)$, the formula for the sectional curvature $K(u,v)$ in the directions u, v has the form:

$$K(u,v) = \frac{3}{4}\Big\|[u,v]\Big\|^2 - \frac{1}{4}\Big\|\mathrm{ad}_u^\dagger v + \mathrm{ad}_v^\dagger u\Big\|^2 + \frac{1}{2}\Big\langle [u,v], \mathrm{ad}_u^\dagger v - \mathrm{ad}_v^\dagger u\Big\rangle + \Big\langle \mathrm{ad}_u^\dagger u, \mathrm{ad}_v^\dagger v\Big\rangle. \tag{4.11}$$

The expression (4.11) coincides with Arnold's formula in [Ar66].

4.2.6 Sectional curvature in the Fourier basis

In this subsection we will derive the expression for the sectional curvature of the WP metric in the planes spanned by the Fourier basis vectors e^{inx} and on the planes, spanned by $\sin nx$ and $\cos nx$.

We will follow the notation used in [BR87]. We have the Fourier basis $L_m = z^{-m+1}\partial/\partial z = -ie^{-imx}\partial/\partial x$ on the circle. Where $x \in [0, 2\pi]$ is a coordinate on a circle, z is a coordinate on a complex plane $\mathbb{C}$. The complexified Weil-Petersson norm is given by:

$$\langle L_m, L_n\rangle = |m^3 - m|\delta_{m,-n}, \quad \omega_m := \langle L_m, L_{-m}\rangle = |m^3 - m|.$$

According to [BL88] the curvature tensor R has the following representation:

$$\langle R(L_{-m}, L_n)L_m, L_{-n}\rangle = (m+2n)(n+2m)\frac{\omega_m\omega_n}{\omega_{m+n}} - (n+m)\left\{\begin{matrix} (2n-m)\omega_m, & n \geq m \\ (2m-n)\omega_n, & m \geq n \end{matrix}\right\}, \tag{4.12}$$

where $n, m > 1$.

In the previous section we have demonstrated that Arnold's formula for the sectional curvature still holds in our case of the metric on the quotient space. We will follow the footsteps of Arnold ([Ar66]) in deriving the same result as Bowick and Lahiri.

$$\begin{aligned} R(L_{-m}, L_n)L_m &= [\nabla_{L_{-m}}, \nabla_{L_n}]L_m - \nabla_{[L_{-m},L_n]}L_m \\ &= \nabla_{L_n}\nabla_{L_{-m}}L_m - \nabla_{L_{-m}}\nabla_{L_n}L_m - \nabla_{[L_{-m},L_n]}L_m. \end{aligned}$$

First, we compute some identities that would be helpful, for example the Lie bracket for right-invariant vector fields:

$$[L_k, L_l] = L_l(L_k)_x - L_k(L_l)_x = (l-k)L_{k+l}.$$

Bilinear operator B defined on Lie algebra $\mathfrak{g}$ as $\langle B(u,v), w\rangle = \langle u, [v,w]\rangle$, or in other words:

$$B(L_k, L_l) = -(k+2l)\frac{\omega_k}{\omega_{k+l}}L_{k+l}.$$

Covariant derivative:

$$\begin{aligned} \nabla_{L_k}L_l &= \frac{1}{2}\left(-[L_k, L_l] + B(L_k, L_l) + B(L_l, L_k)\right) \\ &= \frac{1}{2}\left((k-l) - (k+2l)\frac{\omega_k}{\omega_{k+l}} - (l+2k)\frac{\omega_l}{\omega_{k+l}}\right)L_{k+l}. \end{aligned}$$

Using the above identities we can derive:

$$\begin{aligned} \langle \nabla_{L_n}\nabla_{L_{-m}}L_m, L_{-n}\rangle &= 0, \\ \langle \nabla_{L_{-m}}\nabla_{L_n}L_m, L_{-n}\rangle &= -\langle \nabla_{L_n}L_m, \nabla_{L_{-m}}L_{-n}\rangle \\ &= \frac{(n-m)^2\omega_{n+m}^2 - ((n+2m)\omega_n + (m+2n)\omega_m)^2}{4\omega_{n+m}}, \\ \langle \nabla_{[L_{-m},L_n]}L_m, L_{-n}\rangle &= \frac{n+m}{2}[(2m-n)\omega_n + (2n-m)\omega_m + (n+m)\omega_{n-m}]. \end{aligned}$$

Combining all the ingredients we get the final formula for the sectional curvature. One can check that it agrees with formula (4.12):

$$\boxed{\begin{aligned}\langle R(L_{-m}, L_n)L_m, L_{-n}\rangle =& \frac{((n+2m)\omega_n + (m+2n)\omega_m)^2 - (n-m)^2\omega_{n+m}^2}{4\omega_{n+m}} \\ &- \frac{n+m}{2}[(2m-n)\omega_n + (2n-m)\omega_m + (n+m)\omega_{n-m}]\end{aligned}}$$

If we take $s_n = \sin nx$ and $c_n = \cos nx$, then the expression for the sectional curvature in the plane spanned by s_n, c_n simplifies and has the following form (notice, that $\|s_n\|_{WP}^2 = \|c_n\|_{WP}^2 = \omega_n/2$):

$$\begin{aligned}\langle R(s_n, c_n)s_n, c_n\rangle &= \frac{9n^2\omega_n^2}{4\omega_{2n}} - \frac{n^2\omega_n}{2}, \\ K(s_n, c_n) &= \frac{9n^2}{\omega_{2n}} - \frac{2n^2}{\omega_n}.\end{aligned} \tag{4.13}$$

In Figure 4.1 you can see plots for the sectional curvature $K(L_{-m}, L_n) = \frac{\langle R(L_{-m},L_n)L_m,L_{-n}\rangle}{\omega_m\omega_n}$ and $K(s_n, c_n) = 4\frac{\langle R(s_n,c_n)s_n,c_n\rangle}{\omega_n^2}$.

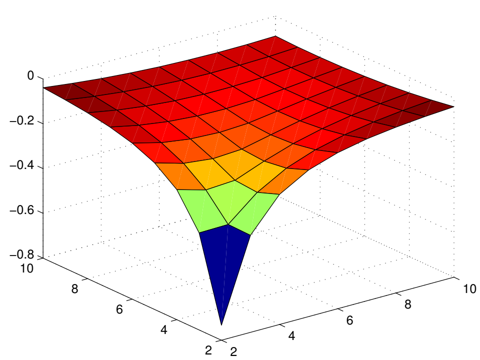

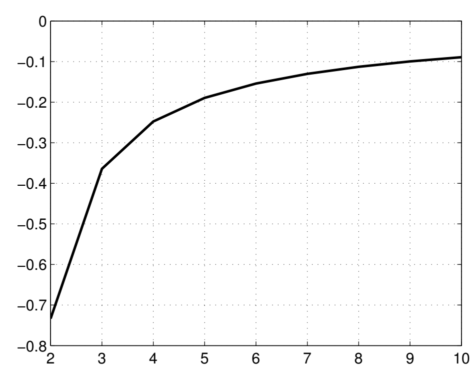

Figure 4.1: Left: sectional curvature $K(L_{-m}, L_n)$, where $L_m = -ie^{-imx}\partial/\partial x$. Right: sectional curvature $K(\sin nx, \cos nx)$.

In Subsection 5.3.6 we will demonstrate the effects of negative sectional curvature on the geometry of the geodesic triangle. And in Section 5.4 we will demonstrate numerically the divergence of geodesics according to the formula (4.1).

4.2.7 Ricci curvature

The Ricci curvature tensor at the origin of the universal Teichmüller space $T(1)$ is defined by the following series

$$\mathcal{R}_{k\bar{l}} = \sum_{n=2}^{+\infty} R_{k\bar{n}n\bar{l}}. \tag{4.14}$$

Here, we are using the convention $\bar{n} = -n$.

We will state the theorem from [TT06] without a proof regarding the Ricci tensor.

Theorem 6. *The Ricci tensor at the origin of $T(1)$ is well-defined and is given by*

$$\mathcal{R}_{k\bar{l}} = -\frac{13}{12\pi}\delta_{kl}.$$

Since the Weil-Petersson metric on $T(1)$ is right-invariant, it follows that the Ricci tensor is well defined everywhere on $T(1)$, not only at the origin.

You can see that the Ricci curvature is finite. That means that high-frequency sectional curvatures are going to zero, and they are tending to zero fast enough to guarantee the convergence of the series (4.14). That tells us that the shooting algorithm of finding geodesics would be less sensitive to the high-frequency component of the initial velocity, than to the lower-frequency components. The higher the frequency, the closer to zero the sectional curvature is, hence the more 'flat' the geometry of the space becomes. That will allow us to tackle high-frequency noise in the geodesic finding problems.

4.3 Discussion

Knowing curvature is a very important tool in the study of the shape space. Firstly, it tells us how geodesics behave, and what happens to neighboring geodesics. Secondly, knowing curvature allows us to do better statistics. Currently, statistics on the shape space is done in the following way [VMTY05]. Given n shapes s_k, the Karcher mean m is found. It is defined as a shape m, such that it minimizes the following sum $\sum_{k=1}^{N} dist(m, s_k)^2$. The shapes are linearized: instead of s_k one considers vectors v_k, that are the initial vectors of the geodesic, connecting m and s_k's. Therefore, analysis is transfered from a non-linear space of shapes, to a linear space, tangent space at the Karcher mean m. But the analysis is not entirely correct if we are not taking curvature into the account. In some planes the space is more 'curved' than in others. For example, given two pairs of vectors u_1, u_2 and v_1, v_2, such that the sectional curvature $K(u_1, u_2) > K(v_1, v_2)$. From the point of view of the tangent space, if vectors have the same norm and the same angle between them, two pairs of shapes will look the same. But this is not the case if we account for the curvature: the shapes, corresponding to vectors u_1, u_2 will spread from each other further away, than the shapes, produced from vectors v_1, v_2. This is reflected in the formula (4.1). In Section 5.4 I have demonstrated numerically the 'spreading apart' of geodesics. This is one of the major reasons why Weil-Petersson metric is interesting: its sectional curvatures are known and we can compute them relatively easy, employing the formula (4.11).

Chapter 5

Numerical methods of finding geodesics

5.1 From shapes to fingerprints

Given a 2D shape Γ, we need to construct its fingerprint. This is done via constructing two conformal maps, ϕ_{int} and ϕ_{ext}. Respectively, these map the interior of the disk to the interior of the shape, and the exterior of the disk to the exterior of the shape. By composing these maps and restricting their action to the circle one gets the fingerprint $\Psi = \phi_{\text{int}}^{-1} \circ \phi_{\text{ext}}|_{S^1}$.

The shape Γ is represented via the collection of N points $\{z_n\}_{n=1}^{N}$, spaced uniformly with arclength in the complex plane. Recall, that for the construction of the fingerprint we find two conformal maps ϕ_{int} and ϕ_{ext}, such that:

$$\phi_{\text{int}} : \mathbb{D}_{\text{int}} \to \Gamma_{\text{int}},$$
$$\phi_{\text{ext}} : \mathbb{D}_{\text{ext}} \to \Gamma_{\text{ext}},$$

where $\mathbb{D}$ is the unit disk and Γ is the shape. Shape Γ is given by the collection of points $\{\Gamma_k\}$ in the complex plane. This two maps allow us to define a fingerprint and its inverse: $\Psi = \phi_{\text{int}}^{-1} \circ \phi_{\text{ext}}|_{S^1}$ and the inverse $\Psi^i = \phi_{\text{ext}}^{-1} \circ \phi_{\text{int}}|_{S^1}$. We define two sets of points, θ^{int} and θ^{ext}, on the circle:

$$\theta_k^{\text{int}} = \phi_{\text{int}}^{-1}(\Gamma_k),$$
$$\theta_k^{\text{ext}} = \phi_{\text{ext}}^{-1}(\Gamma_k).$$

In this notation we can write the fingerprints:

$$\Psi^i(\theta^{\text{int}}) = \theta^{\text{ext}}, \quad \Psi(\theta^{\text{ext}}) = \theta^{\text{int}}.$$

There are several methods of computing the conformal map between a disk and a shape given by a collection of points:

- the SC package developed by Toby Driscoll and L.N.Trefethen [DT], `http://www.math.udel.edu/~driscoll/SC/`
  or
- the 'zipper' algorithm developed by Donald Marshall [MR07], `http://www.math.washington.edu/~marshall/zipper.html`.

The SC package computes the conformal map using the Schwarz-Christoffel formula. It will produce a conformal map between a disk and the interior (as well as the exterior) of a polygon, with vertices given by points $\{z_n\}_{n=1}^N$. The SC package is not very accurate if the regions in question are very elongated, or have large protrusions. For the shapes 'close' to circular shapes we have used the SC algorithm. For more complex shapes (e.g. fish) we have used the zipper algorithm.

There are several advantages to the 'zipper' algorithm. First of all, it is very fast and can handle a large number of points (up to $10,000$). Secondly, the resulting conformal map is a composition of elementary transformations (linear fractional maps, squares and square roots), which can be computed with high accuracy and can be inverted explicitly.

There are several versions of the 'zipper' algorithm. The one that we will use is the geodesic 'zipper' algorithm. It computes the conformal map between a disk and a domain, bounded by a C^1 curve, that goes through the points $\{z_n\}_{n=1}^N$.

When contructing the fingerprint, we would need to have an appropriate sampling of θ^{ext} and θ^{int}, which will give a dense enough sampling in terms of the arclength on the curve. In Figure 5.5 you can see that spacing of θ^{int} could be of the order of 10^{-8}. This will pose some problems, which we are going to explain later in this chapter.

5.2 From fingerprints to shapes

After finding a geodesic path in the space of fingerprints we need to visualize how this path looks in the shape space. We use a fast and an easily implementable algorithm, based on the Hilbert transform.

The shape defined by $F(\theta) := f_{\text{ext}}(e^{i\theta}) = f_{\text{int}}(e^{i\theta}) \circ \Psi$ can be found as a solution of an integral equation

$$K(F) + F = e^{i\theta}, \tag{5.1}$$

where K is the following operator:

$$K(F)(\theta_1) = \frac{i}{2} \int_{S^1} \left(\cot\left(\frac{\theta_1 - \theta_2}{2}\right) - \Psi'(\theta_2) \cot\left(\frac{\Psi(\theta_1) - \Psi(\theta_2)}{2}\right)\right) F(\theta_2) d\theta_2.$$

We can discretize the linear operator K, using the fact that the Hilbert kernel could be integrated explicitly:

$$\int_a^b \cot(x/2)dx = 2\log\left|\frac{\sin(a/2)}{\sin(b/2)}\right|.$$

When $0 \in [a,b]$ the above integral should be taken in the principal value sense. The discretization of the linear operator K is then given by:

$$K_{\alpha,\beta} = 2\log\left|\frac{\sin(\theta^\alpha - \theta^{\beta+1/2})\sin(\Psi(\theta^\alpha) - \Psi(\theta^{\beta-1/2}))}{\sin(\theta^\alpha - \theta^{\beta-1/2})\sin(\Psi(\theta^\alpha) - \Psi(\theta^{\beta+1/2}))}\right|,$$

where $\theta^\alpha = 2\pi\alpha/N$, and $\theta^{\alpha+1/2} = (\theta^\alpha + \theta^{\alpha+1/2})/2$. By inverting operator $I+K$ in the equation (5.1) we will find the shape $F(\theta)$. For details refer to [SM06].

5.3 Geodesic finding

5.3.1 Energy discretization

Given two shapes represented by fingerprints $\Psi_0(\theta)$ and $\Psi_1(\theta)$, we are looking for a geodesic path $\Psi(\theta,t) \in \mathbf{Diff}(S^1)$, such that $\Psi(\theta,0) = \Psi_0(\theta)$ and $\Psi(\theta,1) = \Psi_1(\theta)$, which minimizes the length of the path

$$L(\Psi_0,\Psi_1) = \int_0^1 \|\Psi_t(\Psi^{-1}(\theta,t),t)\|_{WP}dt.$$

Here, $\Psi^{-1}(\theta,t)$ is the inverse in θ variable, i.e. for any fixed t we have $\Psi(\Psi^{-1}(\theta,t),t) = \Psi^{-1}(\Psi(\theta,t),t) = \theta$.

It turns out ([MD10]) that minimizing the path length $L(\Psi_0,\Psi_1)$ is equivalent to minimizing the WP energy, $E(\Psi_0,\Psi_1)$:

$$E(\Psi_0,\Psi_1) = \int_0^1 \|\Psi_t(\Psi^{-1}(\theta,t),t)\|^2_{WP}dt. \tag{5.2}$$

To make the computation of the gradient of the above energy more convenient, we use the following identity (which is easy to check):

$$\Psi_t(\Psi^{-1}(\theta,t),t) = -\frac{(\Psi^{-1})_t(\theta,t)}{(\Psi^{-1})_\theta(\theta,t)}. \tag{5.3}$$

Therefore instead of minimizing (5.2), we need to minimize

$$E(\Psi_0,\Psi_1) = \int_0^1 \left\| \frac{\Psi_t^{-1}(\theta,t)}{\Psi_\theta^{-1}(\theta,t)} \right\|_{WP}^2 dt. \tag{5.4}$$

We denote the inverse of the fingerprint $\Psi^i(\theta,t) := \Psi^{-1}(\theta,t)$. We have the following discretization: the time $t \in [0,1]$ is discretized at equally-spaced points $t_k = \frac{k}{M}$, for $k = 0,\ldots,M$. We discretize the variable $\theta \in [0,2\pi]$ into N uniformly-spaced points $\theta_l = 2\pi l/N$, for $l = 0,\ldots,N-1$. We will always use $M = 2^m$ and $N = 2^n$ for suitable n and m. The geodesic path $\Psi^i(\theta,t)$ will be represented as a set of $N \times (M+1)$ points: $\{\Psi^i(\theta_l,t_k)\}_{lk}$, for $l = 0,\ldots,N-1$ and $k = 0,\ldots,M$.

For the computation of the energy (5.4) it is convenient to use the shifted time grid, denoted t_s. The grid is defined as $t_s = \frac{1}{2M} + \frac{s}{M}$, for $s = 1,\ldots,M$. Therefore the points of the grid t_s are the midpoints between those of the grid t_k. Denote $t_{s-} = t_s - \frac{1}{2M}$ and $t_{s+} = t_s + \frac{1}{2M}$, i.e. $t_{s\pm}$ coincide with the points of the original grid t_k. Discretized version of the initial and target fingerprint we will denote $\widetilde{\Psi}_0$ and $\widetilde{\Psi}_1$ respectively.

Therefore we have the discretizations of the derivatives

$$\Psi_\theta^i(\theta_k,t_s) = \frac{1}{2}\left(\frac{\Psi^i(\theta_{k+1},t_{s+}) - \Psi^i(\theta_{k-1},t_{s+})}{4\pi/N} + \frac{\Psi^i(\theta_{k+1},t_{s-}) - \Psi^i(\theta_{k-1},t_{s-})}{4\pi/N} \right),$$

$$\Psi_t^i(\theta_k,t_s) = \frac{\Psi^i(\theta_k,t_{s+}) - \Psi^i(\theta_k,t_{s-})}{1/M}.$$

Thus we obtain the following discretization of the velocity of the geodesic path (see

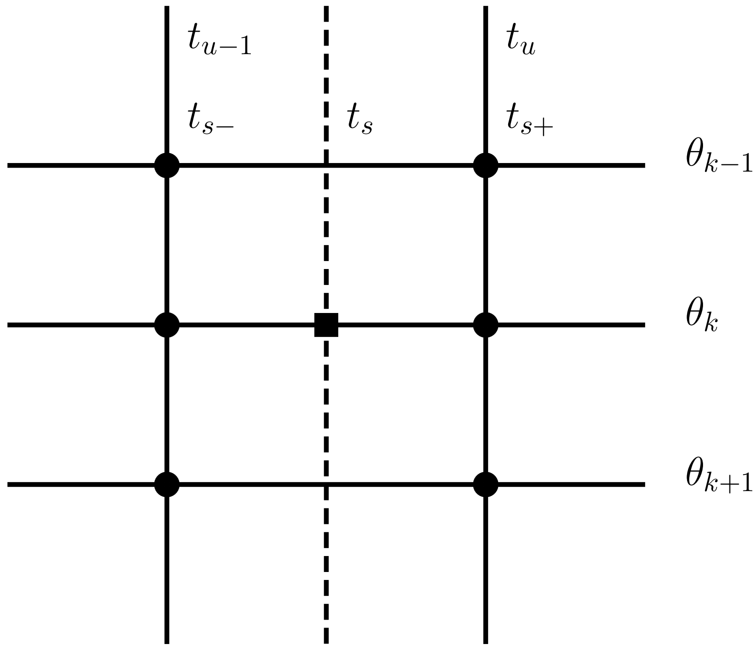

Figure 5.1: The value of $\frac{\Psi^i_t(\theta_k,t_s)}{\Psi^i_\theta(\theta_k,t_s)}$ is computed at the point marked by the square, using values of the fingerprint $\Psi^i(\theta_l, t_s)$ at points marked by dots.

Figure 5.1):

$$\frac{\Psi^i_t(\theta_k, t_s)}{\Psi^i_\theta(\theta_k, t_s)} = \frac{8\pi M}{N} \frac{\Psi^i(\theta_k, t_{s+}) - \Psi^i(\theta_k, t_{s-})}{\Psi^i(\theta_{k+1}, t_{s+}) - \Psi^i(\theta_{k-1}, t_{s+}) + \Psi^i(\theta_{k+1}, t_{s-}) - \Psi^i(\theta_{k-1}, t_{s-})}$$

To compute the discretized version of the WP norm we will need to use a discrete Fourier transform. If, in general, velocity has the following Fourier expansion

$$\frac{\Psi^i_t(\theta, t)}{\Psi^i_\theta(\theta, t)} = \sum_{n=-\infty}^{\infty} a_n(t) e^{in\theta},$$

then its WP norm will be simply

$$\left\| \frac{\Psi^i_t(\theta, t)}{\Psi^i_\theta(\theta, t)} \right\|^2_{WP} = \sum_{n=-\infty}^{\infty} |a_n(t)|^2 |n^3 - n|.$$

Using the discrete Fourier transform:

$$\frac{\Psi_t^i(\theta_k, t_s)}{\Psi_\theta^i(\theta_k, t_s)} = \frac{1}{N}\sum_{n=0}^{N/2} a_n(t_s) e^{2\pi i n k/N}, \quad a_{N-n}(t_s) = \overline{a_n(t_s)}.$$

Now everything is set to compute the geodesic $\{\Psi^i(\theta_l, t_k)\}_{lk}$. For that we need to minimize the discretized version of the energy (5.4) (up to a multiplicative constant):

$$\widetilde{E}(\widetilde{\Psi}_0^i, \widetilde{\Psi}_1^i) = \sum_{s=1}^{M}\sum_{n=2}^{N-2} |a_n(t_s)|^2 (n^3 - n).$$

5.3.2 Computing the gradient of the energy

For minimizing the energy we need to have the expression for the gradient. It will be used in the gradient descent or the conjugate gradient algorithms. Denote $\widetilde{E} := \widetilde{E}(\widetilde{\Psi}_0^i, \widetilde{\Psi}_1^i)$, $\Psi_{ku}^i = \Psi^i(\theta_k, t_u)$ and $\Psi_{k,s\pm}^i = \Psi^i(\theta_k, t_{s\pm})$.

Define $\{w_l\}_{l=0}^{N-1}$ to be an inverse discrete Fourier transform of $\{\widehat{w}_l\}_{l=0}^{N-1}$. In other words,

$$w_l = \sum_{k=0}^{N-1} \widehat{w}_k e^{2\pi i k l/N},$$
$$\widehat{w}_l = \tilde{k}^3 - k, \text{ where } \tilde{k} = \min(k, N-k).$$

Action of the WP operator in the Fourier domain amounts to multiplying by $|n^3 - n|$, therefore after the inverse discrete Fourier transform this will correspond to a convolution. In other words,

$$\widetilde{E} = \sum_{i,j,s} w_{i-j}\, v_{j,s}(\Psi^i)\, v_{i,s}(\Psi^i), \text{ where } v_{k,s} := \frac{\Psi_t^i(\theta_k, t_s)}{\Psi_\theta^i(\theta_k, t_s)}. \tag{5.5}$$

Hence we can compute the gradient

$$\frac{\partial \widetilde{E}}{\partial \Psi^i_{k,u}} = 2 \sum_{i,j,s} w_{i-j}\; v_{j,s}\, \frac{\partial v_{i,s}}{\partial \Psi^i_{k,u}}. \tag{5.6}$$

Notice that for each fixed entry (k,u) the derivative $\partial v_{i,s}/\partial \Psi^i_{k,u}$ will be non-zero only for six (j,s) entries. Specifically, when $j = k, k \pm 1$, and when $s_+ = u$ and $s_- = u$.

5.3.3 Choosing a representative fingerprint

Recall that each shape is represented by a fingerprint $\Psi \in \mathrm{PSL}_2(\mathbb{R})\backslash \mathbf{Diff}(S^1)$, or equivalently by its inverse $\Psi^i \in \mathbf{Diff}(S^1)/\mathrm{PSL}_2(\mathbb{R})$. The geodesic in the coset space $\mathbf{Diff}(S^1)/\mathrm{PSL}_2(\mathbb{R})$ will have the form $\Psi^i(t)\cdot \mathrm{PSL}_2(\mathbb{R})$, in other words, it is a geodesic path in the space of left cosets of $\mathrm{PSL}_2(\mathbb{R})$. For any map $A \in \mathrm{PSL}_2(\mathbb{R})$, $\Psi^i \circ A$ will also be a fingerprint for the same shape. Weil-Petersson energy doesn't 'see' changes that happen in the vertical space $psl_2(\mathbb{R})$. This creates an ambiguity in the geodesic $\Psi^i(\theta, t)$, thus we need to choose a representative fingerprint in the coset space. For any fingerprint Ψ^i we can find a unique map $A \in \mathrm{PSL}_2(\mathbb{R})$ such that $\hat{\Psi}^i = \Psi^i \circ A$ will fix three prescribed angles. The fingerprint $\hat{\Psi}^i$ will be called a normalized fingerprint.

Three prescribed angles that the normalized fingerprint will fix are $-\pi, \alpha, \beta$. In general the map $A(z) \in \mathrm{PSL}_2(\mathbb{R})$ that preserves the unit circle will have the form:

$$A(z) = \frac{az + b}{\bar{b}z + \bar{a}}, \quad |a|^2 - |b|^2 = 1,$$

where $a = a_1 + ia_2$, $b = b_1 + ib_2$. If one takes $z = e^{i\theta}$, then we get a map on the circle:

$$\tan(A(\theta)/2) = \frac{(a_2 + b_2) + (a_1 - b_1)\tan(\theta/2)}{(a_1 + b_1) - (a_2 - b_2)\tan(\theta/2)}.$$

We construct a fingerprint using the 'zipper' algorithm such that $\Psi^i(-\pi) = -\pi$. By taking $a_2 = b_2$ we guarantee that $A(-\pi) = -\pi$, therefore $\hat{\Psi}^i(-\pi) = -\pi$. We need to specify two more constraints. We take:

$$A(\theta) = 2\arctan(c + d\tan\theta/2),$$

where $A(-\pi) = -\pi$ for any $c, d > 0 \in \mathbb{R}$. We choose c, d such that $\Psi^i \circ A(\alpha) = \alpha$ and $\Psi^i \circ A(\beta) = \beta$. Such c and d are given by the solution of the system:

$$\begin{aligned} c + d\tan\frac{\alpha}{2} &= \tan\frac{\Psi(\alpha)}{2}, \\ c + d\tan\frac{\beta}{2} &= \tan\frac{\Psi(\beta)}{2}. \end{aligned}$$

Notice, on the right-hand side we have $\Psi(\theta) = (\Psi^i)^{-1}(\theta)$. The above system has a unique solution for $\alpha \neq \beta$. In the minimization of energy we have used angles $\alpha = -\pi/4$, $\beta = \pi/2$.

5.3.4 Minimizing the energy

Given two fingerprints $\Psi_0^i(\theta)$ and $\Psi_1^i(\theta)$, we are looking for the geodesic path that connects them and minimizes the WP energy. We start the minimization with the coarse grid $M = 8, N = 32$. The initial guess for the geodesic would be a circle, whose normalized fingerprint is the identity map. In other words the initial guess is:

$$\begin{aligned} &\Psi^i(t_u, \theta_k) = \theta_k, \text{ for } u = 1, \ldots, M-1, k = 0, \ldots, N-1, \\ &\Psi^i(0, \theta_k) = \Psi_0^i(\theta_k), \\ &\Psi^i(1, \theta_k) = \Psi_1^i(\theta_k). \end{aligned}$$

After the minimum is achieved at the coarse grid $M = 8, N = 32$ we pass to the finer grid with the same time discretization $M = 8$, but θ is now discretized with $2N = 64$ points. The geodesic path from minimization on the coarser grid will be used as an initial guess for the fine grid. We continue this process until we reach a sufficient level of discretization in theta. In all the cases presented in this thesis, the finest grid had $N = 256$ points, unless otherwise specified.

Gradient descent

At every step of the algorithm we start with some approximation of the geodesic path $g(\theta_k, t_u)$ and compute the gradient ∇E according to (5.6). Then we update $g_{\text{new}}(\theta_k, t_u) = g_{\text{old}}(\theta_k, t_u) - \lambda \nabla E$. Traditionally in the minimization procedures, λ is chosen using some kind of a line search algorithm. This algorithm searches for the minimum of some function f in the direction of v, i.e. finds λ that minimizes $f(x + \lambda v)$, for some fixed starting point x in the direction given by the vector v. In our case the function f is the Weil-Petersson energy, and the vector v is the negative of the gradient.

In our numerical experiments it turned out that the multiple evaluations of energy in the line search procedure greatly slowed down the convergence. Instead we decided to use constant λ, thus making constant steps in the direction of the negative gradient. If the energy decreases we continue with chosen λ; if the energy increases, we roll back by one step, and try again in the same direction, but with $\lambda_{\text{new}} = \lambda/2$. We set the minimal λ to be Matlab's machine precision, which is $2.2 \cdot 10^{-16}$.

Conjugate gradient

The conjugate gradient algorithm for minimizing the energy is an improvement over the gradient descent method. We will briefly describe it. For a thorough treatment refer to [PTVF07].

In the gradient descent procedure, the new gradient will always be perpendicular to the previous one. This slows down the minimization of the energy. The conjugate gradient algorithm chooses a different minimization direction, which will be conjugate to the previous one, and will lead to the minimum faster than pure gradient descent.

The m-th update step is

$$g_{\text{new}}(\theta_k, t_u) = g_{\text{old}}(\theta_k, t_u) + \lambda h_m.$$

Here, h_m substitutes the gradient of the energy and is computed using the previous value h_{m-1} and values of the energy gradient ∇E at m-th and $(m-1)$-st step:

$$h_m = \nabla E_m + \frac{\nabla E_m \cdot \nabla E_m}{\nabla E_{m-1} \cdot \nabla E_{m-1}} h_{m-1}.$$

At the first step $h_0 = -\nabla E_0$. The value of λ, as in the previous case, is fixed. If the energy on the next step becomes larger, we roll back one step to half λ and try again. The algorithms stops when we achieved the minimum λ, which is set to be the machine precision in Matlab, $2.2 \cdot 10^{-16}$ in our case.

In Table 5.1, one can see the computational times of gradient descent and conjugate gradient algorithms with various initial guesses. Conjugate gradient (CG) outperforms the gradient descent (GD) exactly because of the reasons described above: it chooses a better descent direction and arrives at the minimum faster.

In the simulations presented below (except for the comparison Table 5.1), we have used a combination of gradient descent and conjugate gradient methods. First we apply the CG method, and if the CG algorithm can not proceed any further, we switch to the gradient descent. The number of minimization iterations at each refinement level was capped by 10^6 steps.

5.3.5 Local minimum

In general, the gradient (or conjugate gradient) descent procedure does not guarantee that we will arrive at the global minimum of the energy. The algorithm could get stuck in the local minimum. Depending on where we start — in other words, depending on the initial guess for the geodesic — we might end up at different local minima.

To address this issue we will start a minimization of the WP energy with four different initial guesses for the geodesic:

- Guess [1]. All intermediate shapes are the same as the first shape.
- Guess [2]. All intermediate shapes are the same as the second shape.
- Guess [linear]. Intermediate shapes are represented by the fingerprint $\Psi(\theta, t_u) = (1 - t_u)\Psi_1 + t_u\Psi_2, t_u = u/M, u = 1, \ldots, M - 1$.
- Guess [circle]. Intermediate shapes are circles.

We have computed four geodesics, using four different initial guesses, between a horizontal ellipse and an ellipse rotated clockwise by $\pi/3$ from the horizontal one. All of them have eccentricity $e = a/b = 2$. The resulting geodesics turned out to be visually the same (see Figure 5.10). In Table 5.2 you can see L^1-errors that we get, if we start off with four different initial guesses. In Table 5.1 you can see the comparison of energies and the run times. This example does not prove per se that in general we will end up at the global minimum, but we argue that we can choose a linear guess for the geodesic and get a minimal path, and the resulting path would not differ from other minimal paths if we had chosen a different initial guess.

Guess	[1]	[2]	[circle]	[linear]
Energy (GD)	5.328	5.328	5.328	5.3287
Time (GD), sec	2305	2400	1800	1650
Energy (CG)	5.3208	5.3208	5.3208	5.3208
Time (CG), sec	322	286	207	161

Table 5.1: Comparison of WP energies and run-times of minimizations using various initial guesses. The computed geodesic connects horizontal ellipse and an ellipse rotated clockwise by $\pi/3$ from the horizontal one, eccentricity $a/b = 2$ (see Figure 5.10). The row 'Time (GD)' is the computational time of the gradient descent algorithm, row 'Time (CG)' is the computational time of the conjugate gradient algorithm.

Guess	$\Psi^{[1]}$	$\Psi^{[2]}$	$\Psi^{[circle]}$	$\Psi^{[linear]}$
Initial guess	1.5083	1.4138	1.1954	0.3236
Final geodesic	$6.8 \cdot 10^{-4}$	$3.8 \cdot 10^{-4}$	$6.0 \cdot 10^{-4}$	0

Table 5.2: The L^1 error between the final geodesic using the linear initial guess and other paths. First line is the L^1 error between initial guesses and the final geodesic path $\Psi^{[linear]}(\theta, t)$. Second line is the L^1 error between final geodesic paths when starting with different initial guesses and the final geodesic path $\Psi^{[linear]}(\theta, t)$. The computed geodesic connects horizontal ellipse, $e = 2$, and an ellipse rotated clockwise by $\pi/3$ from the horizontal one (see Figure 5.10).

5.3.6 Geodesic triangle

In Figure 5.2 we heuristically depicted the local geometry of the shape space. At the vertices are three ellipses: the first one is horizontal, the second one tilted by $\pi/3$ counterclockwise and the third one tilted by $2\pi/3$ counterclockwise from the horizontal ellipse. The semi-major axis is $a = 2$ and the semi-minor axis is $b = 1$, thus the eccentricity is $e = b/a = 2$. On the lines connecting the vertices you can see the shapes, corresponding to the geodesic path connecting respective shapes.

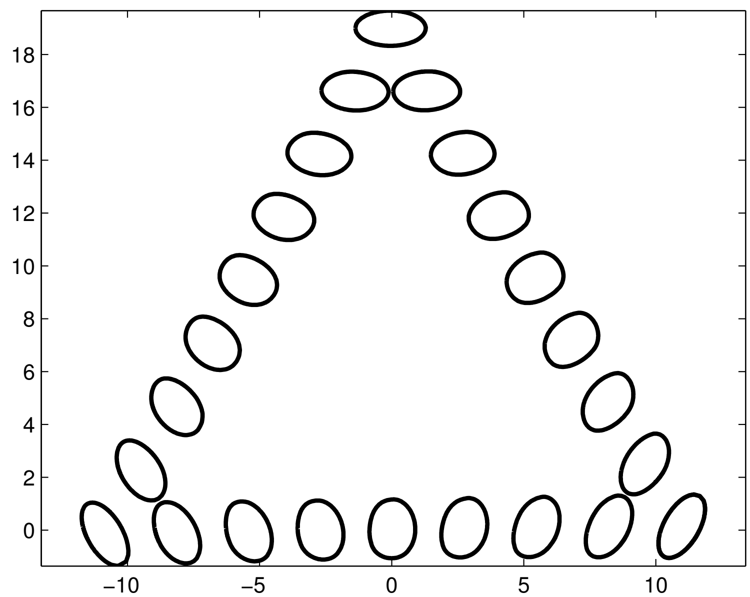

Figure 5.2: A geodesic triangle. Shapes along the edges represent the geodesics between the shapes, depicted at vertices. Notice the reversion to more circular shapes in the middle of geodesics.

Geodesics are not just rotations of one ellipse to another. Rotation of the shape is represented by shifting of the fingerprint. This shifting preserves the high-frequency Fourier coefficients. So the path that has a pure rotation in it will cost more in the WP metric, since we have $|n^3 - n|$ term in the metric. Therefore the geodesic 'smooths' the shape out, preferring to shift in lower frequencies.

This property of the WP metric manifests itself in the fact that the 'mean' shapes — shapes in the middle of the geodesic — tend to be more circular than the ellipses we started with. We can picture a circle shape being in the center of this triangle and the sides of the triangle bending toward the circle, thus exhibiting the typical shape of the triangle in the negatively curved space. Below we compute the angles in the corners of the geodesic triangle and show that they sum to less than π.

Given a geodesic $\Psi(t)$ connecting two shapes Ψ_1 and Ψ_2 we can obtain two velocity vectors $v_{12} = (\Psi(\Delta t) - \Psi(0))/\Delta t, v_{21} = (\Psi(1-\Delta t) - \Psi(1))/\Delta t$. They lie in their corresponding tangent spaces to the manifold of fingerprints M, i.e. $v_{12} \in T_{\Psi_1}M, v_{21} \in T_{\Psi_2}M$. A vector and an initial point uniquely determine a geodesic. The two vectors v_{12}, v_{21} are initial vectors for their corresponding geodesics, i.e. if we start at shape Ψ_1 with the initial velocity v_{12} and trace the geodesic, then at time $t = 1$ (given the appropriate scaling of the vector v_{12}) we will arrive at the second shape Ψ_2. Conversely, starting at shape Ψ_2 with initial velocity v_{21} we 'shoot' a geodesic, and at time $t = 1$ we will get a first shape Ψ_1. If we have a third shape Ψ_3 and two geodesics connecting first and second shape to Ψ_3 we obtain six vectors $v_{12}, v_{13}, v_{21}, v_{23}, v_{31}, v_{32}$ in their respective tangent spaces. These vectors allow us to measure a local geometry of the shape space. Just like in a Euclidean space, we can find angles between vectors, say v_{12} and v_{13}. Thus we can find an angle α_1 at one vertex of the geodesic triangle in Figure 5.2. To be specific:

$$\alpha_1 = \arccos \frac{\langle v_{12}, v_{13}\rangle_{\Psi_1}}{\|v_{12}\|\|v_{13}\|}, \tag{5.7}$$

$$\langle v_{12}, v_{13}\rangle_{\Psi_1} = \left\langle v_{12}.(\Psi_1^{-1})_\theta, v_{13}.(\Psi_1^{-1})_\theta \right\rangle_e$$

Remember, the vectors v_{12}, v_{13} lie in the tangent space $T_{\Psi_1}M$. In order to compute their norm or the WP product between them, we need to translate vectors back by

	α_1	α_2	α_3	$\alpha_1+\alpha_2+\alpha_3$
radians	0.73579	0.7358	0.73562	2.2072
degrees	42.1576°	42.1583°	42.1478°	126.5°
energy of the side opposite to α_k	5.2693	5.2674	5.2671	

Table 5.3: Angles α_k of the geodesic triangle on Figure 5.2.

Ψ_1^{-1} to the tangent space at the identity T_eM. This can be done by right or left translations. If shapes Ψ_k are given by fingerprints in $\mathbf{Diff}(S^1)/\mathrm{PSL}_2(\mathbb{R})$ (that is the case for the minimization of WP energy), then the translation in (5.7) is carried by left translations. See Subsection 5.3.1 for details. At the identity the WP inner product is simply $\langle u, v\rangle_e = \int_{S^1} Lu.vd\theta = \int_{S^1} Lv.ud\theta$.

Similarly to (5.7), we compute the angles α_2 and α_3. In the case depicted in Figure 5.2, shape 1 is a horizontal ellipse, shape 2 is the ellipse rotated clockwise by $\pi/3$, and shape 3 is the ellipse rotated clockwise by $2\pi/3$ from the horizontal. The table 5.3 has the angles α_k in the vertices of the geodesic triangle.

Notice that the sum of all three angles is less than π. This is characteristic of the negatively curved spaces, and we have shown experimentally that it holds true.

The choice of normalization

It should be noted that the author had to choose a particular normalization of fingerprints to achieve the desired results. In Figure 5.3 one can see that for the fingerprint normalization that fixes angles $\alpha = -\pi/4, \beta = \pi/2$ we obtained three ellipses that were not rotations of each other. This is another disadvantage of using uniform grid in θ^{int}-variable (disadvantages of the uniform sampling in θ^{int} will be explored in Subsection 5.3.7). The above normalization changed fingerprints of the tilted ellipses by 'stretching' some parts and 'squeezing' others. Thus it changed density of sampling points on two tilted shapes, but did not alter significantly the density of points on the horizontal ellipse. Energies of the three geodesic paths were $5.5741, 5.3117, 5.7032$, and the opposite angles turned out to be $43.5°, 38.2°, 44.2°$.

In Figure 5.4 we have the normalization, that gave us the results in Table 5.3. Observe that the values of energy changed by about $5-7\%$, when the normalization changed. Thus normalization does not have a big impact on distances, but if one wants to measure fine effects, such as curvature, one should pay attention to the proper choice of the normalization. This is one of the disadvantages of using the uniform grid. More fundamental problem with the uniform grid will be discussed in Subsection 5.3.7.

5.3.7 Uniform vs. non-uniform grid

In the energy minimization we have discretized the fingerprint Ψ on the uniform grid. This allowed us to efficiently compute the WP energy by employing the fact that WP energy has a simple expression in the Fourier domain: $\|v\|^2_{wp} = \sum_n |n^3 - n||v_n|^2$. This was sufficient for shapes that we have encountered so far: ellipses, squares and rectangles. However, if we take the outline of a fish (see Figure 5.5) it turns out that uniform discretization in the θ^{int} domain (y-axis) is not enough to resolve the shape.

Let us elaborate. Recall that fingerprints can be written in two equivalent forms:

$$\Psi^i(\theta^{\text{int}}) = \theta^{\text{ext}}, \quad \Psi(\theta^{\text{ext}}) = \theta^{\text{int}}.$$

We can write the energy of the path using both representations, Ψ and Ψ^i:

$$\int_0^1 \left\|\Psi_t(\Psi^{-1}(\theta,t),t)\right\|^2_{wp} dt = \int_0^1 \left\|\frac{\Psi^i_t(\theta,t)}{\Psi^i_\theta(\theta,t)}\right\|^2_{wp} dt.$$

Notice that the domain under the integration sign is always θ^{int}, no matter which

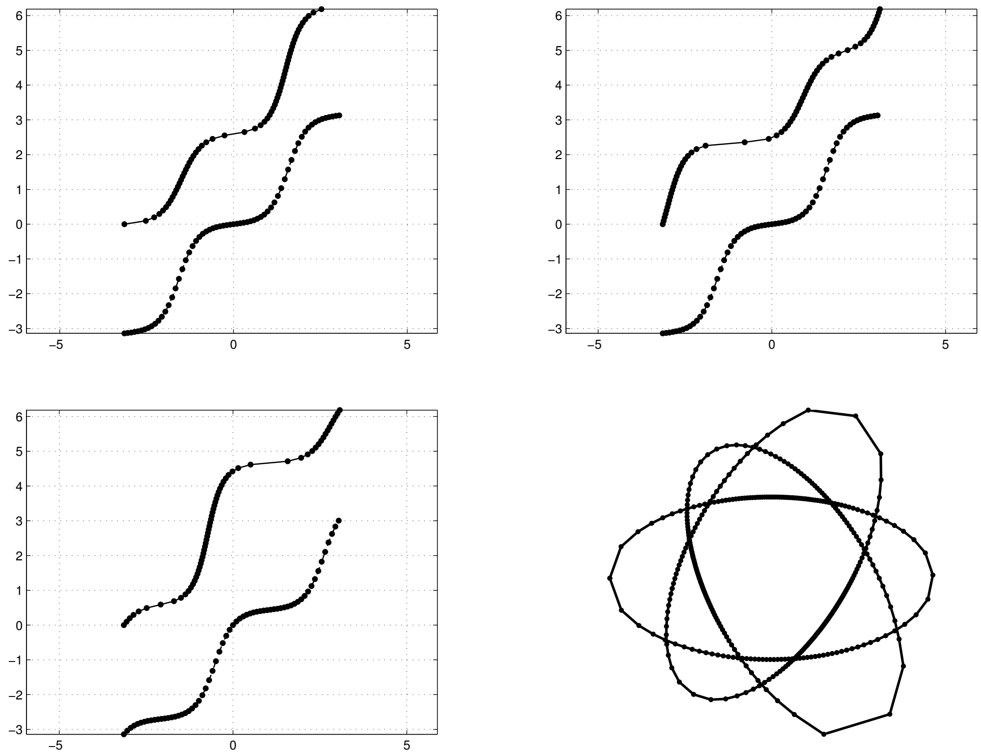

Figure 5.3: Incorrect normalization of fingerprints of ellipses for the geodesic triangle. Normalized fingerprint is plotted above the non-normalized fingerprint. Fingerprints were normalized to fix angles $-\pi, -\pi/4, \pi/2$. Every fourth point is shown to emphasize non-uniform distribution of points. Notice how two tilted ellipses become non-symmetric with the given normalization, while the horizontal one remains symmetric. Therefore the three ellipses are not rotations of each other.

representation we use. That means that for the minimization procedure we have implemented, we need to make a uniform grid in θ^{int} domain.

We have taken the fish shape from Figure 5.5, represented by uniformly-spaced points and constructed conformal maps $\phi_{\text{ext}}, \phi_{\text{int}}$. In Figure 5.6 you can see the log-plot of boundary derivatives $\partial\theta^{\text{ext}}(s)/\partial s = \partial\phi_{\text{ext}}^{-1}(s)/\partial s$ and $\partial\theta^{\text{int}}(s)/\partial s = \partial\phi_{\text{int}}^{-1}(s)/\partial s$. The function ϕ_{ext} is rather benign, as evidenced by the plot of the derivative. In contrast, the derivative $\partial\theta^{\text{int}}(s)/\partial s$ exhibits very small and very large derivatives.

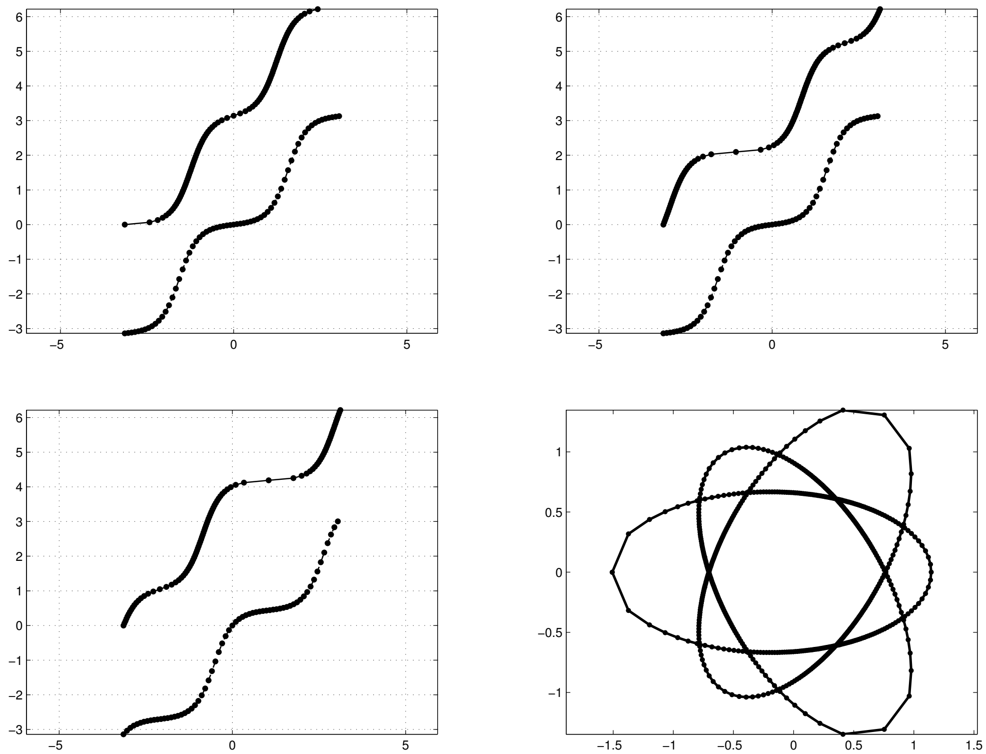

Figure 5.4: Correct normalization of fingerprints for the geodesic triangle. Normalized fingerprint is plotted above from the non-normalized fingerprint. Fingerprints were normalized to fix angles $-\pi, -\pi/3, \pi/3$. Every fourth point is shown to emphasize non-uniform distribution of points. Notice that here three ellipses are rotations of each other.

The ratio between the smallest and the largest derivative is of the order 10^8. The smallest spacing of the θ^{ext} is $1.2 \cdot 10^{-3}$, the smallest spacing of the θ^{int} is $1.5 \cdot 10^{-8}$. This behavior of boundary derivatives is seen not only for this particular shape, but for almost all the fish shapes. And in general, the more elongated the shape is, the smaller the derivative $\partial\theta^{\text{int}}(s)/\partial s$ gets. The influence of the local geometry — in particular the curvature of the shape — affects derivatives of the boundary maps as well, as could be seen in formula (1.2), Subsection 1.3.3.

The above points to the fact that uniform sampling of θ^{int} is inadequate for

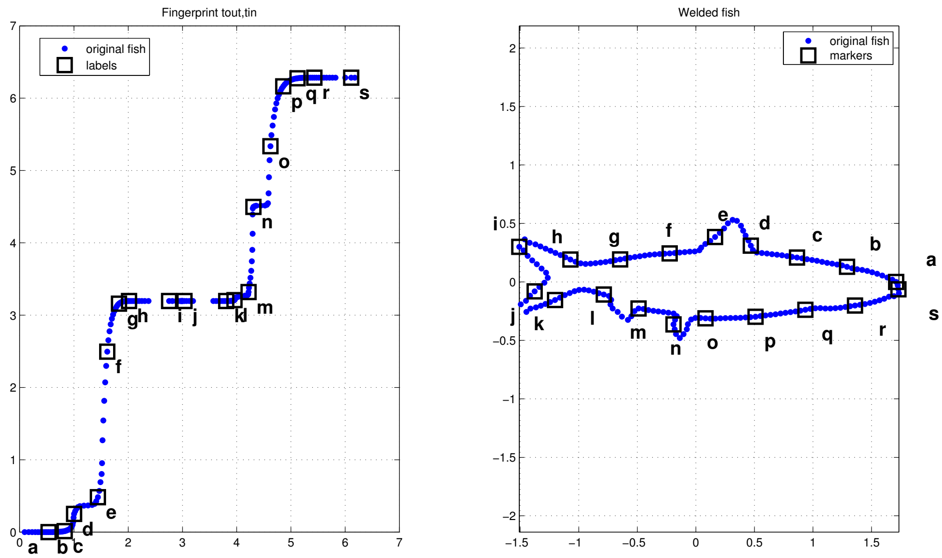

Figure 5.5: The outline of the fish and its fingerprint. Corresponding points on the fish and the fingerprint are marked by squares and labeled by letters from ‘a’ to ‘r’. The smallest spacing of θ^{ext} is $1.2 \cdot 10^{-3}$, the smallest spacing of θ^{int} is $1.5 \cdot 10^{-8}$.

representing shapes with low and high derivatives of $\theta^{\text{int}}(s)$, as in the case of a fish. Almost any shape that is not close to a circular shape will exhibit this trait. In Figure 5.7 you can see the fingerprint of the fish from Figure 5.5, and the shape, reconstructed from the corresponding fingerprint. We used 100 and 1000 points, spaced uniformly in the θ^{int} domain. The tail and head of the fish are not resolved properly, because these parts correspond to parts of the fingerprint with very small derivatives. Hence when we are taking uniform grid in the range θ^{int}, we cannot resolve the tail and the head of the fish. Even 1000 points is not enough to resolve the shape. That is no surprise, since the $\theta_k^{\text{int}} = \phi_{\text{int}}^{-1}(\Gamma_k)$ in general has much worse behavior (extremely large and extremely small derivatives), than $\theta_k^{\text{ext}} = \phi_{\text{ext}}^{-1}(\Gamma_k)$. It is possible to find a shape, such that $\{\theta_k^{\text{ext}}\}$ also has very large and very small derivatives, but for a wider variety of shapes behavior of θ^{ext} is decent. Given the estimates of the derivative of $\theta^{\text{int}}(s)$, we conclude that we need to have about 10^8

points to give a fair representation of such a shape as a fish. This is impractical from the computational perspective.

The solution to this problem will be to devise a numerical minimization scheme that deals with a non-uniform grid in θ^{int}-domain. That means that we cannot use discrete Fourier transform to compute the Weil-Petersson energy. Fourier transform on the non-uniform grid is slow and not very accurate. In this case we need to compute the WP operator L explicitly, by taking derivatives and applying a Hilbert transform. Another approach would be to use singular solutions of the EPDiff(S^1), Teichons, to approximate the geodesic path. Teichon solutions are also geodesic paths in $\mathrm{PSL}_2(\mathbb{R})\backslash\mathbf{Diff}(S^1)$. We have seen in Chapter 3 that Teichon evolution is governed by a simple system of odinary differential equations. Trajectories of $a_k(t)$'s and $b_k(t)$'s will give us the trajectory $v(t) = \sum_{k=1}^{N} a_k G(\theta - b_k)$. By integrating this velocity field we will obtain a geodesic in the fingerprint space, and hence equivalently we will get a geodesic in the shape space. In Chapter 3 we argued that by using a relatively small number of Teichons, we can get a wide variety of shapes with fingerprints that would have very large and very small derivatives. But in this case, this is not an issue, since we do not need to compute the L operator at all. The Teichon integration case eliminates the issue of the local minimum in the minimization of WP energy as well. The trajectory $a_k(t), b_k(t)$ is the geodesic, up to the precision of the numerical scheme, used for integration.

In Chapter 3 we have presented a numerical scheme to solve an initial value problem, i.e. given an initial velocity, find the geodesic path. Finding geodesics is the boundary value problem: given two shapes, what is the velocity with which we should launch the geodesic from the first shape to get to the second shape. Therefore in order to apply Teichons to the geodesic-finding problem some modification of the shooting method should be used, or a boundary value problem should be reformulated in terms of singular solutions of EPDiff.

5.4 Sectional curvature

In Section 4.1 we have demonstrated the following formula, relating the norm of the Jacobi vector fields and sectional curvature:

$$\langle J(t), J(t)\rangle_{g(t)} = \langle w, w\rangle t^2 - K(v,w)\frac{t^4}{3} + O(t^5), \tag{5.8}$$

where $J(t) = (d\exp_P)_{tv}(tw)$ is the Jacobi vector field along the geodesic $g(t) = \exp_P(tv)$ and $K(v,w)$ is the sectional curvature in the plane v, w. In other words, the Jacobi vector fields measure how the geodesic with initial vector v varies if we perturb it in the direction of w by a small amount, i.e. launch a geodesic with initial vector $v + s.w$, for some small s. For negative sectional curvature $K(v,w)$ there will be an excess of $-K(v,w)\frac{t^4}{3}$, when compared to the Euclidean case.

We are going to compute numerically the sectional curvatures $K(\sin(n\theta), \cos(n\theta))$ and compare them to the theoretical results in Figure 4.1. For this, we choose $v(\theta) = \cos(n\theta)/\|v\|_{WP}, w(\theta) = \sin(n\theta)/\|w\|_{WP}$, with $n = 2, \dots, 6$. For each fixed n we compute two geodesics $g_+(t) = \exp_{Id} t(v+s.w)$ and $g_-(t) = \exp_{Id} t(v-s.w)$ using forward integration described in Section 5.6. In our experiment we have chosen $s = .001$. Then we compute the Jacobi vector fields along the geodesic $g(t) = \exp_{Id}(tv)$:

$$J(t) = (g_+(t) - g_-(t))/(2s).$$

Notice that $J(t) \in T_{g(t)}(\mathrm{PSL}_2(\mathbb{R})\backslash\mathbf{Diff}(S^1))$. We then compute the WP norm of $J(t)$, bearing in mind that we need to translate it back to the identity by right translations:

$$\langle J(t), J(t)\rangle_{g(t)} = \langle J(t)\circ g^{-1}(t), J(t)\circ g^{-1}(t)\rangle_e$$

In Figure 5.8 we plotted $-3(\langle J(t), J(t)\rangle_{g(t)} - \langle w, w\rangle t^2)/t^4$ and the theoretical sectional curvature from (4.13). It is clear that the crude forward integration we used captures relatively well the geometry of the shape space, at least for some initial time t.

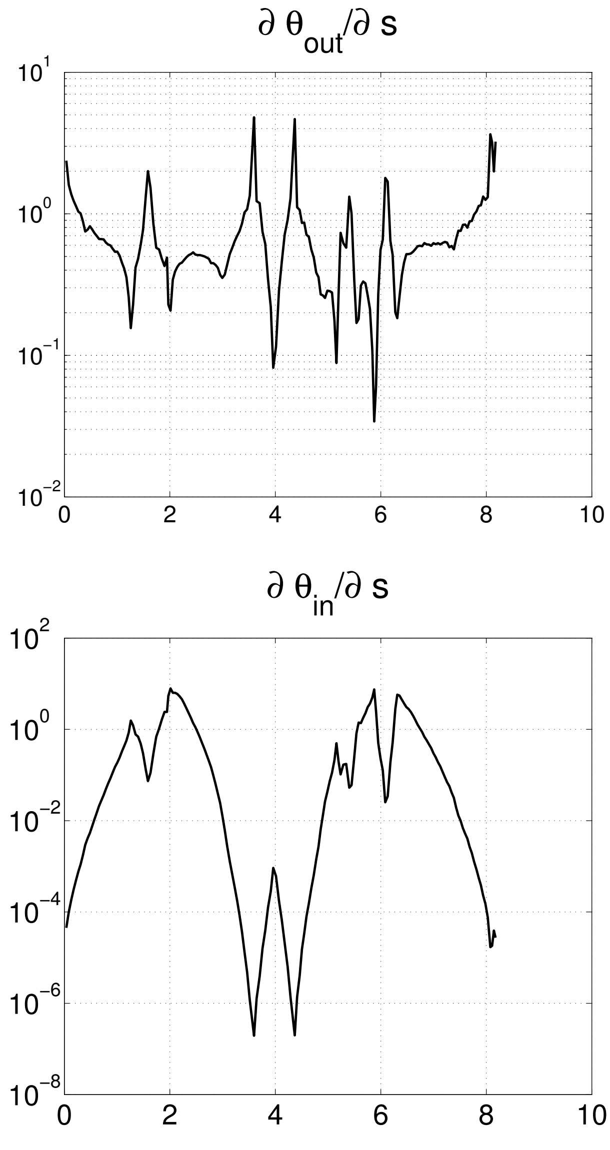

Figure 5.6: Log-plot of derivatives of $\theta^{\mathrm{ext}}(s)$ (top) and $\theta^{\mathrm{int}}(s)$ (bottom) with respect to the arclength s on the fish shape (Figure 5.5).

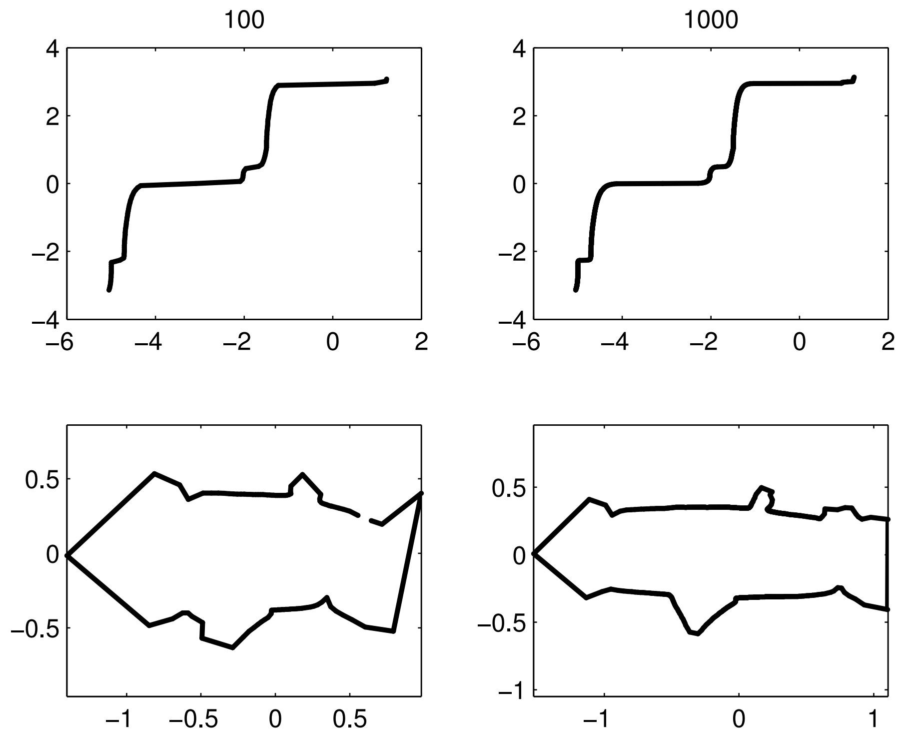

Figure 5.7: Uniform sampling of the fingerprint of the fish (Figure 5.5) with $N = 100$ points and the welded shapes (left column); $N = 1000$ points and the welded shape (right column).

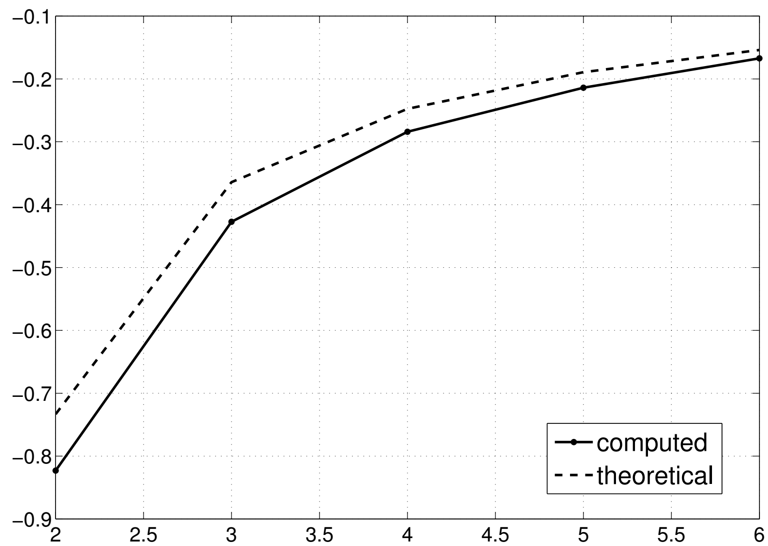

Figure 5.8: Comparison of the theoretical sectional curvature (dashed line), with the numerically computed sectional curvature $K(\cos(n\theta), \sin(n\theta))$.

5.5 Examples of geodesics

Below in Figures 5.9–5.17 are examples of geodesics obtained using the combination of conjugate gradient and gradient descent algorithms on the WP energy. The figures should be read from left to right, from top to bottom. The starting shape is in the upper left corner, the final shape is in the bottom right corner. Notice that in the middle of geodesics, shapes tend to be more circular than starting or final shapes. As we mentioned before, this is a reflection of the negative curvature of the shape space with the Weil-Petersson metric. This fact is especially pronounced for the pair of geodesics in Figures 5.9, 5.10. In the first figure ellipse with eccentricity $e = 1.5$ is morphed into the rotated one with the same eccentricity. In the second figure, the same geodesic is displayed for ellipses with $e = 2$. The middle shapes closely resemble ellipses with smaller eccentricities, $e = 1.2$ and 1.3 respectively. Both of them are rotated by $\pi/6$ counter-clockwise.

The energy of the path is displayed in the caption to each figure. It is exactly the squared length of the path connecting two shapes (see for example [MD10]). Intuitively, the larger the distance between shapes, the more 'different' should the shapes be in some sense. For example, compare the geodesics with rotated ellipses in Figures **??** and **??**. In the case of $e = 1.5$ the energy $E = 1.62$, for $e = 2$ the energy is $E = 5.2671$. It takes more energy to rotate more oblong ellipse, than the one with $e = 1.5$.

Moreover, the path from the circle to the square (Figure 5.13) is shorter than the path connecting the ellipse, $e = 1.5$, and the square (Figure 5.14), which is in turn shorter than the path from the ellipse, $e = 2$ to the square (Figure 5.15). The energies are $E = 2.80, E = 3.80$, and $E = 5.91$ respectively.

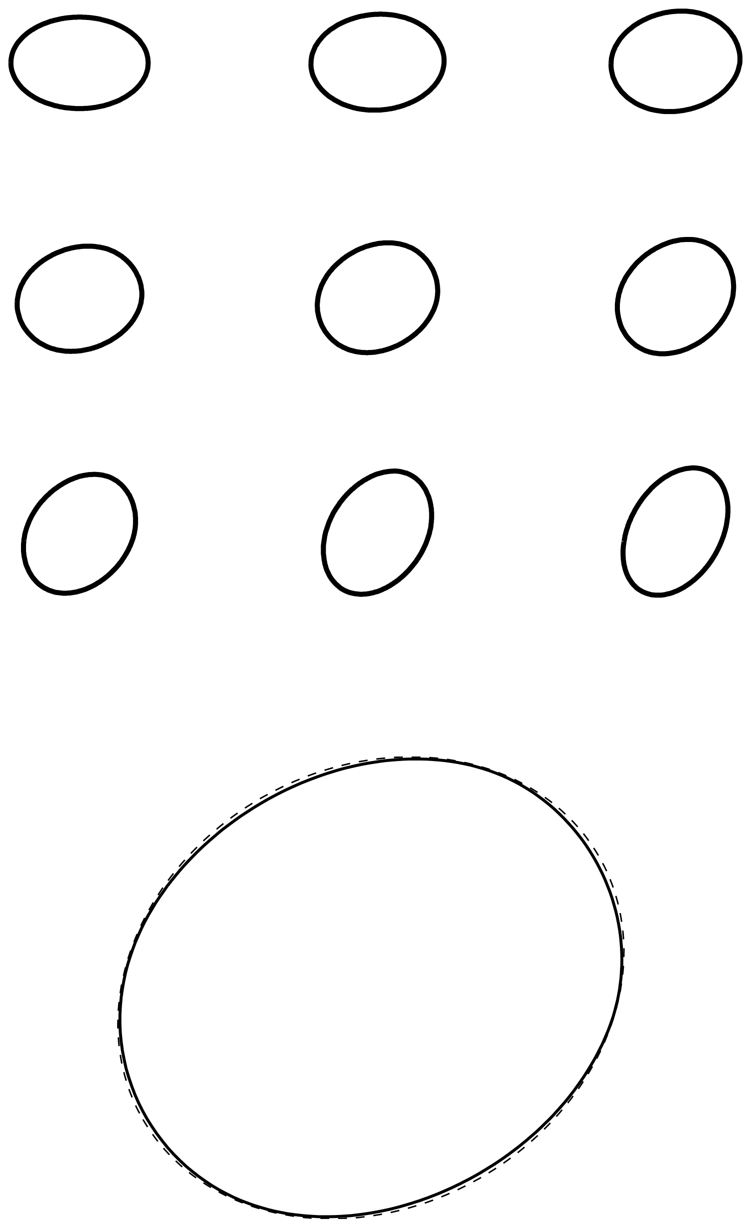

Figure 5.9: Energy $E = 1.62$. The geodesic, connecting the horizontal ellipse with the ellipse rotated by $\pi/3$ from the horizontal one. The ellipses' eccentricity is $e = 1.5$. Below is the middle shape of the geodesic, overlayed with the dashed ellipse, eccentricity 1.2, rotated by $\pi/6$ counter-clockwise.

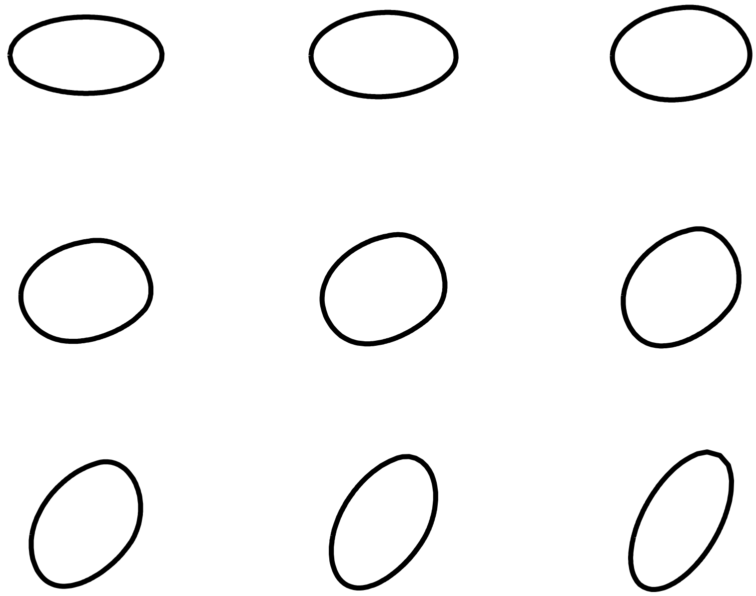

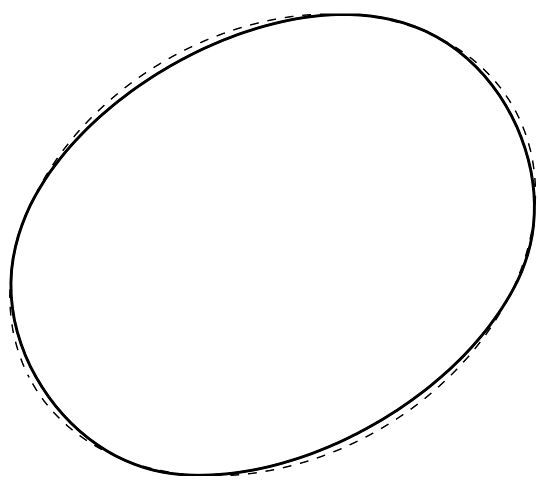

Figure 5.10: Energy $E = 5.2671$. The geodesic, connecting the horizontal ellipse with the ellipse rotated by $\pi/3$ from the horizontal one. The ellipses' eccentricity is $e = 2$. Below is the middle shape of the geodesic, overlayed with the dashed ellipse, eccentricity 1.3, rotated by $\pi/6$ counter-clockwise.

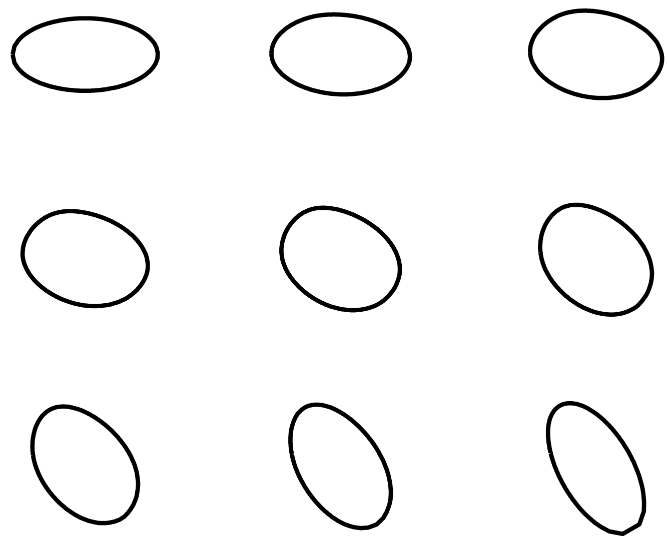

Figure 5.11: Energy $E = 5.2674$. The geodesic, connecting the horizontal ellipse with the ellipse rotated by $2\pi/3$ counter-clockwise. The ellipses' eccentricity is $e = 2$.

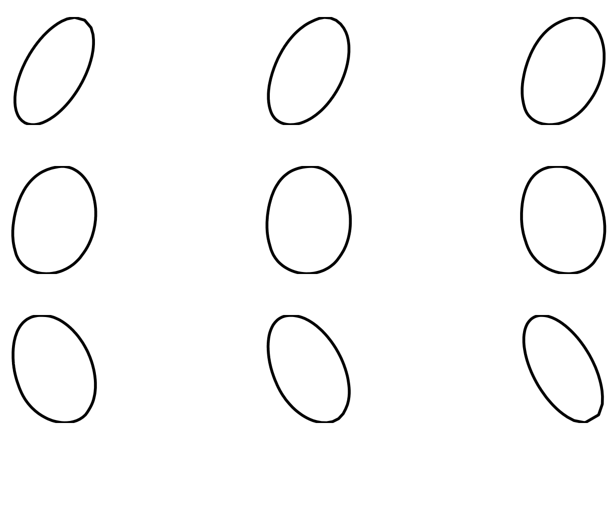

Figure 5.12: Energy $E = 5.2693$. The geodesic, connecting ellipse rotated by $\pi/3$ with the ellipse rotated by $2\pi/3$ from the horizontal one. The ellipses' eccentricity is $e = 2$.

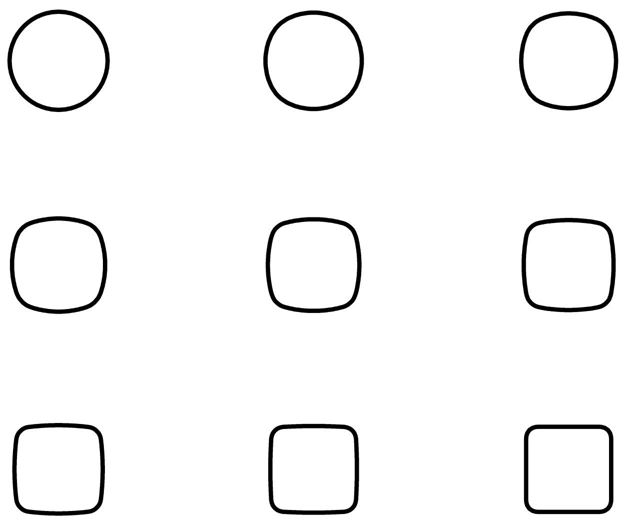

Figure 5.13: Energy $E = 2.80$. The geodesic path, connecting the circle with the square.

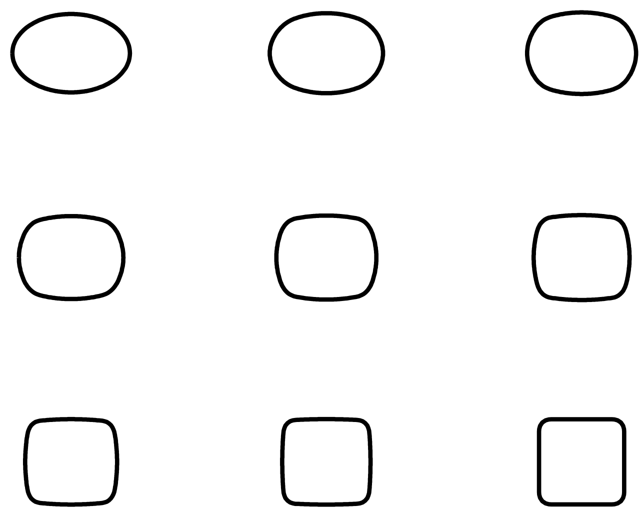

Figure 5.14: Energy $E = 3.80$. The geodesic, connecting the horizontal ellipse, with $e = 1.5$, and the square.

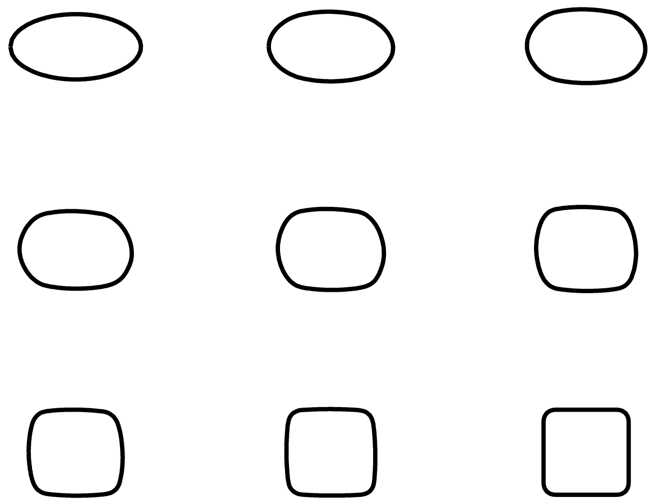

Figure 5.15: Energy $E = 5.91$. The geodesic, connecting the horizontal ellipse, $e = 2$, and the square.

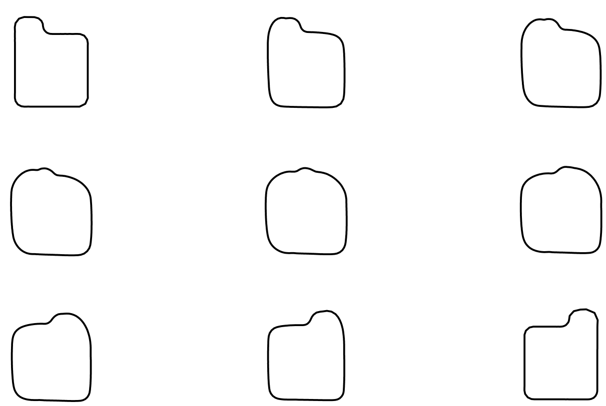

Figure 5.16: Energy $E = 12.90$. The geodesic, connecting the square with the upper-left bump with the square with the upper-right bump.

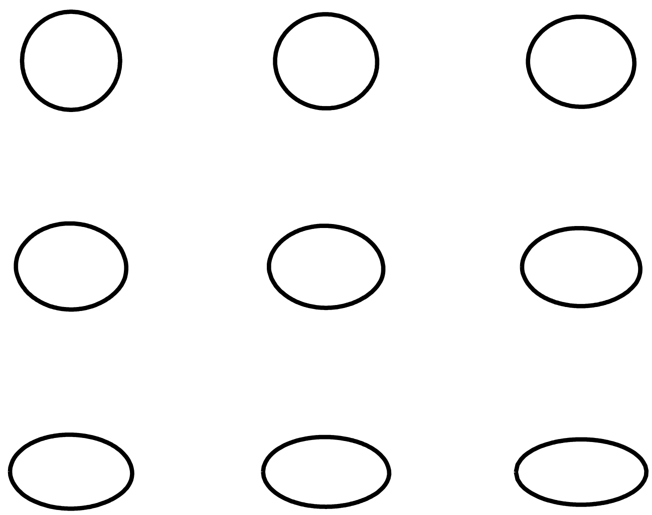

Figure 5.17: Energy $E = 1.65$. The geodesic path, connecting the circle with the horizontal ellipse, $e = 2$.

5.6 Forward integration of the EPDiff

Recall that the solution of the EPDiff(S^1) also minimizes the energy of the path. The path of minimal energy that we obtained from minimization is not guaranteed to be the global minimum, i.e. is not guaranteed to be a solution of the EPDiff(S^1). In this section we will describe a crude integration scheme for the forward solution of the EPDiff(S^1) and compare results from this forward integration scheme with the minimization of the WP energy.

Remember, that the EPDiff could be written as:

$$v_t = -G * (2Lv.v_\theta + Lv_\theta.v), \tag{5.9}$$

where $L = -\mathcal{H}(\partial_\theta^3 + \partial_\theta)$ is the Weil-Petersson operator, and G is its Greens function, i.e. its inverse. This is an integro-differential equation. We have solved the initial value problem numerically in the special case of singular solutions in Chapter 3. The numerical scheme that we used was fairly robust: it preserved the energy and momentum with high accuracy. For the case of general initial v we are going to use a simple Runge-Kutta solver, implemented in Matlab by the `ode45` function.

The right-hand side of (5.9) is computed using the Fourier representation of operator L and its inverse G. As a reminder, if $f = \sum_n \hat{f}_n e^{in\theta}$, then (for $n \neq 0, \pm 1$):

$$(Lf)\widehat{}_n = |n^3 - n|\hat{f}_n, \quad (G * f)\widehat{}_n = \frac{1}{|n^3 - n|}\hat{f}_n.$$

As in (5.5) we compute $2Lv.v_\theta + Lv_\theta.v$ at t_i's using the discrete Fourier transform of the L operator in the form of $\{w_k\}_{k=0}^{N-1}$:

$$(2Lv.v_\theta + Lv_\theta.v)(i) = \sum_{j=0}^{N-1} 2w_{i-j}.v(i).v_\theta(j) + w_{i-j}.v_\theta(i).v(j),$$

where $v(i), v_\theta(j)$ are values of velocity $v(\theta)$ and its derivative $v_\theta(\theta)$ on the discrete uniform grid $\{\theta_k\}$. Then we perform the convolution $G * (2Lv.v_\theta + Lv_\theta.v)$ using the discrete Fourier transform and the fact that $\hat{G}(i) = \dfrac{1}{|i^3 - i|}$. Below is the Matlab code of the function `epdiff_rhs`, that provides the right-hand side of the EPDiff (5.9), and the code of the function `convg`, that implements convolution with $G(\theta)$ via FFT.

```
function du = epdiff_rhs(t,u,W,ghat)
% Function du = epdiff_rhs(t,u,W,ghat) computes the rhs
% of the EPDiff.
% Input u is an Nx1 velocity vector,
% ghat(n) = 1/|n^3-n|, are the Fourier coefficients
% of the Green's function G,
% W is the discretization of the WP operator L.

N = length(u);
dtheta = 2*pi/N;

utheta  = ([u(2:end); u(1)] - [u(end); u(1:end-1)])/(2*dtheta);
du      = - convg( (W*utheta).*u + 2*(W*u).*utheta, ghat);

%%%%%%%%%%%%%

function y = convg(x,ghat)
% Function y = convg(x,ghat) computes the convolution
% of the vector x with Green's function.
% ghat are the Fourier coefficients of the Green's function G.
```

```
N = length(x);
omega = ( -N/2 : N/2-1 )';
factor = exp(1i*omega*pi);
xhat = factor.*fftshift(fft(x))/N;

y = real(ifft(ifftshift(N*xhat.*ghat./factor)));
```

We will compare the performance of this crude forward solver with the minimization of the WP energy procedure.

We have compared almost all the geodesics in Figures 5.9–5.13. In the case of the rotated ellipses with $e = 2$, the forward solver of the EPDiff diverged, before reaching $T = 1$. The code was able to integrate until $T = 0.9$, therefore, the comparison was performed upto time $T = 0.9$.

The geodesic path $\Psi^i(\theta, t)$ that we get from the minimization of energy, will yield an initial vector $v_0 = \Psi^i_t(\theta, t)/\Psi^i_\theta(\theta, t)|_{t=0}$. Remember that the geodesic path in the minimization of energy lies in the space $\mathbf{Diff}(S^1)/\mathrm{PSL}_2(\mathbb{R})$, but the EPDiff$(S^1)$ is the geodesic equation on the $\mathrm{PSL}_2(\mathbb{R})\backslash\mathbf{Diff}(S^1)$ space with a right-invariant metric. That means that the initial velocity for the EPDiff will be $-v_0$ (see equation (5.3)).

We plug in $-v_0$ as the initial vector in the EPDiff (5.9), and solve forward using `ode45`, with the right-hand side discretization as described above, with $\Delta t = .01$.

The EPDiff forward solver and the minimization procedure deal with different representations of the geodesic. The forward solver outputs the velocity trajectory $v(\theta, t)$ in the tangent space at the identity. To get the geodesic path we need to integrate it. The minimization path deals with the discrete version of the geodesic path $\Psi^i(\theta, t)$. To get the velocity field one needs to take $v = (\Psi^i)_t/(\Psi^i)_\theta$. Errors will invariably add up when we pass from v to Ψ and vice versa. In this section we choose to compare velocity fields v^f ('f' for the forward integration of the EPDiff) and v^m

(‘m’ for the minimization of the WP energy). After solving the EPDiff forward, we interpolate it to the same grid that $v^m(\theta_k, t_s)$ is computed on, i.e. for $t_s = \frac{1}{2M} + \frac{k}{M}$, $k = 0, \ldots, M-1$.

At the end we compare v^f and $-v^m$ (negative sign because of the reasons explained above). In Figures 5.18, 5.19 you can see plots of L^1 errors $\|v^f + v^m\|_{L^1}$ for different times t_k for different geodesics. We have refined guesses for the initial velocity v_0 by increasing the number of time steps M in the minimization procedure.

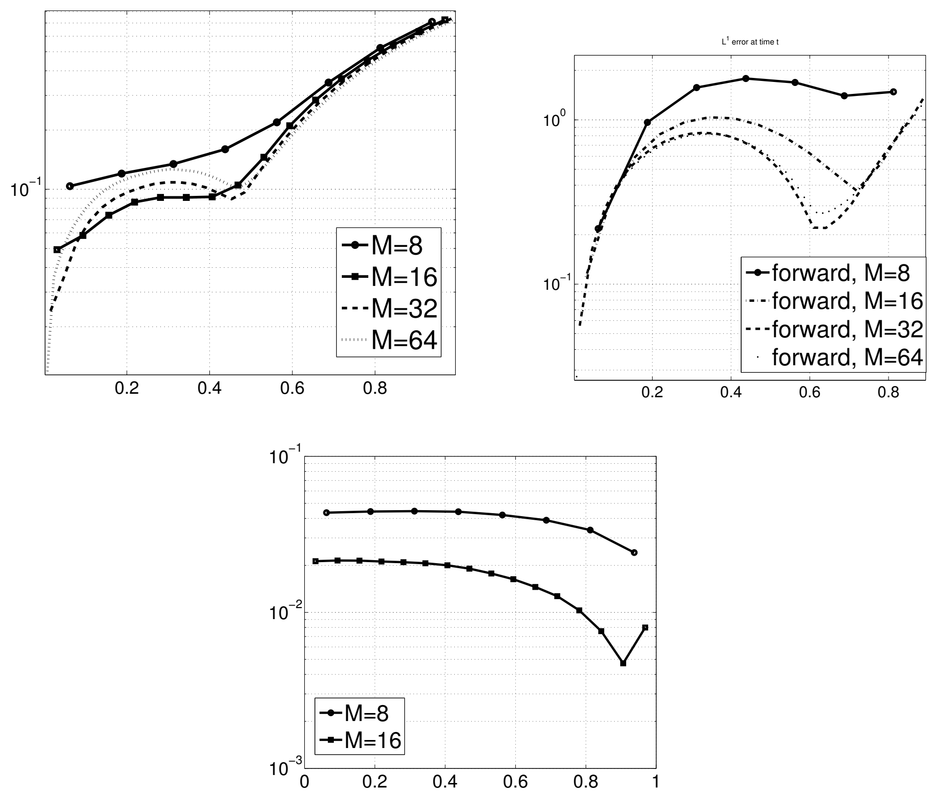

Figure 5.18: L^1 errors $\|v^f + v^m\|_{L^1}$ for different geodesics. From left to right, top to bottom: **1)** the geodesic connecting an ellipse, $e = 1.5$, with the same one rotated by $\pi/3$ counter-clockwise (Figure 5.9); **2)** the geodesic connecting the horizontal ellipse with the ellipse rotated by $\pi/3$ counter-clockwise, $e = 2$ (Figure 5.10); **3)** the geodesic connecting the circle and the ellipse, $e = 2$ (Figure 5.17).

Observe that in most of the plots L^1-error decreases initially with the increase of M, i.e. with the refinement of the time discretization. But at times close to $t = 1$ almost all initial guesses turn out to have the same L^1-error.

Judging from Figures 5.20 and 5.21 we can assume that the forward integration of the EPDiff is a very crude approximation to the geodesic. The energy $\|v\|^2_{WP}$ should be conserved under the flow of the EPDiff, but it is not constant. In the third plot in Figure 5.20 the energy is conserved best by the EPDiff forward solver, and the L^1-error plot (the third plot in Figure 5.18) acts accordingly — the error is one of the smallest among examples presented.

Notice, the larger the energy, the worse the forward solver behaves, both in terms of the energy conservation and in terms of the L^1-error.

The effect of the refinement of the t-grid is mostly noticeable in the first L^1-error plot (Figure 5.18, the circle to the square). By increasing M, i.e. by increasing the time discretization in the geodesic algorithm, we get better solutions for some initial time. As t approaches 1, all the advantages of the finer t-discretization disappear — the error is the same for high and low M's.

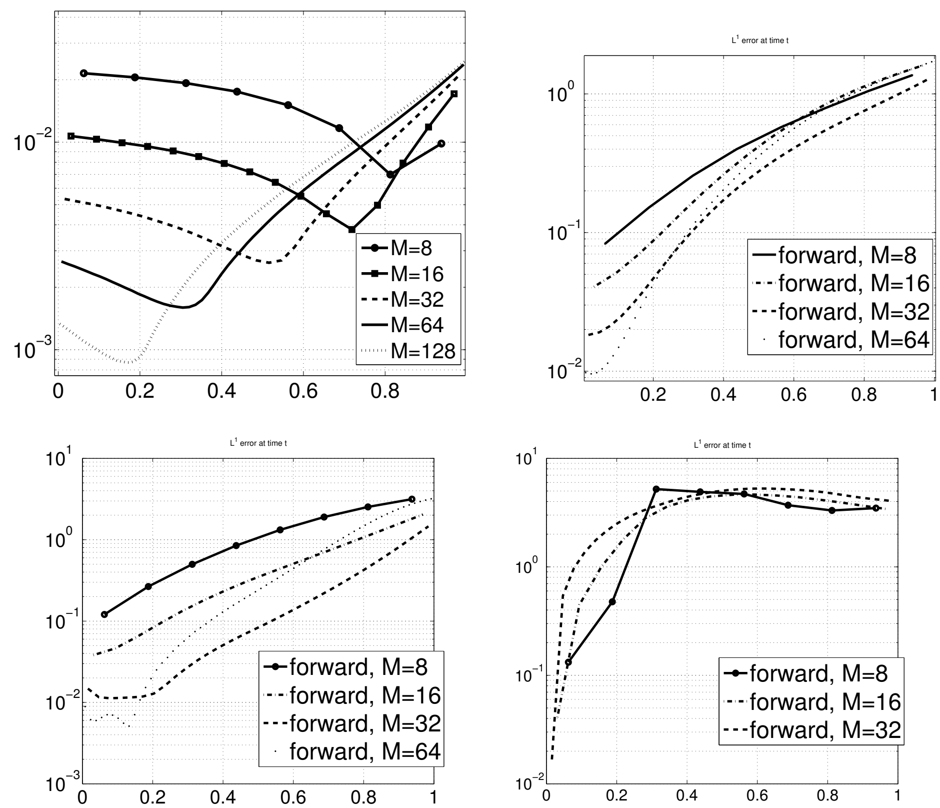

Figure 5.19: L^1 errors $\|v^f + v^m\|_{L^1}$ for different geodesics. From left to right, top to bottom: **1)** the geodesic connecting the circle and the square (Figure 5.13); **2)** the geodesic connecting the ellipse, $e = 1.5$, and the square (Figure 5.14); **3)** the geodesic connecting the ellipse, $e = 2$ and the square (Figure 5.15); **4)** the geodesic connecting the square with the upper-left bump with the square with the upper right bump (Figure 5.16).

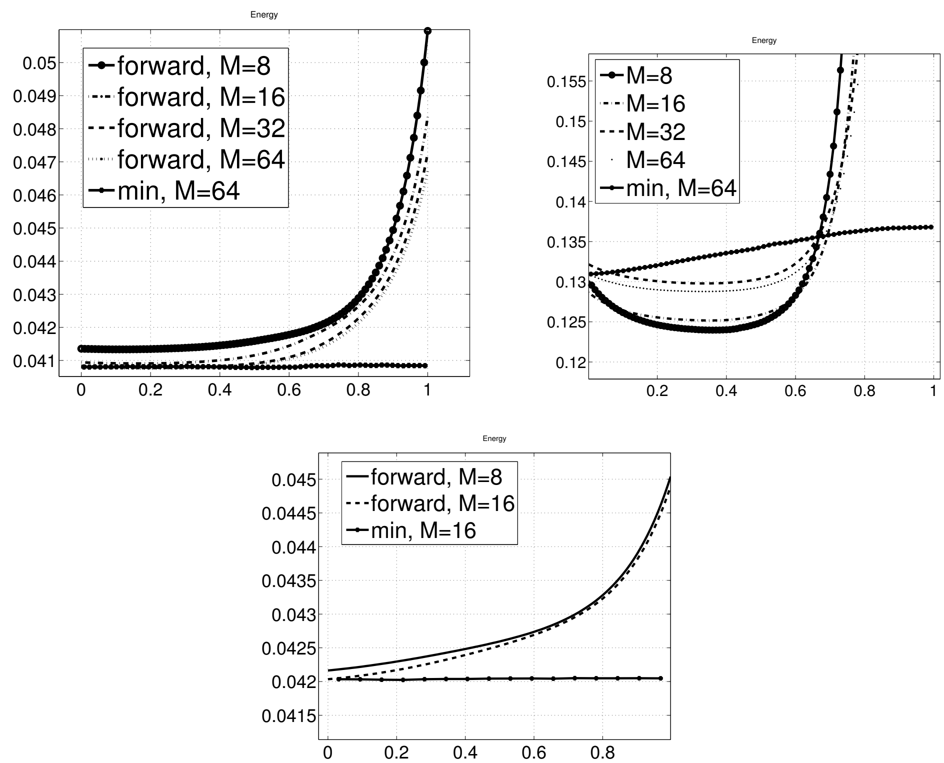

Figure 5.20: Energy of geodesic paths v^f and v^m, computed via forward solution of the EPDiff and minimization respectively. From left to right, top to bottom: **1)** the geodesic connecting the ellipse, $e = 1.5$, with the same one rotated by $\pi/3$ counter-clockwise (Figure 5.9); **2)** the geodesic connecting the horizontal ellipse with the ellipse rotated by $\pi/3$ counter-clockwise, $e = 2$ (Figure 5.10); **3)** the geodesic connecting the circle and the ellipse, $e = 2$ (Figure 5.17).

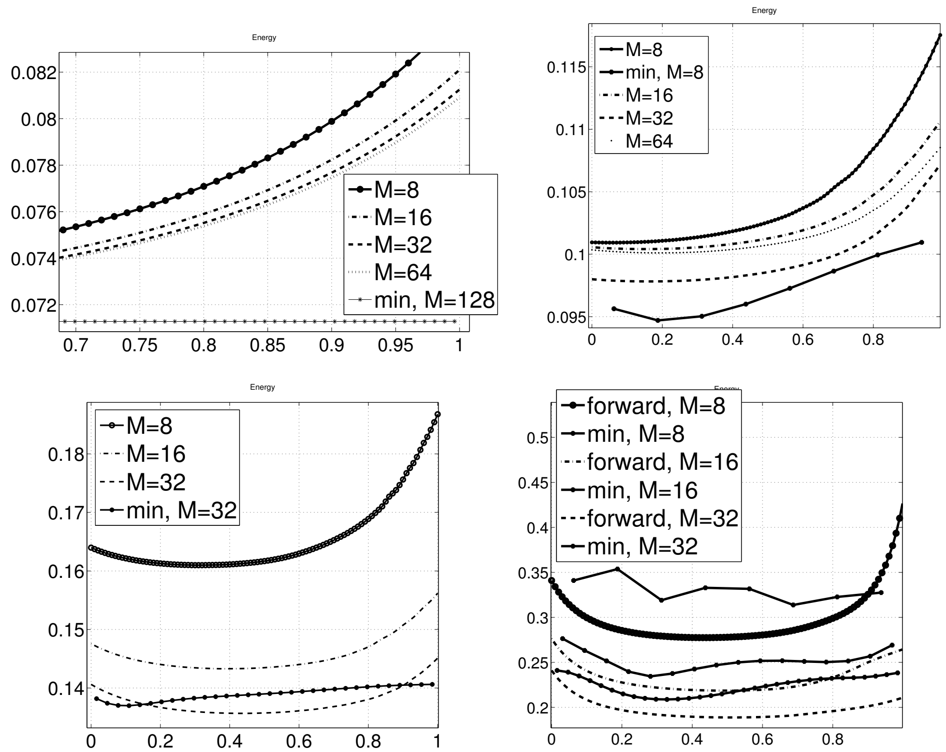

Figure 5.21: Energy of geodesic paths v^f and v^m, computed via forward solution of the EPDiff and minimization respectively. From left to right, top to bottom: **1)** the geodesic connecting the circle and the square (Figure 5.13); **2)** the geodesic connecting the ellipse, $e = 1.5$, and the square (Figure 5.14); **3)** the geodesic connecting the ellipse, $e = 2$ and the square (Figure 5.15); **4)** the geodesic connecting the square with the upper-left bump with the square with the upper right bump (Figure 5.16).

Consider the geodesic connecting the ellipse, $e = 1.5$, with the same one rotated by $\pi/3$ counter-clockwise (Figure 5.9). As a side-by-side comparison, in Figure 5.22 we have plotted velocities v^f and v^m, and the absolute value of their difference. In Figure 5.23 you can compare the final shapes at $t = 1$, from the forward solution of the EPDiff and the minimization of energy. In these plots we can observe that the better the guess for the initial velocity (in other words, for high M), the closer the final shape will be to the final shape of the minimization procedure.

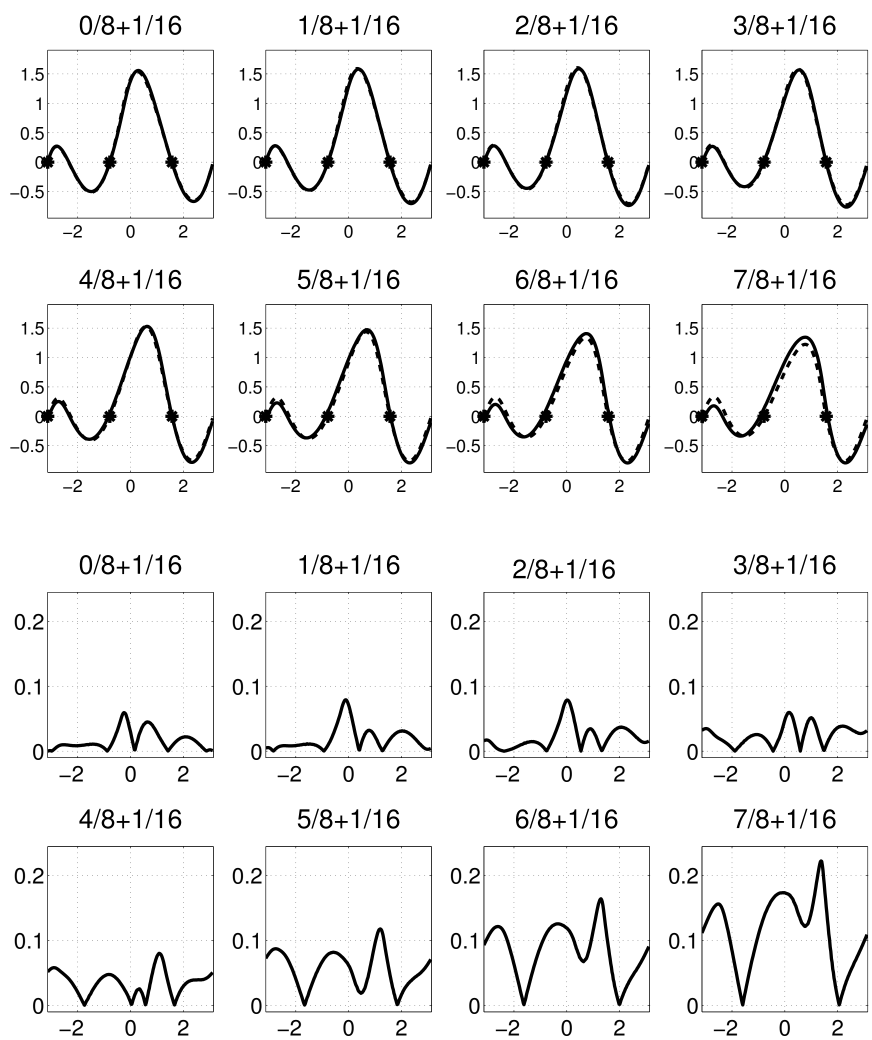

Figure 5.22: Velocities v^f and v^m (top two rows), and $|v^f - v^m|$ (bottom two rows) for the geodesic connecting an ellipse with $e = 1.5$ with the same one rotated by $\pi/3$ counter-clockwise (Figure 5.9), $M = 8, N = 256$. Dashed line corresponds to the output of the minimization procedure, solid line is the output of the forward solver.

As the shapes get further apart (larger values of energy E), it is harder for the forward solver to 'arrive' at the final shape at time $t = 1$. For the geodesic connecting a circle with a square (Figure 5.13) the final shapes are basically indistinguishable. But as we get further apart, e.g. in Figures 5.25, 5.26 we need more refinements of the t-grid to get a better approximation to the final shape. Note, for $M = 64$ in Figure 5.26 the final shapes are not very close to each other. This is due to the fact that the minimization procedure didn't converge completely, thus it didn't provide us with the good guess for the initial velocity.

The worst behavior of the forward solver was demonstrated in the geodesic connecting squares with bumps. In Figure 5.27 observe that final shapes are very different. Although, as M increases we obtain better results. This is the geodesic with the highest energy among all our cases. The energy of the solution v^f of the forward integrator (Figure 5.21) does not diverge exponentially, like in most other cases. The energy stays close to the constant energy of the minimization path. It might be that in this case we are observing the effects of negative curvature. Small changes in the initial vector can lead to very different shapes. And this effect is emphasized by the length of the geodesic.

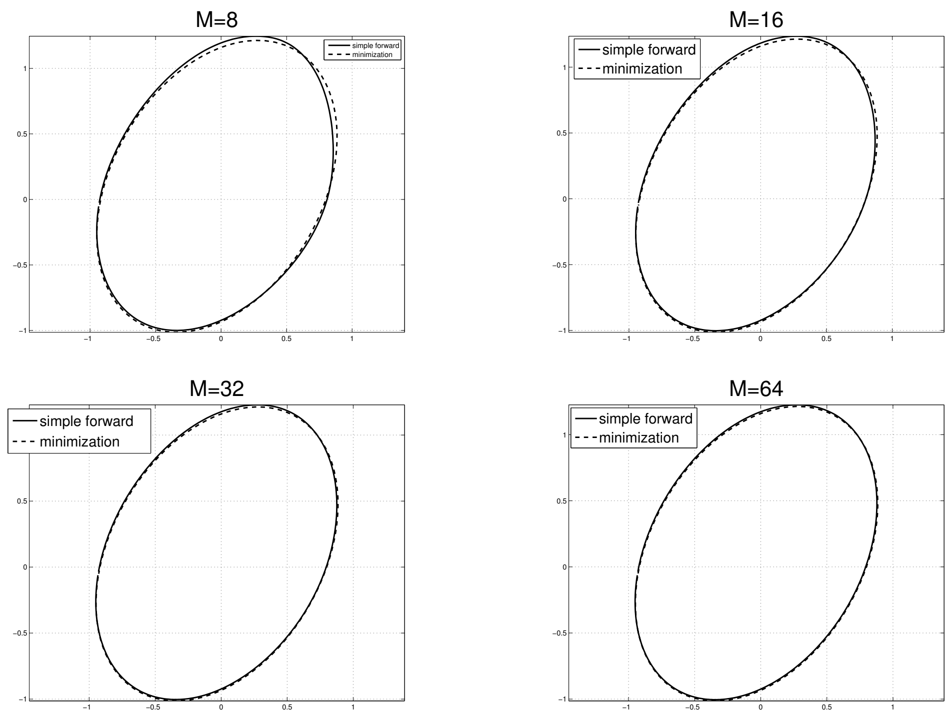

Figure 5.23: Comparison of final shapes at $t = 1$ of the forward integration of the EPDiff (solid line) and the minimization of the energy (dashed line). The geodesic connects the horizontal ellipse with the ellipse rotated by $\pi/3$ counter-clockwise, $e = 1.5$ (Figure 5.9). $E = 1.62$.

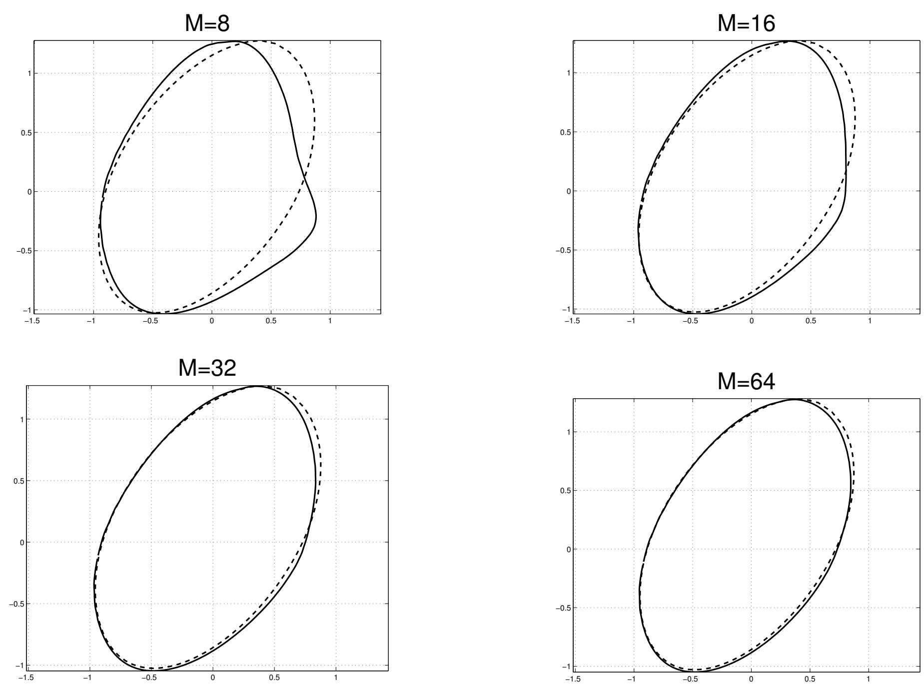

Figure 5.24: Comparison of final shapes at $t = 1$ of the forward integration of the EPDiff (solid line) and the minimization of the energy (dashed line). The geodesic connects the horizontal ellipse with the ellipse rotated by $\pi/3$ counter-clockwise, $e = 2$ (Figure 5.10). $E = 5.2671$.

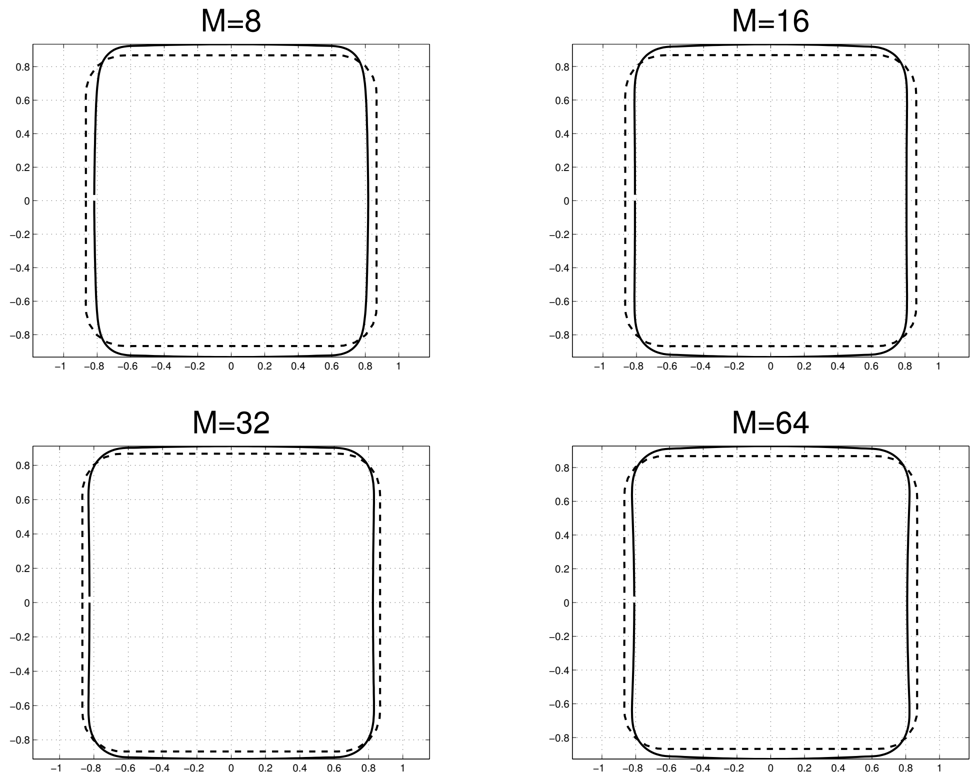

Figure 5.25: Comparison of final shapes at $t = 1$ of the forward integration of the EPDiff (solid line) and the minimization of the energy (dashed line). The geodesic connects the horizontal ellipse ($e = 1.5$) with the square (Figure 5.14). $E = 3.80$.

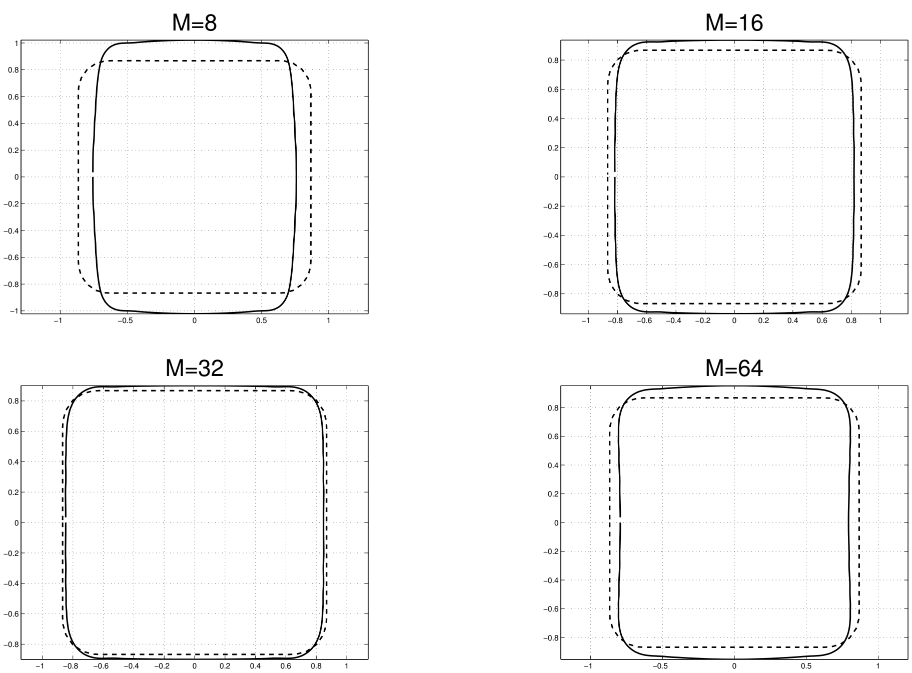

Figure 5.26: Comparison of final shapes at $t = 1$ of the forward integration of the EPDiff (solid line) and the minimization of the energy (dashed line). The geodesic connects the horizontal ellipse ($e = 2$) with the square (Figure 5.15). $E = 5.91$.

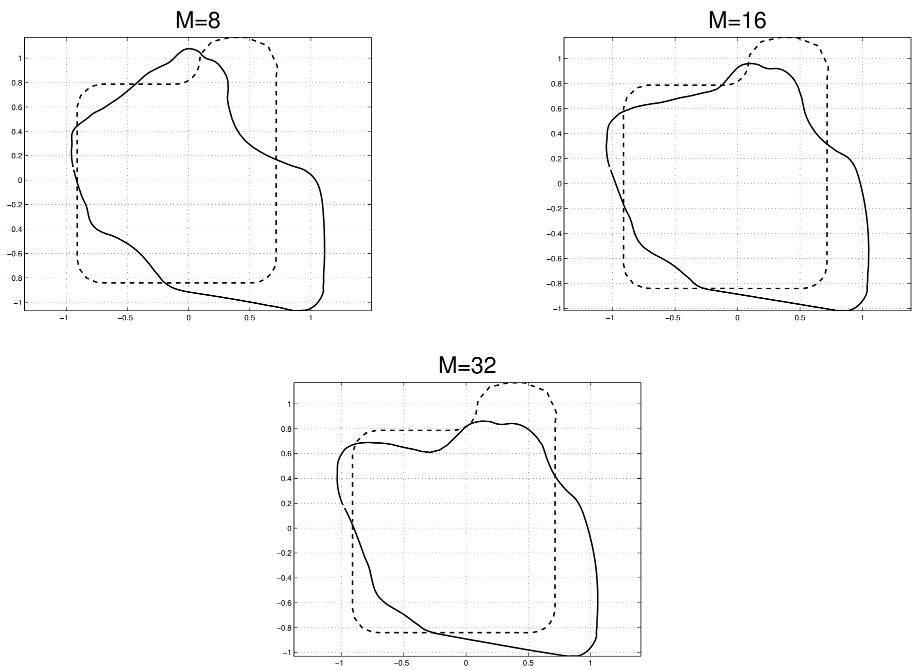

Figure 5.27: Comparison of final shapes at $t = 1$ of the forward integration of the EPDiff (solid line) and the minimization of the energy (dashed line). The geodesic connects the square with the left bump with the square with the right bump (Figure 5.16). $E = 12.90$.

5.7 Forward integration of the EPDiff vs Teichon integration

In Chapter 3 we have investigated the singular solutions of the EPDiff, Teichons, and demonstrated the performance of a symplectic integrator Lobatto IIIAB, that allowed us to obtain evolution of the Teichon with high accuracy.

In this section we will compare the performance of the forward solver of the EPDiff (Section 5.6) with the forward Teichon solver in the following way. We will integrate forward until time $T = 0.3$ the EPDiff using `ode45` with initial velocity $v(t = 0) = \sin(n\theta)$, for $n = 2, \ldots, 8$. We will compare this to the output of the Teichon solver. We initialize the Teichon solver by the momenta $m = \sum a_k\delta(\theta - b_k)$, that will approximate the momenta $m(t = 0) = Lv(t = 0) = |n^3 - n|\sin(n\theta)$. In this case we will take $b_k = 2\pi k/N_d, k = 0, \ldots, N_d - 1$ and $a_k = |n^3 - n|\sin(nb_k)/N_d$. Here, N_d is the number of approximating delta functions. We have tested $N_d = 64, 128, 256$. After that we will compare the output of the forward solver v^f with the output of the Teichon solver v^t ('t' for Teichon), where $v^t = \sum_k a_k G(\theta - b_k)$.

In Figure 5.28 you can see the plots of the L^1 error $\|v^f - v^m\|_{L^1}$ with different number of delta functions N_d in the approximating momenta. As N_d increases, the L^1 error for initial time smaller, due to the better approximation of the initial v. At the final time $t = 0.3$ the errors are the same. Sine the Teichon forward solver is a high-order solver we conclude that the forward EPDiff solver from Section 5.6 is not a good approximation of the solution of the EPDiff.

It is worth pointing out that the WP norm of the initial velocity vector $\|sin(n\theta)\| = \sqrt{|n^3 - n|/2}$. For example, $\|sin(2\theta)\| = \sqrt{3} \approx 1.73$ and $\|sin(8\theta)\| = \sqrt{252} \approx 15.87$. In Figure 5.29 you can see the L^1 error $\|v^f - v^t\|_{L^1}$ in the case of the normalized initial velocity: $v = \frac{\|\sin(2\theta)\|_{WP}}{\|\sin(n\theta)\|_{WP}}\sin(n\theta)$. It is normalized so that $\|v\|_{WP} = \|\sin(2\theta)\|_{WP} = \sqrt{3}$. As you can see the error does not depend much on the frequency n. We can conclude that as the norm grows, the forward EPDiff solver starts diverging. Some of the norms of the initial vectors of geodesics:

- the ellipse $e = 1.5$ to the rotated ellipse, Figure 5.9, $\|v\|_{WP} = 1.27$;
- the ellipse $e = 2$ to the rotated ellipse, Figure 5.10 $\|v\|_{WP} = 2.29$;
- the circle to the square, Figure 5.13, $\|v\|_{WP} = 1.67$;
- the ellipse $e = 1.5$ to the square, Figure 5.14, $\|v\|_{WP} = 1.99$;
- the ellipse $e = 2$ to the square, Figure 5.15, $\|v\|_{WP} = 2.53$;
- the square with the left bump to the square with the right bump, Figure 5.16, $\|v\|_{WP} = 3.65$;
- the circle to the ellipse, Figure 5.17, $\|v\|_{WP} = 1.28$.

The highest of the above norms corresponds to $\|\sin(3\theta)\|_{WP} = \sqrt{12} \approx 3.46$. Yet the L^1 error for $v(t = 0) = \sin(3\theta)$ is not that large as the error when matching the square with the left bump to the square with the right bump. But the tendency is clear: the higher the norm of the initial vector, the worse the behavior is of the `ode45` forward EPDiff solver.

In Figure 5.30 you can see why we cannot use the forward Teichon solver to verify the geodesics. Even in the simplest case we cannot use the momenta to approximate the initial velocity, the momenta is too jagged and the approximating Teichon velocity is very different from the v from the minimization procedure.

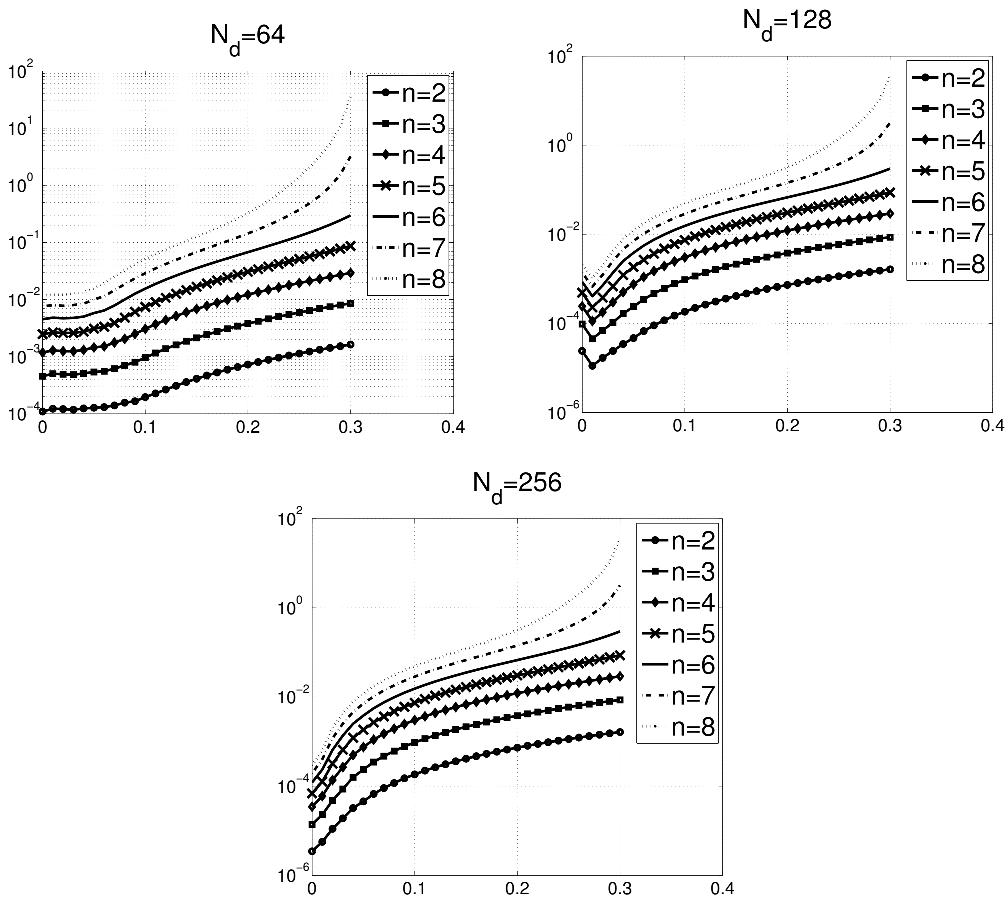

Figure 5.28: Initial velocity $v(t=0) = \sin(n\theta)$. Comparison of L^1 errors $\|v^f - v^t\|_{L^1}$, where v^f is the output of the forward solver of the EPDiff (Section 5.6), v^t output of the Teichon solver (Section 3.4).

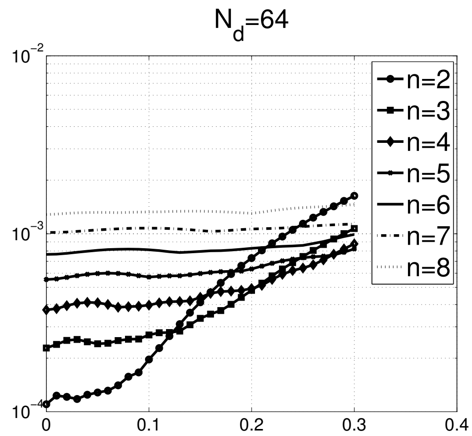

Figure 5.29: Normalized initial velocity $v = \frac{\|\sin(2\theta)\|_{WP}}{\|\sin(n\theta)\|_{WP}}\sin(n\theta)$. Comparison of L^1 errors $\|v^f - v^t\|_{L^1}$, where v^f is the output of the forward solver of the EPDiff (Section 5.6), v^t output of the Teichon solver (Section 3.4).

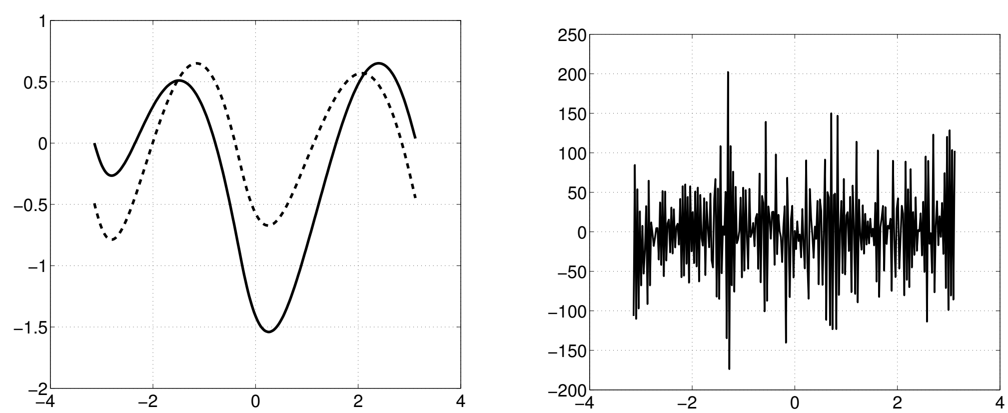

Figure 5.30: Initial velocity v (left) and initial momenta m (right) for the geodesic connecting the horizontal ellipse $e = 1.5$ to the one rotated by $\pi/3$ counter-clockwise (Figure 5.9). Dashed line is the Teichon approximation of the initial velocity v.

Bibliography

[Ar66] Arnold V.I., *Sur la géométrie différentielle des groupes de Lie de dimension infinie et ses applications à l'hydrodynamique des fluides parfaits,* Ann. Inst. Fourier 16 (1966), 316-361.

[AK98] Arnold, V.I., Khesin, B., *Topological methods in hydrodynamics,* Applied Mathematical Sciences, v.125, Springer, 1998.

[BR87] Bowick, M. J. and Rajeev, S. G., *String Theory as the Kähler Geometry of Loop Space*, Physical Review Letters, **58**, pp.535-538, 1987.

[BL88] M.J. Bowick and A. Lahiri, *The Ricci curvature of* $Diff(S^1)/SL(2,R)$, J. Math. Phys. 29 (1988) (9), pp. 19791980.

[CH93] R. Camassa and D. D. Holm, *An integrable shallow water equation with peaked solitons*. Phys. Rev. Lett. 71, (1993), pp.1661-1664.

[DT] T. Driscoll and L.N. Trefethen. *Schwarz-Chrsitoffel Mapping*. Cambridge Univ. Press, 2002.

[Fe08] M. Feiszli. *Conformal Shape Representation.* Ph.D. Thesis, Division of Applied Mathematics, Brown University, 2008.

[GR00] Gradshteyn, I.S., Ryzhik, I.M., *Table of integrals, series, and products,* 6th edition, Academic Press, 2000

[GM98] U. Grenander and M. I. Miller. *Computational anatomy: an emerging discipline*. Quarterly of Applied Mathematics, 56(3):617694, Sept. 1998.

[Ha02] Hairer, E., Lubich, C. and Wanner, G., *Geometric Numerical Integration. Structure Preserving Algorithms for Ordinary Differential Equations.* 2nd edition, Springer, 2002

[HM04] D. D. Holm and J.E. Marsden, *Momentum maps and measure valued solutions (peakons, filaments, and sheets) of the Euler-Poincare equations for the diffeomorphism group.* In The Breadth of Symplectic and Poisson Geometry, A Festshrift for Alan Weinstein, J.E. Marsden and T.S. Ratiu, Editors, Birkhauser Boston, Boston, MA, Progr. Math., 232, (2004) pp. 203-235.

[Ho04] Holm, D.D., Rananather, J.T., Trouve, A., Younes, L.: *Soliton dynamics in computational anatomy.* NeuroImage 23 (2004), S170178, http://arxiv.org/abs/nlin.SI/0411014.

[Hu06] Hubbard, John, *Teichmüller Theory*, Matrix Editions, Ithaca, 2006.

[JM00] S. C. Joshi and M. I. Miller. *Landmark matching via large deformation diffeomorphisms*. IEEE Transactions on Image Processing, 9(8):13571370, Aug. 2000.

[Jo05] Jost, Jürgen, *Riemannian geometry and geometric analysis,* 3rd edition, Springer, 2005.

[Ku09] S. Kushnarev, *Teichons: Soliton-like Geodesics on Universal Teichmüller Space* Source: Experiment. Math. Volume 18, Issue 3 (2009), 325-336.

[KM97] Kriegl, A. and Michor, P., *The Convenient Setting for Global Analysis*, Surveys and Monographs of the Amer. Math. Soc., **53**, 1997.

[Le97] Lee, John, *Riemannian Manifolds. An introduction to curvature,* Springer, 1997.

[Leh87] Lehto, O. *Univalent Functions and Teichmüller Space*, Pringer-Verlag, 1987.

[MR07] Donald E. Marshall, Steffen Rohde, *Convergence of a Variant of the Zipper Algorithm for Conformal Mapping*, SIAM Journal on Numerical Analysis, Volume 45, Issue 6, October 2007.

[M08] M. Micheli. *The Differential Geometry of Landmark Shape Manifolds: Metrics, Geodesics, and Curvature.* Ph.D. Thesis, Division of Applied Mathematics, Brown University, 2008.

[Michor 08] Michor, Peter W. (2008), *Topics in differential geometry*, American Mathematical Soc..

[MM05] P. W. Michor and D. B. Mumford. *Vanishing geodesic distance on spaces of submanifolds and diffeomorphisms.* Documenta Mathematica, 10:217245, 2005.

[MM06] P. W. Michor and D. B. Mumford. *Riemannian geometries on spaces of plane curves.* Journal of the European Mathematical Society, 8:148, 2006.

[MM07] P. W. Michor and D. B. Mumford. *An overview of the Riemannian metrics on spaces of curves using the Hamiltonian approach.* Applied and Computational Harmonic Analysis, 23:74113, 2007.

[MTY02] M. I. Miller, A. Trouvé, and L. Younes. *On the metrics and Euler-Lagrange equations of computational anatomy.* Annual Review of Biomedical Engineering, 4:375405, 2002.

[MTY06] M. I. Miller, A. Trouvé, and L. Younes. *Geodesic shooting for computational anatomy.* Journal of Mathematical Imaging and Vision, 24(2):209228, Mar. 2006.

[Mu91] D. Mumford. *Mathematical Theories of Shape: do they model perception?* Proc. Conference 1570, Soc. Photo-optical & Ind. Engineers, pages 210, 1991.

[MD10] Mumford, D. and Desolneux, A. *Pattern theory: the Stochastic Analysis of Real World Signals*, to appear, 2010, based on notes of a course given in 1998 at the Institut Henri Poincaré.

[NV90] S. Nag and A. Verjovsky, $\mathbf{Diff}(S^1)$ *and the Teichmüller spaces*, Commun. Math. Physics, 130 (1990), 123-138.

[Pa95] Pandey, J.N., *The Hilbert transform of Schwartz distributions and applications,* Pure and applied mathematics, A Wiley-Interscience Series of Texts, Monographs, and Tracts, 1995.

[PTVF07] William H. Press, Saul A. Teukolsky, William T. Vetterling, Brian P. Flannery, *Numerical Recipes 3rd Edition: The Art of Scientific Computing*, Cambridge University Press, 3 edition.

[Sch93] Schumacher,G. *The curvature of the Petersson-Weil metric on the moduli space of Kähler-Einstein manifolds.* In Complex analysis and geometry, Univ. Ser. Math., pages 339-354. Plenum, New York, 1993.

[SM06] Sharon, E. and Mumford, D., *2D-Shape Analysis using Conformal Mapping*, International Journal of Computer Vision, Volume 70, Number 1 / October, 2006, pages 55-75

[Siu86] Siu, Y.T. *Curvature of the Weil-Petersson metric in the moduli space of compact Kähler-Einstein manifolds of negative first Chern class.* In Contributions to several complex variables, Aspects Math., E9, pages 261-298. Vieweg, Braunschweig, 1986.

[TT06] Takhtajan, T. and Teo, L.-P. *Weil-Petersson Metric on the Universal Teichmüller Space*, Memoirs of the Amer. Math. Soc., bf 183, 2006.

[Wo86] Wolpert, S.A. *Chern forms and the Riemann tensor for the moduli space of curves.* Invent. Math., 85(1):119-145, 1986

[YMSM08] L. Younes, P. W. Michor, J. Shah, and D. B. Mumford. *A metric on shape space with explicit geodesics.* Rendiconti Lincei Matematica e Applicazioni, 9:2557, 2008.

[KSMJ04] E. Klassen, A. Srivastava, W. Mio, and S. Joshi. *Analysis of planar shapes using geodesic paths on shape spaces.* IEEE Transactions on Pattern Analysis and Machine Intelligence, 26(3):372383, Mar. 2004.

[VMTY05] M. Vaillant, M. Miller and A. Trouve, L. Younes: Statistics on Diffeomorphisms via Tangent Space Representation, Neuroimage (2005)

[Wang et al 07] L. Wang, F. Beg, T. Ratnanather, C. Ceritoglu, L. Younes, J. C. Morris, J. G. Csernansky, and M. I. Miller. *Large deformation diffeomorphism and momentum based hippocampal shape discrimination in dementia of the Alzheimer type.* IEEE Transactions on Medical Imaging, 26(4):462470, Apr. 2007.